ISSN: 2795-1944

Date of Printing: June, 2022

Date of Publishing: June, 2022

Editor: Er. Bikesh Kunwar

Publication:

SET – Advanced College of Engineering and Management

Kalanki, Kathmandu

Science Engineering and Technology (SET) Conference - 2021

Proceedings

of

3rd National Conference

on

Science, Engineering and Technology

(SET Conference 2021- Innovation and Technology for Global Pandemics)

Vol: 3

December 4, 2021

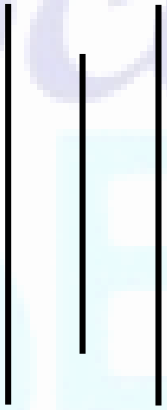

Associate Editors:

Er. Prabin Dawadi

Er. Subeksha Khanal

Er. Laxmi Prasad Bhatt

Er. Sameer Sitoula

Committee Members of SET Conference – 2021

Patron

- Er. Lochan Lal Amatya

Advisory Board

- Prof. Shashidhar Ram Joshi, Ph.D.
- Prof. Dr. Geeta Bhakta Joshi
- Prof. Dr. Subarna Shakya
- Prof. Dr. Gokarna Bahadur Motra
- Prof. Dr. Vinod Parajuli
- Assoc. Prof. Bikash Bahadur Shrestha
- Assoc. Prof. Laxmi Bhakta Maharjan
- Assoc. Prof. Dhaneshwor Sah
- Er. Prashant Ghimire
- Er. Ajaya Shrestha
- Er. Santosh Niraula
- Mr. Rajendra Poudel
- Er. Prerana Khwaunju

Members

Er. Narayan K.C.
Er. Raisha Shrestha
Er. Bigyan Karki
Er. Sameer Sitoula
Er. Subeksha Khanal
Er. Prabin Dawadi
Mr. Gunanidhi Gyawali
Er. Arjun Basnet
Er. Sandip Adhikari
Er. Babita Sharma
Dr. Raksha Dangol
Er. Kritika Gulati

Executive Committee

President
Er. Amit Kumar Rauniyar

Vice President
Er. Prem Chandra Roy

Secretary
Er. Bikash Acharya

Technical Coordinator
Er. Neha Karna

Media Coordinator
Er. Bikesh Kunwar

Finance Coordinator
Er. Laxmi Prasad Bhatt

Conference Coordinator
Er. Sujata Dahal

Event Management Team

Mr. Shyam Mani Acharya
Mr. Som Tamang
Mr. Ashok Kumar Sah
Mr. Suman Gurung
Mr. Ukesh Lal Shrestha
Mrs. Shiksha Karki
Ms. Taniya Rana
Mr. Kiran Basnet

TABLE OF CONTENTS

Part I: Communication Engineering

Part II: AI and Decision Support Systems

Part III: Software Engineering

Part IV: Hydrology and Hydropower

Part V: Building Technology

Science Engineering and Technology (SET) Conference - 2021

Part I: Communication Engineering

Implementation of Turbo Code in CDMA 2000

Damodar Kandel [1], Roshan Chitrakar [2]

[1] *Communication Directorate, Nepal Polices*
[2] *Nepal College of Information Technology*
[1] *damumsic@yahoo.com*, [2] *roshanchi@gmail.com*

Abstract

For efficient and reliable communication, channel coding is performed. Among channel coding, Turbo code is one used in wireless communication system. Carrier division multiple access (CDMA) is efficient technique in wireless communication system because it serves an unlimited number of users. Turbo code performs on a capability close to Shannon limit. It is recursive in nature and provides better performance. In this paper, we study performance of convolutional encoder in AWGN channel, performance of Turbo encoder in AWGN and Rayleigh fading channel, effect of number of iterations in Turbo decoder and Turbo code is implemented in forward link of CDMA 2000. Simulation result in forward link of CDMA showed that if probability of error decreases SNR value increases.

Keywords*: Turbo Code, CDMA, Shannon limit, Channel coding, Convolutional code, Rayleigh fading channel.*

1. Introduction:

There are mainly two types of channel codes, namely block codes and convolutional codes. Block codes are based rigorously on finite field arithmetic and abstract algebra. They can be used to either detect or correct errors. They accept a block of k information bits and produce a block of n coded bits. By predetermined rules, $n-k$ redundant bits are added to the k information bits to form the n coded bits. Convolutional codes are one of the most widely used channel codes in communication systems. These codes are developed with a separate strong mathematical structure and are primarily used for real time error correction. Convolutional codes convert the entire data stream into one single code word. The encoded bits depend not only on the current K input bits but also on past input bits. The wide acceptance of convolutional codes advances to extend and improve the basic coding schemes, namely, trellis coded modulation and Turbo codes. TCM adds redundancy by combining coding and modulation into a single operation. The unique advantage of TCM is that there is no reduction in data rate or expansion in Bandwidth. A near channel capacity error correcting code called Turbo code is able to transmit information through the channel with low (approaching zero) bit error rate. Turbo code can achieve performance within 1 dB of channel capacity. The performance of Turbo code is partly due to the random interleaver used to give the turbo code a random appearance. The advantage of Turbo code is enough code structure to decode efficiently. According to Shannon's theorem the maximum capacity of a channel is given by:

$$C = W\ log_2(1+\frac{S}{N}) \quad (1)$$

Where w is the bandwidth of the channel, $(\frac{S}{N})$ is the signal to noise ratio and C is the channel capacity in bits/ s. Shannon postulated that it is practically possible to transmit data over a channel at a rate $< C$. This correspondence to the $\frac{E_b}{N_0} = 0.693 = -1.59\ dB$. In order to reach this limit would require that the codes be of extremely large lengths such that the decoding complexity would be extremely large. Claude Shannon demonstrated that turbo codes could achieve BER of $0.7\ dB$ compared to the Shannon's capacity in an AWGN channel.

The idea about Turbo code was born in France in 1993 when a group of researchers working in France developed turbo codes. The initial results showed that turbo codes could achieve energy efficiencies within only a half decibel of the Shannon capacity [1]. In the paper of Matthew C. Valenti and Jian Sun [4] the idea about how the turbo code is implemented in third generation cellular system like CDMA 2000 and UMTS is described. Linear code is a code for which the modulo -2 sum of two valid code words (found by XOR-ing each bit position) is also a valid code word. Most codes including Turbo codes are linear. The Hamming weight of a code word is the number of one it contains. Thus, a simple linear code could be composed of two code words, {000} and {111}, where hamming weight of the first code word is zero and the hamming weight of the second code word is 3. All linear codes must contain the all- zeros code word, since any code word XOR-ed with itself will produce all zeros. Convolutional codes are used to improve the performance of digital radio, mobile phones, satellite links and Blue tooth to achieve reliable data transfer whereas Turbo codes are used in 3G and 4G mobile telephony, Media FLO, terrestrial mobile television system from Qualcomm and new NASA mission used as MARS Reconnaissance orbiter.

1.1 Convolutional Encoder:

A general convolutional encoder is mechanized with a KK- stage shift register and n modulo-2 address, where K is the constraint length [10]. The constraint length represents the number of K-bit shifts over which a single information bit can influence the encoder output. At each unit of time, K bits are shifted into the first K stages of the register; all bits in the register are shifted k stages to the right, and the outputs of the n address are sequentially sampled to yield the binary code symbols or code bits. These code symbols are then used by the modulator to specify the waveforms to be transmitted over the channel. Since there are n code bits for each input group of K message bits, the code rate is k/n message bit per code, where K>n.

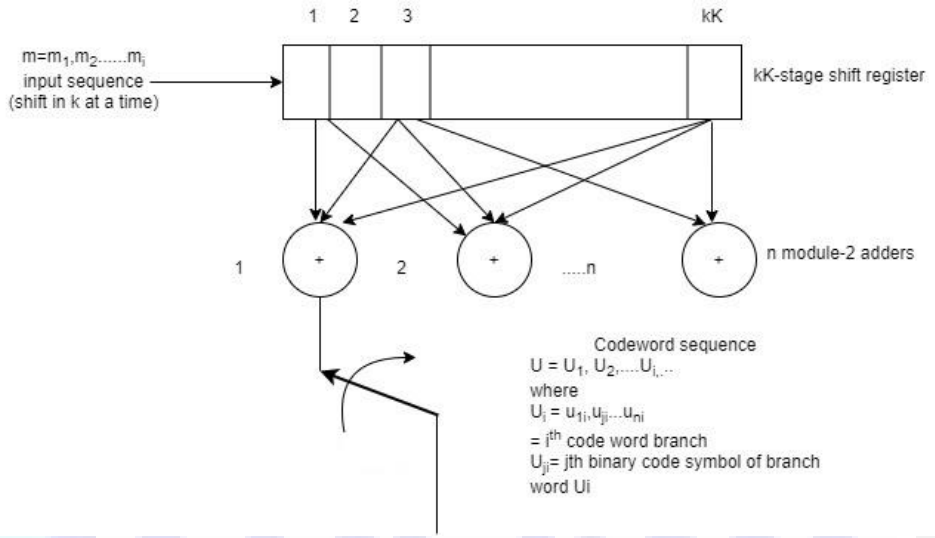

Figure 1. Convolutional encoder with constraint length k and rate k/n

1.1.1 Convolutional encoder representation:

To describe a convolutional code, one need to characterize the encoding function $G(m)$, so that given an input sequence$m$, one can rapidly compute the output sequence U. Several methods are used for representing a convolutional encoder, the most popular being the connection pictorial, connection vectors or polynomials, the state diagram, the tree diagram and the trellis diagram.

1.1.2 Connection representation:

Fig. 2 illustrates a convolutional encoder with constraint length$k = 3$. There are $n = 2$ modulo-2 adders; thus, the code rate $\frac{k}{n}$ is $\frac{1}{2}$. At each input bit time, a bit is shifted into the leftmost stage and the bits in the registers are shifted one position to the right. Next, the output switch samples the output of each modulo-2 adder, thus forming the code symbol pair making up the branch word associated with the bit just inputted. The sampling is repeated for each inputted bit. The connection between the adders and the stages of the register gives rise to the characteristic of the code. Any change in the choice of connections results in a different code.

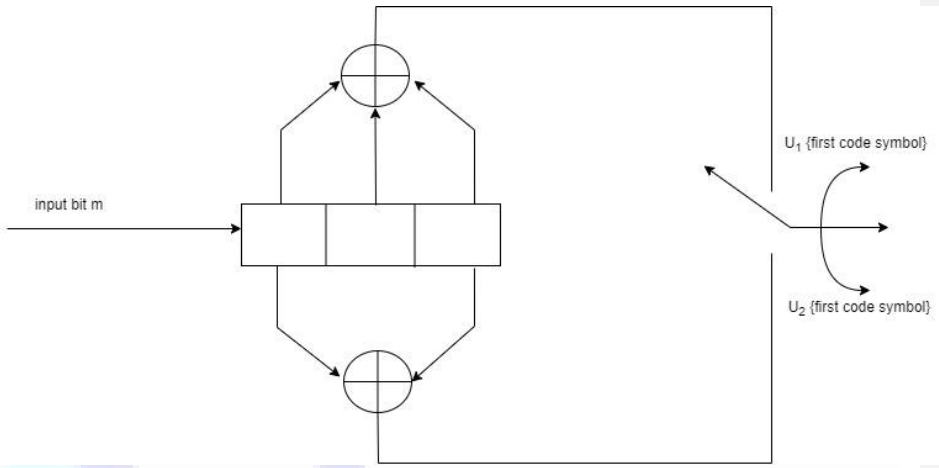

Figure 2. Convolutional encoder (rate ½, k=3)

1.2 Turbo code encoder:

The Turbo code encoder employs two identical systematic recursive convolutional encoders connected in parallel with an interleaver preceding the second recursive convolutional encoder. The two recursive convolutional encoders are called the constituent encoders of the Turbo encoder. The information bits are encoded by both RSC encoders. The first encoder operates on the input bits in their original order, while the second encoder operates on the input bits as permuted by the Turbo interleaver. If the input symbol is of length Kbits and output symbol size is n bits, then the encoder is of code rate $r_c = \frac{k}{n}$. The information bits are always transmitted across the channel. Depending upon the code rate desired, the parity bits from the two constituent encoders are punctured before transmission.

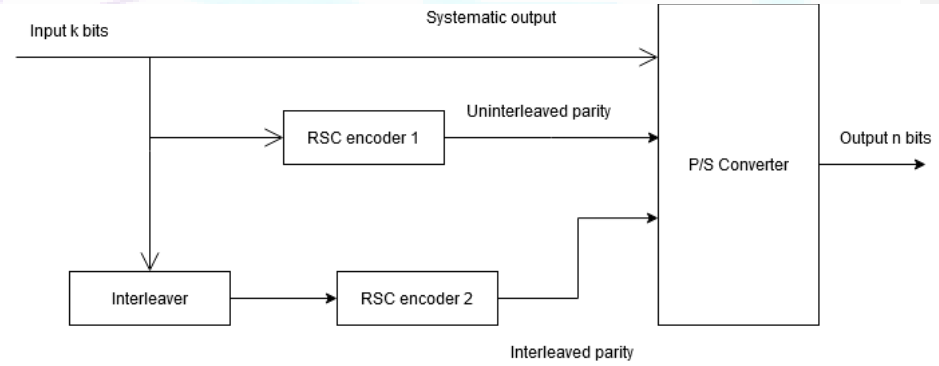

Figure 3. Turbo Code encoder

1.2.1 CDMA 2000 Turbo code*:*

Mohanad Babiker et.al [6] explained CDMA is the third-generation wireless communication and cellular system. The performance of Turbo code and Turbo decode in CDMA depends on interleaver which restricts the size of the frame data. The length of frame is determined in a specific range. In the CDMA the size of the input data has values start from 380 bits per frame and by specific sequence, the frame values reach to 20730 bits per frame [2][3].

Fig. 4 shows a recursive systematic convolutional code (RSC) used by CDMA. The encoder has one input with three-shift register, which produced three outputs (one systematic and two parity) for each input bit. The code rate of this RSC encoder is $R_c = \frac{1}{3}$. The encoder utilized as a part of the parallel linked coding structure [4,5,6].

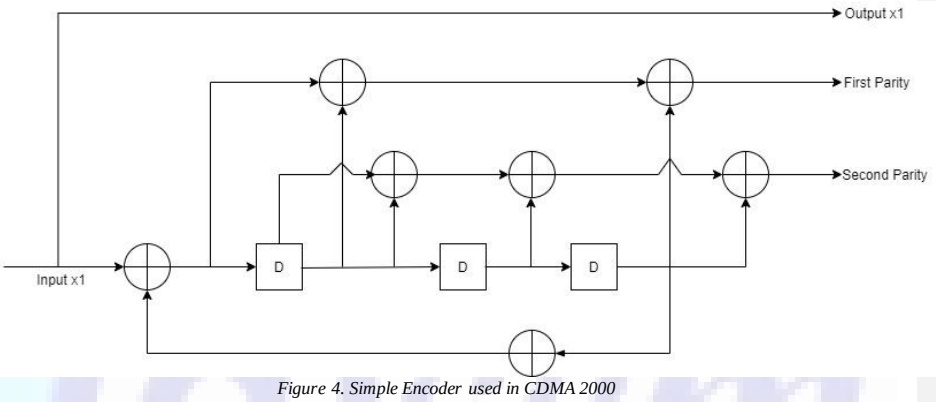

Figure 4. Simple Encoder used in CDMA 2000

1.2.2 Turbo decoder:

The decoding method which is used to minimize probability of sequence of error is Viterbi algorithm. This algorithm is not suitable to generate a posteriori probability (APP) output for each decoded bit. A relevant algorithm was proposed by Bahl et.al. [8]. This algorithm was modified by Berrou, et.al [9] for use in decoding RSC codes. The APP that a decoded data bit $d_k = i$ can be derived from the joint probability $\lambda_k^{i,m}$ defined by

$$\lambda_k^{i,m} = p\{d_k = i, S_k = m | R_1^N\}$$

(2)

Where $S_k = m$ is the encoder state at time$k$, and R_1^N is a received binary sequence from time $k = 1$ through sometime$N$.

The APP that a decoded data bit $d_k = i$, represented as a binary digit, is obtained by summing the joint probability over all states, as follows:

$$p\{d_k = i | R_1^N = \sum_m \lambda_k^{i,m} \quad i = 0,1$$

(3)

Next, the log likelihood ratio is written as the logarithm of the ratio of Apps, as

$$L(\tilde{d}_k) = log\left[\frac{\sum_m \lambda_k^{i,m}}{\sum_m \lambda_k^{0,m}}\right]$$

(4)

The decoder decides, known as the maximum a posteriori decision rule, by comparing $L(\tilde{d}_k)$ to a zero threshold. That is.

$$\tilde{d}_k = 1 \text{ if } L(\tilde{d}_k) > 0$$
$$\tilde{d}_k = 0 \text{ if } L(\tilde{d}_k) < 0$$

(5)

For a systematic code, the LLR $L(\tilde{d}_k)$ associated with each decoded bit $\tilde{d}_k$ can be described as the sum of the LLR of $\tilde{d}_k$, out of the demodulator and of the other LLRs generated by the decoder (extrinsic information).

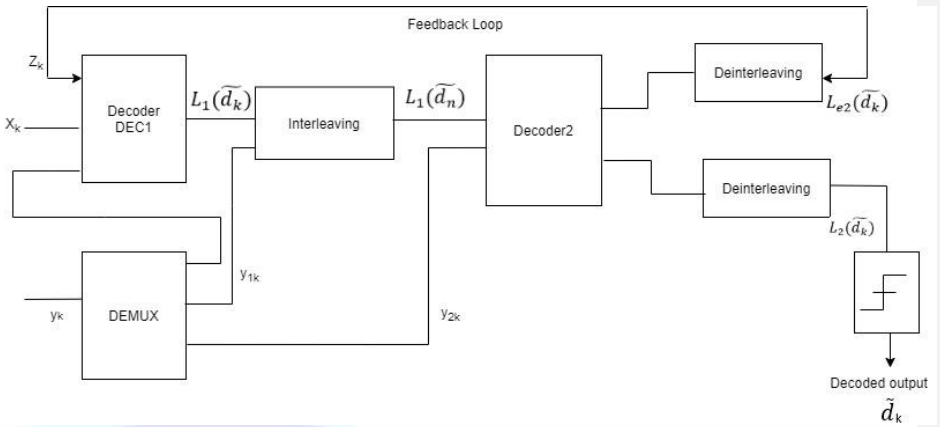

Figure 5. Turbo decoder

1.3 IS-2000 CDMA system:

M. Raja Murali Krishna et.al [7] described there is reverse or forward link fundamental and supplemental channel in IS-2000 CDMA. The data is encoded frame by frame and tail bits are added at the end of each frame. The data bits plus tail bits determined the frame size.

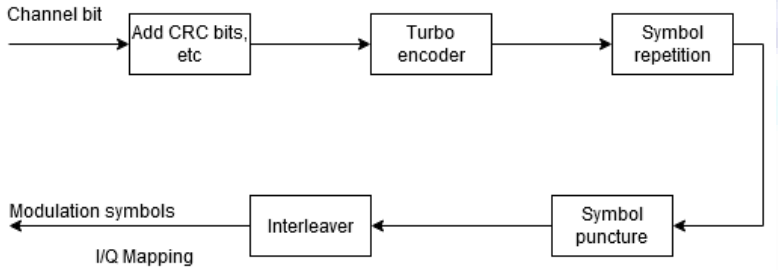

Figure 6. A part of the forward fundamental channel and forward supplemental channel structure

In order to keep a base band symbol at a constant rate of 19.2 kbps, whenever the user rate is less than 9600 bps, each symbol from the encoder is repeated before block interleaving. If the information rate is 2400 bps or 1200 bps, each code symbol is repeated three or seven times, respectively.

Output Puncturing:

M. Raja Murali Krishna et.al [7] described the role of Turbo code puncturing is to periodically delete selected bits to reduce coding overhead. In IS-2000 CDMA Turbo code, the bits in encoder 1 are always transmitted for the non-tail bits whereas the bits in encoder 2 are always punctured for the non-tail bits. Other puncturing patterns depend on the code rate selected.

Interleaver:

Mohanand Babiker et.al [6] explained interleaver is used in turbo code to avoid the error. It can spread and rearrange error without neglecting any bit. There are three types of interleaver namely row column interleaver, helical interleaver and odd even interleaver. The most like interleaver is the one that provide randomness. By using inverse map in de-interleaved the multiple combinations of input sequence is performed [5]. The input sequence is given as Z_1, Z_2, Z_3, Z_4, Z_5, Z_6, Z_7, Z_8, Z_9 and an output is shown in fig. 7.

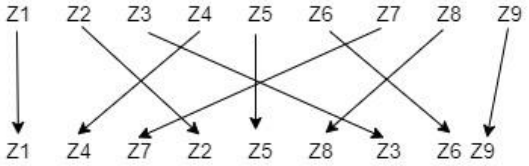

Figure 7. Rearranging of Data in the Interleaver

2. Related Works

M, Raja Murali Krishma in 2014 made a research in Turbo code with AWGN and fading channel in which he observed improve in error correcting coding technique but had limitations in the trade-off between the BER and the number of iterations, output delay is longer and higher coding rate needs more bandwidth. K. Rasadurai & N. kumarathan in 2012 research in Turbo MUD SISO and observed computational complexity and improvement in BER performance but they observed delay during the simulation. Jaswinder singh in 2011 used the technique named Fiber-optic CDMA, Successive interference cancellation, differential detection which resulted better than conventional TDMA and FDMA techniques but had multiple access interferences among the users simultaneously accessing the network.

3. Methodology

The turbo code is employed and implemented in simulation using MATLAB. Our methodology parameters are parallel recursive systematic convolutional code with code rate used is $\frac{1}{2}$ and modulation used is BPSK. Turbo code is implemented in the forward link of CDMA 2000 in which QPSK modulation is used. The simulation was carried out with a frame size of 300 and generator matrix [1 1 1 1; 1 0 1 1].

Figure 8. Simulation process

4. Simulation and Result

a. BER vs. $\frac{E_b}{N_o}$ plot of Convolutional encoder:

$\frac{E_b}{N_o}$ was varied from 1 dB to 4 dB and the BER value at the different $\frac{E_b}{N_o}$ was obtained for convolutional encoder in AWGN channel. It was found that as the $\frac{E_b}{N_o}$ value was increased, BER value was decreased.

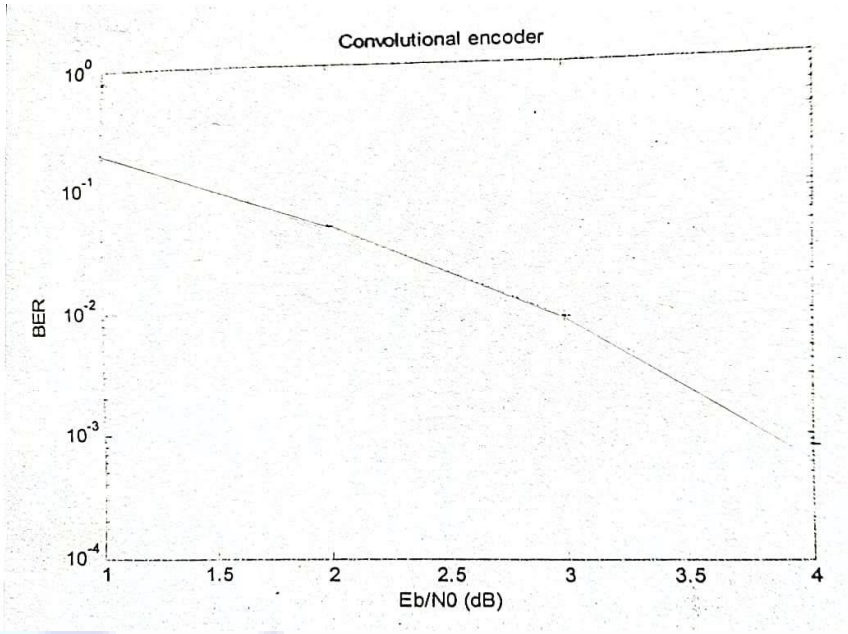

Fig 9. BER vs. $\frac{E_b}{N_o}$ plot for convolutional encoder obtained from simulation.

b. *BER vs. $\frac{E_b}{N_o}$ plot of Turbo encoder:*

$\frac{E_b}{N_o}$ was varied from 1 dB to 5 dB and the BER value at the end of 5 iterations was obtained for AWGN and Rayleigh fading channels. It was found that as the $\frac{E_b}{N_o}$ value was increased, the BER value was

decreased.

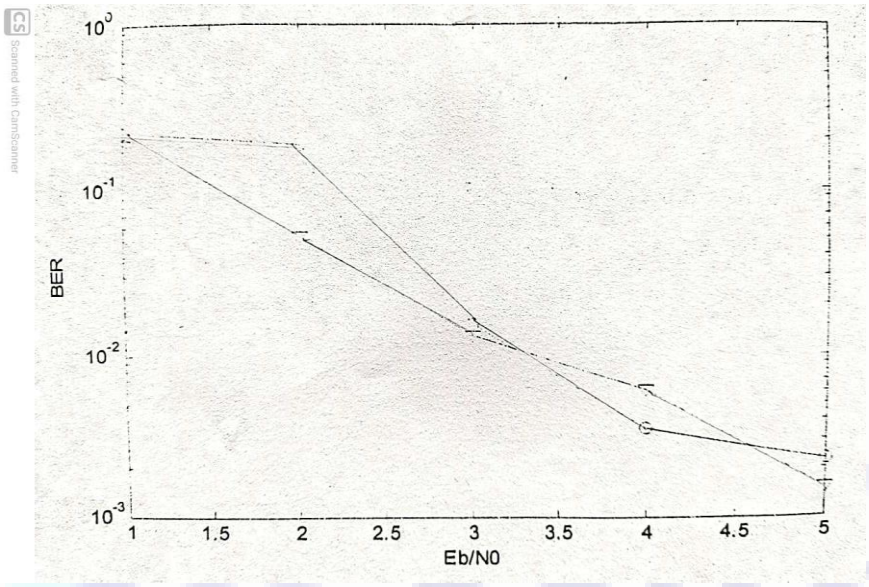

Figure 10. BER vs. $\frac{E_b}{N_o}$ plot for different $\frac{E_b}{N_o}$ obtained from simulation.

c. Effect of Number of iterations of the Turbo decoder:

Simulation was carried out to find the BER by keeping the $\frac{E_b}{N_o}$ value constant. As the number of iterations increased it was found that the AWGN channel with $\frac{E_b}{N_o} = 2.0$ dB showed relatively better convergence in the value of BER. However, with Rayleigh fading channels with $\frac{E_b}{N_o} = 2.0$ dB no signs of convergence were seen. Hence the BER vs. iteration plot for Rayleigh fading channels correspond to $\frac{E_b}{N_o} = 4.0$ dB. Increasing the signal energy, it is observed that the BER is found to converge.

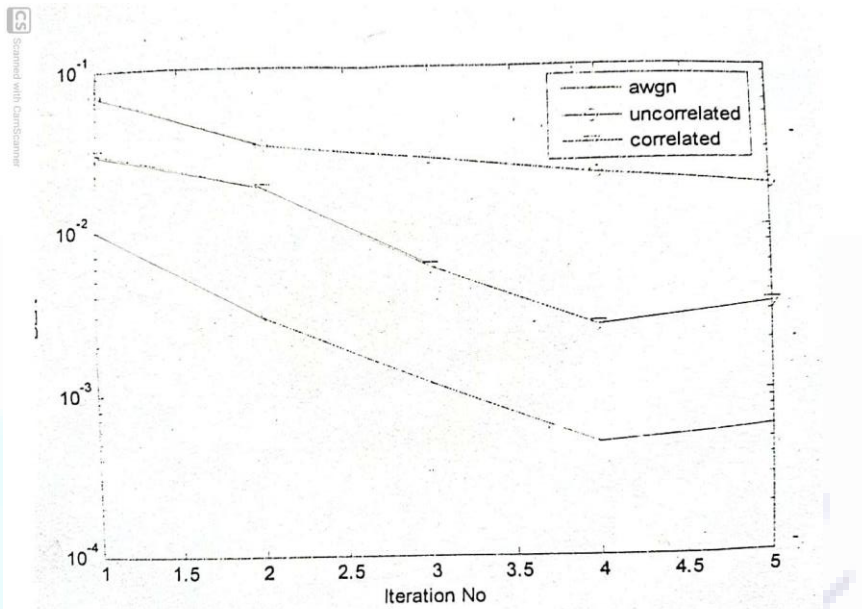

Fig 11. BER vs. Iteration Number plot with $\frac{E_b}{N_0} = 2.0$ dB for AWGN channel and 4.0 dB for Rayleigh fading channel obtained from simulation.

d. Probability of error vs. SNR:

SNR was varied from 1 dB to 4 db. It was found that as the SNR value increases probability of error decreases. QPSK modulation was used.

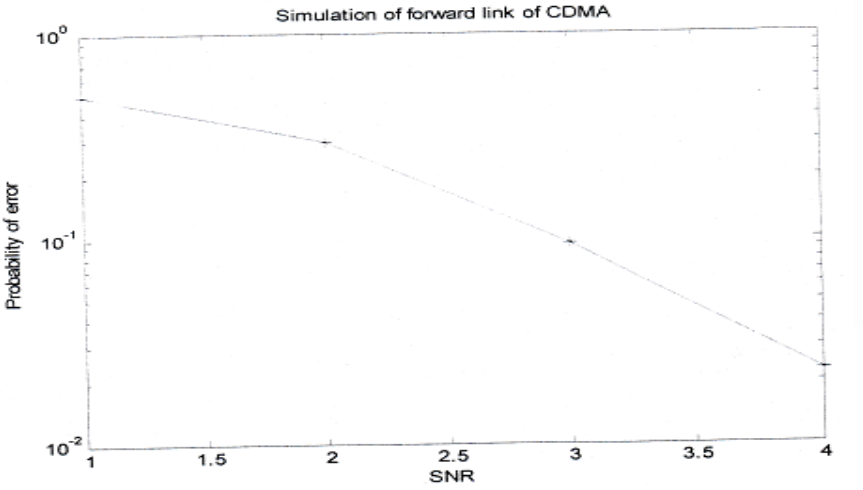

Fig 12. Probability of error vs. SNR obtained from simulation.

5. Conclusion

Turbo code is a powerful coding technique. It works better than convolutional code. It is achieved near Shannon capacity. However, there are many factors need to be considered in the Turbo code design. They are Tradeoff between BER and the number of iterations, effect of frame size on the BER and code rate.

For future work, other types of interleaver can be used to improve the performance. Reducing decoding delay time is another interesting topic. Trellis code can be used in the forward link of CDMA.

References

[1] G. Berrou, A. Glavieuc and P. Thitmajshima, "Near Shannon limit error correcting Coding: Turbo Codes, "in proc.1993. pp.1064-1070.

[2] Vijay K. Garg, "IS-95 CDMA and CDMA 2000", India.

[3] T.S. Rapport, "Wireless Communications Principles and Practice", New Jersey, Prentice- Hall, 1996.

[4] M.C. Valenti and J. Sun, "The UMTS Turbo Code and an efficient decoder Implementation suitable for software-defined radios," International journal of wireless information networks, October 2001, vol.8.

[5] M. Herald, R.L. Gouable, J-F Helard, and J.-Y. Baudais, "Multicarrier CDMA techniques for future wideband wireless networks", Annales des telecommunications, vol.56, (2001), pp.260-274.

[6] Mohanad Babiker, Othman Omran Khalifa, Aisha Hassan Abdullah Hashim, Momoh J.E. Salami and Muhammed Zaharadeen Ahmed, "Performance of Turbo Code in CDMA under AWGN Channel", International journal of Future Generation Communication and Networking vol.10, No.5, pp.19-28, 2017.

[7] M. Raja Murali Krishna, M. Tata Ahish, Ch. Bhuveneswari, H. Vinod, "Performance Analysis of Turbo Codes in CDMA Under AWGN and Fading", IOSR Journal of Electronics and Communication Engineering, vol.9, pp. 46-55, 2014.

[8] G.H. Nortan and S.S.H.Wijayasuriya, "New properties of Convolutional codes and some applications to communication systems, "MTN Networks Pvt.Ltd. Sri Lanka, 1994.

[9] Andrew J. Viterbi, "An Intutive Justification and a simplified Implementation of the MAP decoder for Convolutional Codes," IEE JSAC, Feb. 1998, vol.16, pp255-264.

[10] P.J. Arul Leena Rose, "A study on prevention of Noises in Mobile Communication", International Journal of Advance Engineering and Research Development, vol.5, Issue 02, 2018.

Science Engineering and Technology (SET) Conference - 2021

Part II: AI and Decision Support Systems

Mobile Sales Prediction Using Time Series Analysis

Aakriti Aganja[1], Oshin Gansi[2], Sujata Suwal[3], Jhanak Parajuli[4]

[1]Author, Student, Department of Computer Engineering, Khwopa College of Engineering
Tribhuvan University, Kathmandu, Nepal Email: aganjaaaki@gmail.com

[2]Author, Student, Department of Computer Engineering, Khwopa College of Engineering
Tribhuvan University, Kathmandu, Nepal
Email: os.gansi@gmail.com

[3]Author, Student, Department of Computer Engineering, Khwopa College of Engineering
Tribhuvan University, Kathmandu, Nepal Email:
sujatasuwal644@gmail.com

[3]Supervisor, Lecturer, Department of Computer Engineering, Khwopa College of Engineering
Tribhuvan University, Kathmandu, Nepal
Email: jhanak.parajuli@gmail.com

Abstract

Knowledge about the sales trend and ability to predict the sale of the product keeps the business organizations a step away from the market risks. The accurate sales prediction has the great impact on the success of the business. This paper presents the mobile sales prediction of the African continent using Long Short-Term Memory (LSTM) model, Autoregressive Integrated Moving Average (ARIMA) model and Seasonal Autoregressive Integrated Moving Average (SARIMA) model in time series data. The efficiency of the models used for the prediction is compared in terms of R-Squared value. The obtained R squared values of LSTM, ARIMA and SARIMA are 85.56, 55.34 and 76.61 respectively. The results shows that the LSTM model outperformed the ARIMA and SARIMA model. Additionally, Attention based LSTM networks can be employed for further improvement in accuracy of the sales forecasting model.

Keywords: *ARIMA, SARIMA, LSTM, Sales Forecasting, Time Series*

1. Introduction

In this age of information it won't be wrong to say that data is power and asset of any organization. Using right data with right technique at right time can empower and optimise the organizational performance economically as well as in planning and analysing. A time series is a data set that tracks a sample over time.And time series analysis is the use of the statistical methods to analyse time series data and exact meaningful statistics and characteristics about the data.

A sales analysis report shows the trends that occur in any company's sales volume that may be increasing or declining over time. Sales managers often use the report to identify the market opportunities and the area where improvement must be done. A sales analysis report shows the company's actual sales over a period of time. The seasonal increments in the sales helps the company for additional business during those peak periods.Accurate predictions allow the organization to improve market growth with higher levels of revenue generation. Sales forecasts are essential inputs for various decision-making activities in an organization.

This paper presents the idea of predicting the sales by using scientific methods taking all historical trends and patterns of the transactions into account.

2. Literature Review

The ARIMA model is one of the most widely used techniques for analyzing time series data points or to predict future data points. One research study of [1], Research paper of Ariyo, A.Adewumi, A.O. and Ayo, C.K2014 presented the extensive process of designing time series models for stock price prediction using the ARIMA model.They have used the New York Stock Exchange (NYSE) and Nigeria Stock Exchange (NSE) data for research. The data is composed of four elements, namely: open price, low price, high price, and close price respectively. For research, the closing price was chosen to represent the price of the index to be predicted. The closing price was chosen because it reflects all the activities of the index in a trading day. Analyzing their results revealed that the ARIMA model has short term potential for prediction. As per this study, ARIMA models can compete reasonably well with emerging forecasting techniques in short-term prediction.In the research work [2]]Y. Kaneko and K. Yada ,simple predictive models such as a linear regression model, decision tree, gradient boost tree were used .These models are actually suitable for the
prediction of non - seasonal data

Similarly, in the research work, [3] S. Cheriyan, S. Ibrahim, S. Mohanan, and S. Treesa, social media-based topic analysis and sentiment analysis were combined with a more sophisticated time-series analysis for both feature extractions and predictions. For this ARIMA model was used. Seasonal data are more accurately predicted using the SARIMA model in comparison to other models. Being time dependent and possessing some form of seasonality trends (disparity within particular time frames) makes this different from a regular regression, say, a linear one. Hence, a seasonal ARIMA model is the ideal solution. After constructing the ARIMA model we explore it further to find the best fit using certain criteria and optimize it further. Using this finalized model, we obtain the sales forecast for the desired interval of time. Similarly, in [4] S. P. Shakti, M. K. Hassan, Y. Zhenning, R. D. Caytiles, and I. N. C. SN, ARIMA model was used for the predicting the automobile sales.The
performance of ARIMA is compared with SVM and shows which is better for predicting the temperature within a short time. Also, paper [5] C. Olah, is the most popular RNN (Recurrent Neural Networks) approach and they are networks with loops in them, allowing information to persist. These loops make recurrent neural networks seem kind of strange. A recurrent neural network can be thought of as multiple copies of the same network, each passing a message to a successor.

3.Models Used

3.1. Linear Regression

Linear regression is a basic type of predictive analysis where predictor variables i.e the independent variables are used to predict the dependent variables. It explains the relationship between the dependent

and independent variables. For the data we used, it failed to predict the sales as it could not capture the trend and seasonality of the data.

3.2. LSTM (Long Short-Term Memory)

It is a special kind of recurrent neural network used for sequence modeling. It uses gates to control information flow and cells to store or delete the information as per their importance.

LSTM networks are explicitly designed to overcome the long-term dependency problem as it remembers information for long periods of time.

In this paper, we used an LSTM network with one hidden layer. For the implementation of this model, we aggregated our data at the monthly level and summed up the sales column. To make our forecast easier, we applied some transformations. While training the model, the optimizer used is adam, the loss was calculated using mean squared error and the total number of the epoch was 182. The accuracy of the model was calculated using the basic metrics like R-squared, RMSE, MSE, MAE.

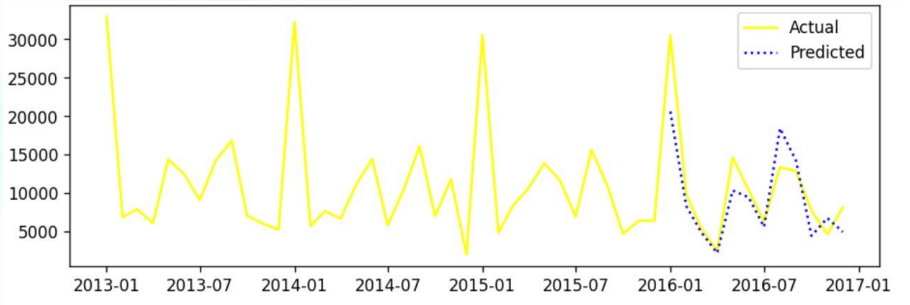

Figure 3.2.1: LSTM forecasting

3.3. ARIMA (Auto Regressive Integrated Moving Average)

It is actually a class of models that explains a given time series based on its own past values, that is, its own lags and the lagged forecast errors, so that equation can be used to forecast future values. An ARIMA model is characterized by 3 terms: p, d, q where, p is the order of the AR term, q is the order of the MA term and d is the number of differencing required to make the time series stationary.

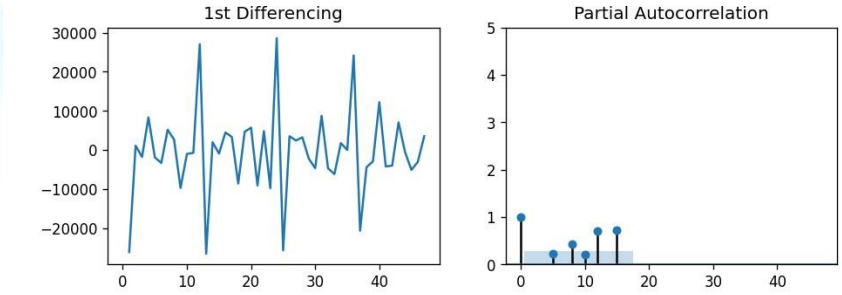

Figure 3.3.1: PACF plot

Here, first the stationarity of the series is checked and if not then it is converted to stationary by differencing. This number of diffencing gives the value of d. Now, the p is obtained from the PACF plot. PACF conveys the pure correlation between a lag and the series which helps to know if that lag is needed in the AR term or not. It is observed that the PACF lag 1 is quite significant since it is well above the significance line. So, the value of p becomes 1.

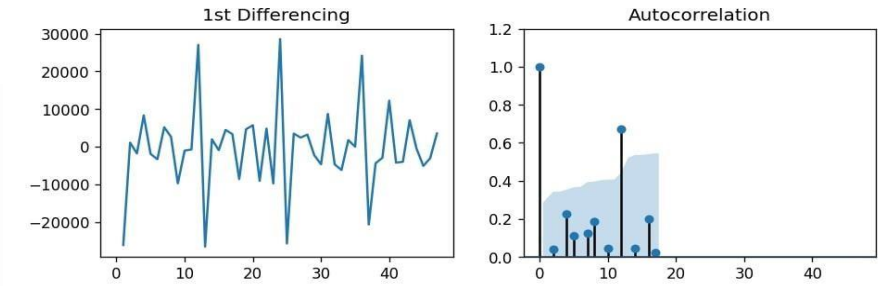

Figure 3.3.2: ACF plot

The value of q is obtained from the ACF plot. The ACF tells how many MA terms are required to remove any autocorrelation in the stationarized series. Using the values of p, d and q ARIMA model is built. By using this model, prediction of the series is done where the training set is used to train the series and testing set is used to test whether the forecasted data is accurate to the actual series or not.

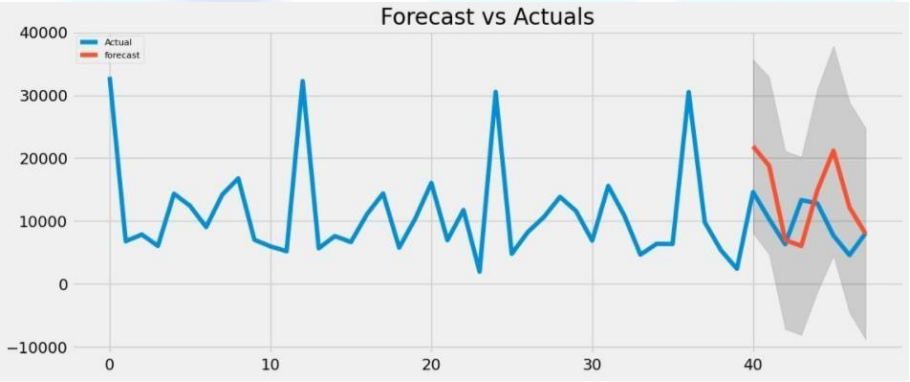

Figure 3.3.3: ARIMA forecasting

3.4. SARIMA (Seasonal Autoregressive Integrated Moving Average)

It is an extension to ARIMA that supports the direct modeling of the seasonal component of the series. It adds three new hyperparameters to specify the autoregression (AR), differencing (I) and moving average (MA) for the seasonal component of the series, as well as an additional parameter for the period of the seasonality. Here, the trend element is calculated as in ARIMA using ACF and PACF plot. But for seasonal elements, it is obtained by the table where the AIC value is least.

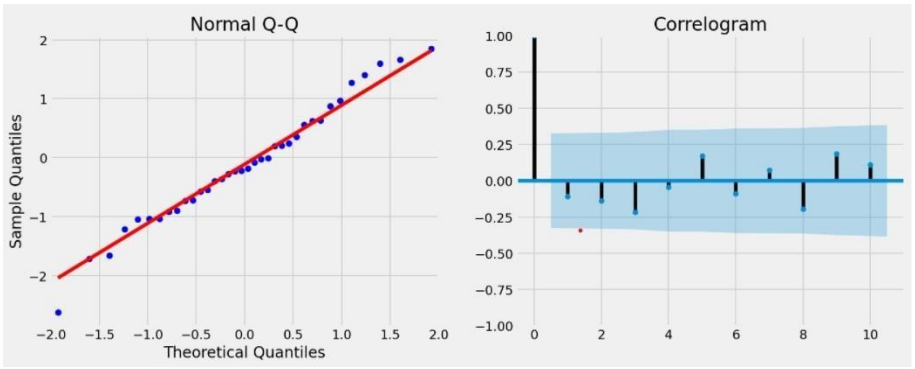

Figure 3.4.1: Model Diagnostics

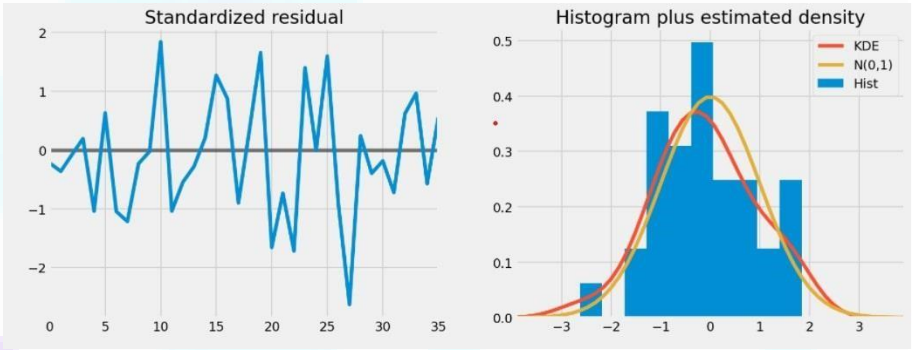

Figure 3.4.2: Model Diagnostics

From the normal Q-Q plot, it can be seen that we almost have a straight line, which suggests no systematic departure from normality. Also, the correlogram on the bottom right suggests that there is no autocorrelation in the residuals, and so they are effectively white noise.

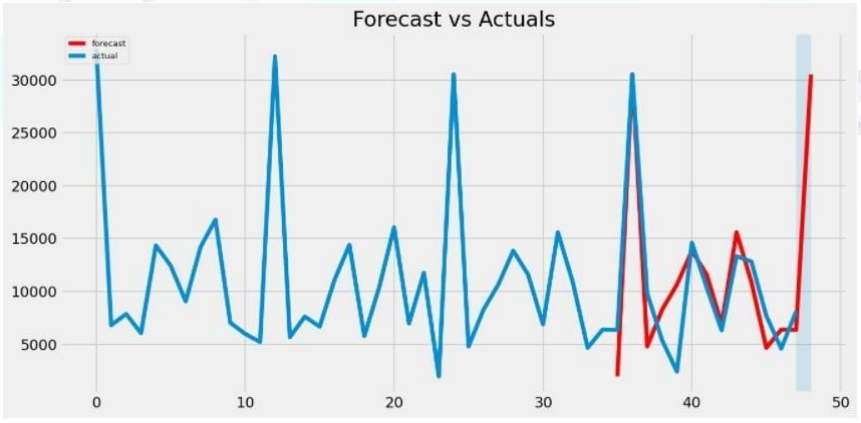

Figure 3.4.3: SARIMA forecasting

4. Comparison

As different models are used to predict the same data of mobile sales, the accuracy of each model is different with each other. All of the models used are also plotted together to show the variety of predictions obtained using respective models.

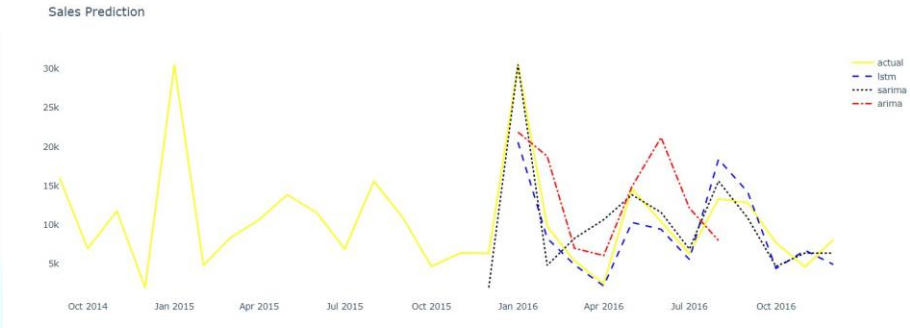

Figure 4.1: Graphical comparison of models

The following table shows the actual sales and the predicted sales from different models.

Table 4.1: Comparison table of actual and predicted sales

Actual Sales	LSTM	ARIMA	SARIMA
30520.06	20586.0		30535.22
9809.85	8271.0		4792.76
5380.60	4868.0		8260.35
2412.08	2153.0		10651.02
14611.95	10297.0	21874.24	13845.18
10344.64	9413.0	18795.94	11582.50
6308.32	5554.0	6983.80	6885.26
13325.11	18393.0	6051.27	15588.65
12816.88	14191.0	14877.19	10867.69
7685.17	4402.0	21191.51	4657.71
4587.75	6708.0	12151.56	6379.50
8097.13	4906.0	7979.25	6349.75

The R-squared value of LSTM is the highest amongst the models used which is 0.8586 and as also seen in the plot, it is the plot which is most accurate to the real data. It means that the forecasting of the sale is almost similar to the actual sale.

The next model used is ARIMA where the R-squared value obtained is 0.5534 which is much lower than LSTM. This change in value can also be seen in the plot where the forecasted data from ARIMA is not much similar to the actual data.

Then comes SARIMA which is the extension of ARIMA or Seasonal ARIMA. The R-squared value obtained is 0.76611 which is higher than ARIMA but lower than LSTM.

Here the R-squared value of SARIMA is greater than ARIMA because four seasonal elements are added.The accuracy of the models is shown in table below:

Model Used	Accuracy
LSTM	85.87%
ARIMA	55.34%
SARIMA	76.61%

Table 4.2: Accuracy table of model

5. Conclusion

ARIMA and SARIMA generated a consistent model when there was a strong seasonal pattern in the data, whereas the LSTM model was able to identify the type of seasonality in the data and decompose the time series based on the type of seasonality and accurately predict it for a given dataset. When comparing the statistical models and neural network, seasonal data is better handled by LSTM model than ARIMA and SARIMA, which suggests that LSTM was able to predict data with a strong pattern.While comparing the R squared for every model for given dataset, it has been observed that the performance of statistical methods differ from Recurrent Neural Network (RNN) method because RNN method is more suitable than statistical models in predicting the sales.

References

[1] A. A. Ariyo, A. O. Adewumi, and C. K. Ayo, "Stock price prediction using the arima model," in 2014 UKSim-AMSS 16th International Conference on Computer Modelling and Simulation. IEEE, 2014, pp. 106–112.

[2] Y. Kaneko and K. Yada, "A deep learning approach for the prediction of retail store sales," in2016 IEEE 16th International Conference on Data Mining Workshops (ICDMW). IEEE, 2016, pp. 531–537.

[3] S. Cheriyan, S. Ibrahim, S. Mohanan, and S. Treesa, "Intelligent sales prediction using machine learning techniques," in 2018 International Conference on Computing, Electronics & Communications Engineering (iCCECE). IEEE,2018, pp. 53–58.

[4] S. P. Shakti, M. K. Hassan, Y. Zhenning, R. D. Caytiles, and I. N. C. SN, "Annual automobile sales prediction using arima model,"International Journal of Hybrid Information Technology , vol. 10, no. 6, pp. 13–22, 2017.

[5] C. Olah, "Understanding lstm networks," 2015.

[6] T. Kim and H. Y. Kim, "Forecasting stock prices with a feature fusion lstm-cnn model using different representations of the same data,"PloS one, vol. 14,no. 2, p. e0212320, 2019.

[7] M. Hiransha, E. A. Gopalakrishnan, V. K. Menon, and K. Soman, "Nse stockmarket prediction using deep-learning models,"Procedia computer science, vol. 132, pp. 1351–1362, 2018.

[8] S. Kohli, G. T. Godwin, and S. Urolagin, "Sales prediction using linear and knn regression," inAdvances in Machine Learning and Computational Intelligence.Springer, 2021, pp. 321–329.

[9] D. C. Montgomery, E. A. Peck, and G. G. Vining,Introduction to linear regression analysis. John Wiley & Sons, 2021.

Science Engineering and Technology (SET) Conference - 2021

Motion Capture using POSENET

Abiral Pokharel [1], Eelisha Pathak [2], Gaurav Regmi [3], Nidwija Bhatta [4], Prof. Dr. Subarna Shakya [5]

[1, 2, 3, 4] *Advanced College of Engineering and Management*

[5] *Pulchowk Campus, Institute of Engineering, Tribhuvan University*

mailto:abiralpokharel001@gmail.com[1], eelisha.pathak@gmail.com[2], grv.damn123@gmail.com[3], nidwizabhatta@gmail.com[4], drss@ioe.edu.np[5]

Abstract

Recovering a 3D full-body human bone rig, which is used to animate a Computer-Generated Image (CGI) model is a challenging problem with many applications although successfully addressed by the motion capture systems with actors with markers worn all over the body with special suit and multiple cameras. In this paper, we detail the bottom-up approach derived from Open Pose, winner of Common Objects in Context (COCO) 2016 KEYPOINTS Challenge, because of its decent quality and robustness of detection of multiple numbers of people in the frame with focus. Proposed network design and optimized post-processing with the full solution of video to 2D conversion run at acceptable speeds. The second part of 2D pose to 3D pose conversion uses a novel Occlusion-Robust Pose-Maps (ORPM) which enables full body pose inference even under strong partial occlusions by other people and objects in the scene. ORPM outputs a fixed number of maps which encodes the 3D joint locations of all people in the scene. Body part associations allow us to infer 3D pose of arbitrary numbers of people without explicit bounding box prediction which increases performance of pose inference. The final combination of the two networks is where a single camera can detect human motion and display the 3D representation in a three-dimensional space in real-time.

Keywords: *Motion Capture, Convolutional Neural Network, Machine Learning, OpenPose, Pose Inference, PoseNet, MobileNet*

1. Introduction

Motion Capture (mo-cap/mocap) is the process of recording the movement of objects or people which is used in military, entertainment, sports, medical, applications, and for validation of computer vision and robotics. In filmmaking and video game development, it refers to recording of human actions using human actors and using that information to animate digital character models already created in 2D or 3D computer animations. When it includes faces and fingers or captures subtle expressions, it is often referred to as performance capture. In many fields, motion capture is sometimes called motion tracking, but in filmmaking and games motion tracking usually refers to match moving. During actual Motion Capture, movements of one or more actors are sampled by times per second, whereas early techniques used images from multiple cameras to calculate 3D positions. Often the purpose of motion capture is to record only the movements of the actors, not his or her visual appearance. This animation data is then mapped to a 3D model so that the model performs the same actions as the actor.

Motion Capture from video feed intends to provide similar output to a motion capture studio. That is to get input of an actor performing different activities and providing an output that will be able to transpose the motion into a 2D model. This transposable output can be implemented as a 3D bone rig which is an

essential part of a 3D model's movement structure. Being able to manipulate bone rigs will make it possible to eradicate the need for a special expensive suit that actors need to wear before performing for a motion capture. It will also eradicate the need for all the expensive equipment required for the motion capture purpose. All this is possible due to implementation of machine learning and artificial intelligence in this field. The software is able to take only a video feed from a camera as live feed or recorded feed and process it to generate a 2D movement rig displayed overlapping on the displaying video and also concurrently convert the 2D rig to 3D representation of the same movement simulating a motion capture. Presently, the use of motion capture is done only with a large budget with complete hardware and an even more complex datasets which is then visualized which is not feasible in the context of Nepal. This paper aims to remove this complexity and provide a simple software solution for simple and cheap motion capture solutions which can be used effectively and in a simpler manner. This research uses a combination of 2D pose estimation and 3D pose estimation of different research combining them to provide best motion capture experience with minimum difference from the motion capture using the expensive hardware solutions. 2D pose estimation is done with the help of convolution neural networks (CNNs). In this paper, an optimized popular method of OpenPose was used for our initial video to 2D pose estimation process. The second phase of 2D to 3D pose conversion uses a newly introduced single shot convolution neural networks (CNN) based method to estimate multi-person 3D pose in general scenes from monocular input. This method is called single shot because it reasons about all people in a scene jointly in a single forward pass and does not require explicit bounding box proposals by a separate algorithm as a preprocessing step. The full convolution method jointly infers 2D and 3D joint locations using newly introduced Occlusion-Robust Pose-Map (ORPM) formulation. ORPM enables multi-person 3D pose estimates under strong occlusions by incorporating redundancy in the encoding, while using a fixed number of outputs regardless of the number of people in the scene. Single person pose estimation, both 2D and 3D, from monocular RGB input is a challenging and widely studied problem in machine vision. It has many applications like activity recognition and content creation for graphical activities. While methods for 2D multi-person pose estimation exist, most 3D pose estimation methods are restricted to a single un-occluded subject. Natural human activities take place with multiple people in cluttered scenes hence exhibiting not only self-occlusions of the body but also strong inter-person occlusions or occlusions by objects. This makes the under-constrained problem of inferring 3D pose (of all subjects) from monocular RGB input even harder and leads to drastic failure of existing single person 3D pose estimation methods. Generally viewing the current motion capture without machine learning and artificial intelligence is an expensive endeavor requiring huge areas for recording studios and very expensive actor gears which is not feasible for many studios and students.

2. Data Collection

The data collection for this paper was done in two phases. First phase was the one converting the images of human subjects into 2D models and displaying the 2D rig. The second phase was the converting of the obtained

2D pose models from the previous phase and converting it into a 3D model rig as well as displaying it in a 3D space. Different data were collected for the two different phases which are described below: The first phase is generally the easier of the two phases as much work had already been done by other research in the field. The data was collected from Microsoft Common Object in Context (MS-COCO) dataset which is a large-scale object detection, segmentation, and captioning dataset. It can be used in object detection, keypoint, panoptic and densePose challenges. Out of all the purposes the dataset was required for keypoint and densePose purposes. The dataset consists of 2,00,000 images of subjects which contains humans and/or other objects and the annotations provided consists of segmentation, bounding box and keypoint coordinates which can be used to train a model to read a video file pick

image from the video frame by frame and feed it into the training phase. The second phase is the complex of the two phases and the data for this model is not as readily available as the 2D pose dataset. The dataset like the Human 3.6M dataset is too big for our purpose and the limitations encountered using this dataset is mentioned in the limitations section. The Multi-Person Dataset described in [1] was used for the purpose of training the second phase of converting the 2D pose data into required 3D pose data. The data was generated by combining in-the-wild multi-person 2D pose data and multi-person multiview motion capture data for 3D annotation would be a straightforward extension of previous (single-person) approaches. Since multi-person 3D motion capture under strong occlusions and interactions is challenging even for commercial systems, often requiring manual pose correction constraining 3D accuracy, the paper [1] employs purely multi-view marker-less motion capture to create the 20 sequences of MuPoTs-3D, the first expressive in-the-wild multi-person 3D pose benchmark. For the much larger training set MuCo-3DHP, [1] resorts to a new compositing and augmentation scheme that leverages the single-person image data of real people to composite an arbitrary number of multi-person interaction images under user control, with 3D pose annotations.

For this result, the initial MS COCO dataset was obtained for video to 3D conversion and processed for the next step described below. The second phase, pre-trained models were used by us which were available freely under non-commercial use for research purposes.

3. Data Preparation

The raw data obtained from MS COCO dataset consisted of 200000 images of objects that can be used for many different purposes like Image Segmentation, Object Detection, Bounding Box generation, Keypoint detection, etc. Out of all these purposes the dataset was required only to generate 2D poses which could be then done with key point detection annotation. Hence, this section describes the process of dataset preparation and cleaning that was performed for the purpose of training the OpenPose model modified to cater to this project.
Initially, the annotation file from MS COCO was available in a json format. To use the obtained data in our model training the json file was read using pandas in python. The image was read using OpenCV. The image was also resized to make all the obtained images to the same resolution for a consistent input for our model. By using pandas, the required key point coordinates, segmentation coordinates and bounding box coordinates were extracted and a csv file was created with the extracted data for our training. The rest of the data was discarded. After creating the csv file, the dataset was divided into training, test and validation sets with 5000 images in the validation set, 40000 images in the test set and the remaining 155000 images in the training set.

After dividing the data, the images were processed, and the images were packed into their respective label data into a numpy array and the three separate numpy files that were generated were normalized and made ready for training. Due to memory limitations of our training machine, the training and test set were further divided into further smaller chunks to prevent high memory usage. The second phase used the pre-trained dataset as mentioned and researched in [1].

4. Training

Like data collection the model training was also divided into two phases. The first phase, as described above, consisted of training of the model to read images and extract 2D pose estimations from the input image. The second phase consisted of training the model to read the 2D pose estimations and generate a 3D pose estimation to simulate motion capture. As described in the previous section, the dataset obtained multiple fractions of data to train the model given below which is the basic OpenPose implementation which is used to generate 2D models from a still image. The training images were fed

into the model and training was performed for 35 epochs with 50 batch size and learning rate of 0.001. The obtained results from the training did not generate effective results so the pretrained OpenPose model called mobilenet was used as a base for extended training. The model was trained with the same processed images in a mobilenet instance not trained in MS COCO dataset for 15 epochs with 50 batch size and variable learning rate ranging from 0.0001 to 0.01 and obtained acceptable results for our video to 2D pose estimation phase with learning rate of 0.005. The OpenPose model also consists of a VGG-19 model embedded inside it which the parameters used for it were available freely for the training use in the model.

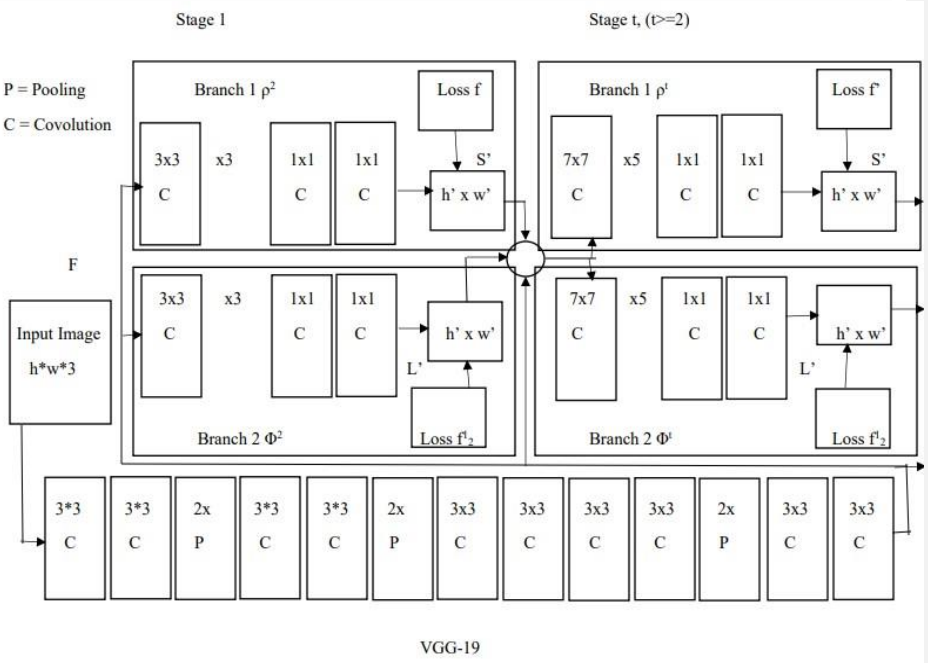

Figure 4.1. OpenPose Model used in paper demonstration

After completing of the first phase, the second phase was promptly started. The training in the second phase consisted of combining both the trained phase in the previous phase to generate a 2D pose and affinity branch that would be used to predict 2D heatmaps and part affinity maps using the Microsoft Common Objects in Context (MS COCO) dataset and the Multi Color 3D Human Poses (MuCo-3DHP) dataset as wasa mentioned in [1]. The training for this phase was carried out using the Caffe framework. The core network's weights were initiated with those trained for 2D pose estimation on MPI and LSP datasets as done in [2]. The core network and the 2D Pose + Affinity branch were trained for multi-person 2D pose estimation using the framework provided by [1]. The researchers of [2] had used the AdaDelta solver, with a momentum of 0.9 and weight decay multiplier of 0.005, and a batch size of 8 and trained for 640000 iterations with a cyclical learning rate ranging from 0.1 to 0.000005. The 3DPose branch was trained with the core network and 2D Pose with the Affinity branch weights frozen. The process defined in [2] used a batch size of 6 and was trained for 360000 iterations with a cyclic learning rate ranging from 0.1 to 0.000001. Better results were led to in the 3D phase training in the 3D pose estimation.

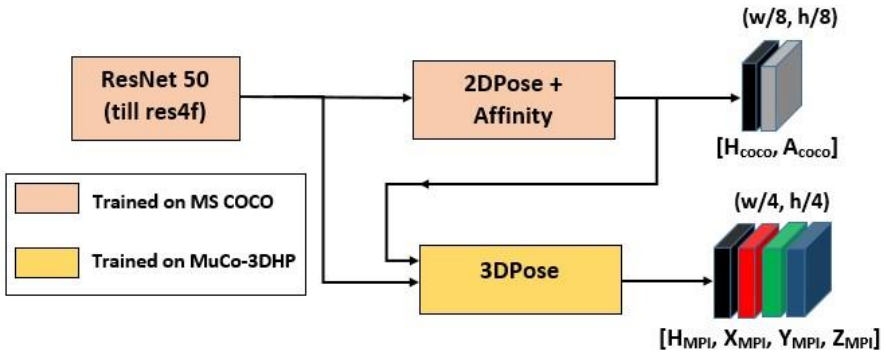

Figure 4.2. Training model for second phase

5. Algorithms and Models

POSENET: When PoseNet processes an image, a heatmap along with offset vectors is returned that can be decoded to find high confidence areas in the image that correspond to pose keypoints. The illustration below captures at a high-level how each of the pose keypoints is associated to one heatmap tensor and an offset vector tensor. Both outputs are 3D tensors with a height and width that we'll refer to as the resolution. The resolution is determined by both the input image size and the output stride according to this formula: Resolution = ((InputImageSize – 1) / OutputStride) + 1

Each heatmap is a 3D tensor of size resolution * resolution * 17, since 17 is the number of keypoints detected by PoseNet. For example, with an image size of 225 and output stride of 16, this would be 15*15*17. Each slice in the third dimension (of 17) corresponds to the heatmap for a specific keypoint. Each position in that heatmap has a confidence score, which is the probability that a part of that keypoint type exists in that position. It can be thought of as the original image being broken up into a 15*15 grid, where the heatmap scores provide a classification of how likely each keypoint exists in each square grid. Each offset vector is a 3D tensor if size resolution * resolution * 34, where 34 is the number of keypoints*2. With an image size of 225 and output stride of 16, this would be 15*15*34. Since heatmaps approximate where the keypoints are, the offset vectors correspond in location to the heatmap points and are used to predict the exact location of the keypoints as by travelling along the corresponding heatmap point. The first 17 slices of the offset vector contain the x-axis of the vector and the last 17 slices contain the y-axis of the vector. The offset vector sizes are in the same scale as the original image.

POSE INFERENCE IN 3D: Read-out of 3D pose of multiple people from ORPMs starts with inference of 2D joint locations and joint detection confidences for each person in the image. Explicit 2D join-to-person association is done with the predicted heatmaps and part affinity fields using the approach described in [1]. Next the 2D joint locations and joint detection confidences in conjunction with Occlusion Robust Pose Maps to infer the 3D pose of all persons in the scene. By virtue of Occlusion Robust Pose Maps, we can read out 3D joint locations at select multiple pixel locations as described above. The extremity joints are defined: the wrists, the ankles, and the head. The neck and pelvis 2D detections are usually reliable, these joints are most often not occluded and lie in the middle of the body. Therefore, the algorithm starts reading the full pose at the neck location. If the neck is invalid, then the

full pose is read at the pelvis instead. If both joints are invalid, then it is considered the subject is not visible in the scene and the prediction is stopped.

6. Block Diagram

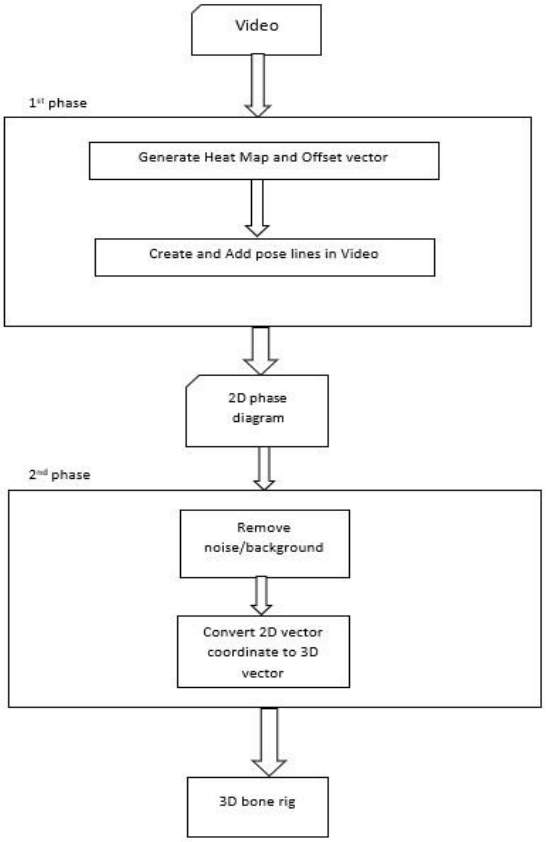

Figure 6.1: Block Diagram

7. Result and Analysis

The output was obtained in a 3D canvas programmed manually and was viewable through normal viewport. The viewport was able to be rotated through to be able to show a 3D spatial environment where the generated 3D pose models were placed.

For the analysis phase, each phase was separate into its own analysis for proper output study. In the initial phase, mobilenet, which is defined in OpenPose in OpenCV library, was used to train our model. Currently training the model up to certain number of convolutional networks have had different varying results which is shown in the table:

Number of Conv Layers trained	Accuracy, %	GFLOPs
Mobilenet_v1 up to 4	37.9	23.3
Mobilenet_v1 up to 5	42.8	27.7
Mobilenet_v1 up to 6	43.2	31.3
Mobilenet_v2 up to 6	39.6	27.2

Table 7.1: Accuracy table First Phase

Here the accuracy was determined by how close the predicted joints were to the actual joint data and each of the 17 joints' accuracy were simply averaged to obtain the required accuracy. The GFLOPs (Giga Floating Operations) is the measure of complexity of the model which was obtained from OpenCV as described in [2].

For the next phase of converting the 2D data into 3D coordinates, the analysis computations are given below: The test in this phase was done on the Human3.6M dataset as explained in the paper in [1].

Poses	Eat	Greet	Phone	Pose	Sit	Wait	Walk	Average
Model Accuracy	61.2	65.7	75.82	62.2	82	65.1	57.6	69.9

Table 7.2: Accuracy table Second Phase

8. Conclusion

Motion Capture is the process of recording the movement of objects or people which is used in military, entertainment, sports, medical applications, and for validation of computer vision and robotics. The process of implementing machine learning and artificial intelligence to be able to take a video feed from a single camera input and process it to generate a 3D projection in a 3D space was researched in this paper. The end results were satisfactory with good test results and accuracy which are shown in the table above.

References

[1] Daniil Osokin. Real-time 2D Multi-Person Pose Estimation on CPU: Lightweight OpenPose. Intel. 2018.

[2] D. Mehta, H. Rhodin, D. Casas, P. Fua, O. Sotnychenko, W. Xu, and C. Theobalt. Monocular 3d human pose estimation in the wild using improved cnn supervision. In 3D Vision (3DV), 2017 Fifth International Conference on, 2017.Han, K. (1993). A study of acetic acid formation in Escherichia coli fermentation.

Pathfinding Algorithm Analyzer and Visualizer

Sankalpa Pokhrel[1], Shashank Kafle[2], Shubham Tamrakar[3] Sulav Bahadur Pradhan[4], Raisha Shrestha[5]

Advanced College of Engineering and Management, Tribhuvan University, Kupondole, Nepal
saankalpaa@gmail.com[1], shashank.kafle0@gmail.com[2], tamrakarshubham23@gmail.com[3], sulavpradhan03@gmail.com[4], raisha.shrestha95@gmail.com[5]

Abstract

Pathfinding is the search for an optimal path from a start location to a goal location in a given environment. Pathfinding algorithms are typically designed as a kind of graph search which are applicable in a wide variety of applications such as computer games, robotics, networks, navigation systems, delivery services, automated guided vehicles and so on. This study implements four different pathfinding algorithms: A, Dijkstra's, Breadth first search (BFS), Depth first search (DFS) and compares their efficiency. It has two parts: (i) analyzer (ii) visualizer where the first part sorts the algorithms considering various performance metrics: elapsed time, shortest path length and number of nodes visited. Likewise, the second part visualizes these algorithms on different scenarios of obstacles in a 2D grid. The Walls and maze functionality used in the study, allows the generation of numerous random search scenarios for efficient testing of the algorithms. Pathfinding on one of the randomly generated scenarios showed DFS as the fastest algorithm with the longest path length. Whereas, A* had the shortest path length with the least number of visited nodes. BFS could also find the shortest path; however, the number of visited nodes was the highest. Similarly, Dijkstra had the shortest path but it took maximum time for the search. The comparison and analysis of results from this study helps to choose a suitable search algorithm depending on the scenario. The visualization of the path finding algorithms may be useful in the learning process as the visited nodes and the shortest path are visually represented on the grid.*

Keywords: *Analyzer, Visualizer, A*, Dijkstra's, Breadth first search (BFS), Depth first search (DFS)*

1. Introduction

1.1 Background Theory

Path finding theory describes a process of finding a path between two points in a certain environment. In most cases the goal is to find the specific shortest path, which would be optimal, i.e., the shortest, or the cheapest. Criteria such as, a path, which emulates path chosen by a person, a path, that requires the lowest resource, or a path from point A to point B through point C is often found relevant in many path finding tasks. The shortest path problem is a pressing issue in many fields, like navigation systems, artificial intelligence, computer simulations and games.

Although all of these fields have their own specific algorithms, there are many general-purpose path finding algorithms which can be successfully applied. Hence our web application helps in comparing the algorithms and gives us an idea which algorithm is efficient for certain paths. The main advantage of this application is that we can visualize different algorithms and it shows the difference between different path finding algorithms visually.

1.2 Problem Statement

Manually finding the path between two points in a complex system is difficult and tedious. Even if we manage to find a path the found path may not be the shortest or the most efficient. It is not always clear what advantages certain algorithm has in comparison to its alternative.

1.3 Scope of Project

This is a web-based application that determines the optimal path for a system using one or more path finding algorithms, graphically represents them and also compares them to find an optimal algorithm for a given scenario.

1.4 Applications

This web application will help the users visualize and compare different path finding algorithms. This can be used in teaching students about path finding algorithms and their differences. This can also be used in various delivery related applications like food delivery and ecommerce.

2. Objective

The objective of this project is to develop a web application that can:

- visualize and compare which of the selected algorithm is the best for the given situation.

3. Materials

The evolution of computer technology has seen various implementation and use of computers widely. Such changes have made computers faster, efficient, accurate and consistent. This has resulted in us humans depending upon the computer much more than before. Problems are mostly solved using computers in the 21st century. Complex calculations, tracing, transactions etc. and many time consuming and tedious tasks have become easier to deal with because of computers. Path finding is also one of the tasks that has become simpler to understand due to advancement in computing world. Over the years, path finding algorithms have received increasing attention in many applications such as video games, robotics, metabolic pathways, augmented reality, and global positioning system. Path finding algorithm addressed the question in the discovery of the shortest route between two positions and avoided obstacles Path finding is a broadly applied algorithm that involves the discovery of routes between two positions by avoiding obstacles at the same time. As a part of this project path finding algorithms A*, Dijkstra's algorithm, BFS

and DFS were implemented to analyze their efficiency in an environment based on a 2D grid. Such factors as traverse node count, execution time and distance travelled are taken into consideration.

Path finding Algorithm Efficiency Analysis in 2D Grid is a system that implemented certain path finding algorithms to analyze their efficiency theoretically. This paper aims to discuss common challenges faced by path finding in video games and providing future trends for optimization. (Rēzeknes Augstskola, Rēzekne, RA Izdevniecība, 2013).

Path finding visualizer that implemented various algorithms to visualize the nodes visited and shortest path for the situation given by the user. User can specify the start and end nodes, add weighted nodes and add various walls manually or select certain patterns generated by the system. (Clément Mihailescu, 2016).

Daniel Shiffman created a system that implemented the A* path finding algorithm to find the optimal path between two points in a 2D grid. The algorithm is written in JavaScript using the p5.js library for rendering. The user has no control over the location of the start and end points and also the obstacles as the walls are generated randomly.

4. Methods

Various pathfinding algorithms were implemented using React JS. The time taken, memory consumed and the shortest path given by each algorithm and was compared to find the best algorithm for each condition.

Firstly, we created the grid array which was mapped using row and column nodes. Then Dijkstra's algorithm was implemented to check if the algorithm runs in the grid. After we implemented the walls and different levels of obstacles we started the animation process for the visualization of the algorithm. The settimeout () function was used to ensure some delay during visualizing process making it easier for the user to visualize and understand how the algorithm works. After we visualized Dijkstra's algorithm we then followed it by adding three more algorithms namely Breadth First Search, Depth first Search and A* algorithm. For the visualization of these algorithms we used the same approach as Dijkstra's algorithm.

With this, the visualization part of the project was completed then we moved on to the analysis part of our project. For this part we used some performance parameters of the algorithms such as no. of visited nodes, shortest path length, time taken for the algorithm to find the shortest path and space consumed by the algorithm while finding the shortest path. To show the user which algorithm was efficient for the given condition these performance parameters were displayed in the table.

As our project is front end based, we decided to use CSS and React JS as it allows us to create reusable UI components in our project.

5. Results

Table 5.1 Analysis of different algorithms in level 1 using 25 different cases

Algorithm	Time taken (ms)	Shortest path length	Number of visited nodes
A*	1.507021	23	47
DFS	1.594	256	640
BFS	2.093	23	601
Dijkstra's	43.664439	23	565

Table 5.2: Analysis of different algorithms in level 2 using 25 different cases

Algorithm	Time taken (ms)	Shortest path length	Number of visited nodes
A*	1.2567	24	53
DFS	1.30411	227	559
BFS	1.7755	24	535
Dijkstra's	40.1934	24	507

Table 5.3: Analysis of different algorithms in level 3 using 25 different cases

sAlgorithm	Time taken (ms)	Shortest path length	Number of visited nodes
A*	1.568	31	109
DFS	0.6958	144	350
BFS	1.049	31	423
Dijkstra's	33.77	31	409

From the graphs below, we can clearly see that A star is most efficient in most of the cases as its elapsed time is the least compared to other algorithms and it occupies less memory compared to others as it visits a smaller number of nodes.

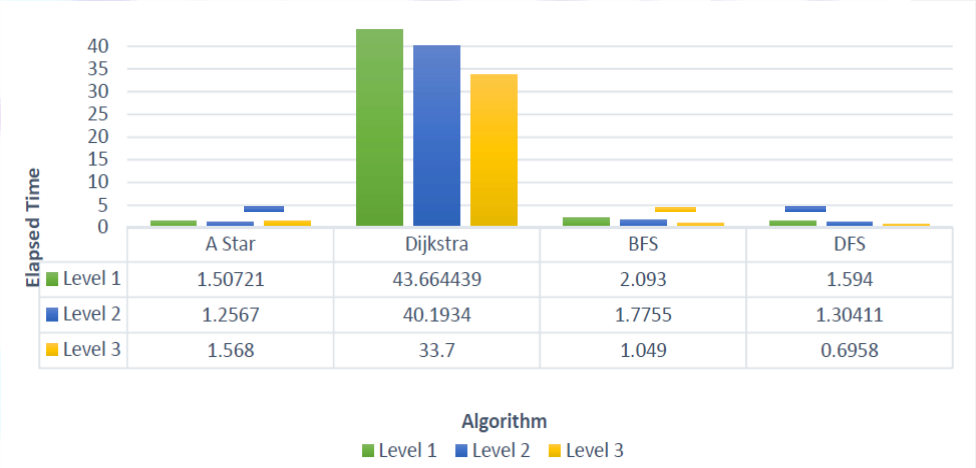

Figure 5.1. Time taken by algorithms when implemented on different level of obstacles

Although DFS takes short time to find the path to the end point compared to some algorithms like Dijktra and breadth-first search but it doesn't guarantee the shortest path and occupies more space as shown by the graph below.

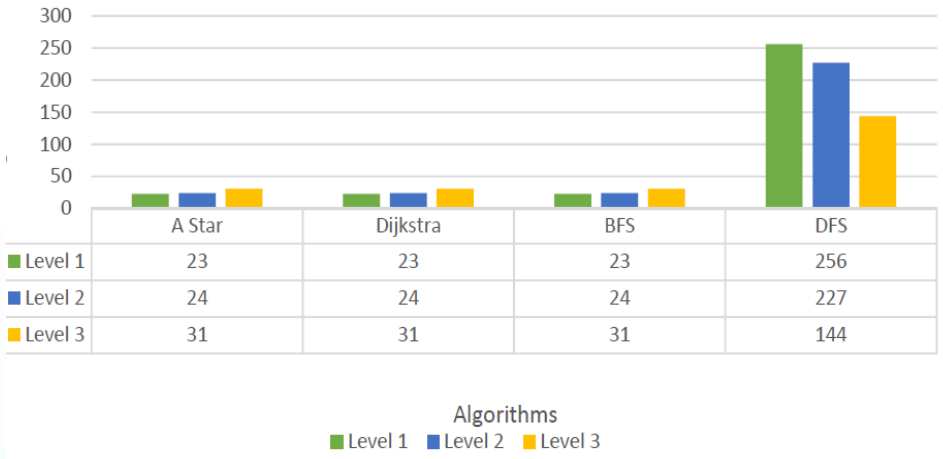

Figure 5.2. Shortest path length taken by algorithms to reach finish node when implemented on different level of obstacles

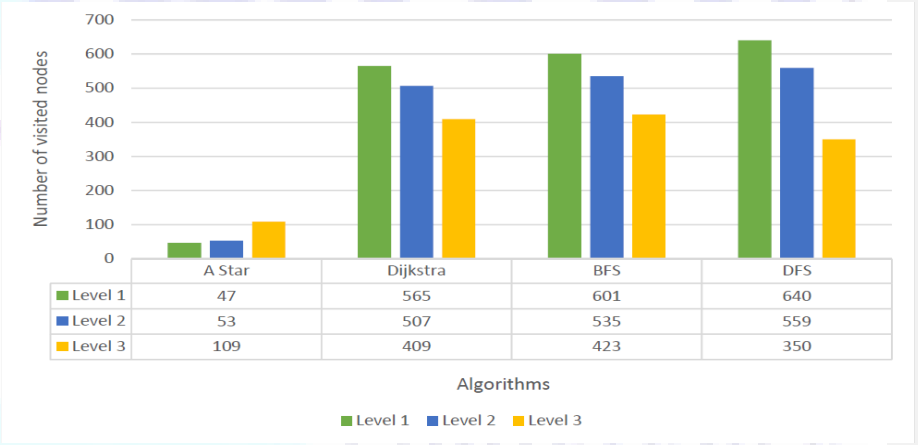

Figure 5.3. Number of nodes visited by algorithms to reach finish node when implemented on different level of obstacle

6. Discussion and Conclusion

Pathfinding algorithm analyzer and visualizer gives the visual representation of the working of different algorithms on different levels of obstacles and their analysis based on the parameters like elapsed time, shortest path length and numbers of nodes visited and shows which algorithms performs best or is the most efficient. Most applications that visualize pathfinding algorithms do

not show the comparison data. Our application overcomes this by providing the analysis along with visualization and also gives the comparison data in a table.

7. Acknowledgements

We would like to express our heartfelt gratitude to IOE and Department of Computer Engineering of Advanced College of Engineering and Management for providing us such a great opportunity to undertake this project. We express our sincere gratitude to the Head of Computer department, Er. Ajaya Shrestha, Deputy Head of computer department, Er. Ram Sapkota for his indispensable guidance and support to harness our skills.

Also, we are grateful to our faculty teachers Er. Abcon Budhathoki and Er. Bikash Acharya for their direct or indirect involvement in our project and for their constant motivation and suggestions. Finally, we would like to thank our college, ACEM for providing us this platform to implement what we have learned so far.

References

[1] “Dijkstra's Shortest Path Algorithm.” https://brilliant.org/wiki/dijkstras-short-path-finder.

[2] “A* Search.” https://brilliant.org/wiki/a-star-search.

[3] “Depth-First Search (DFS).” October 11, 2020 https://brilliant.org/wiki/depth-first-search-bfs.

[4] Kapi, Azyan “A Review on Informed Search Algorithms for Video Games Pathfinding" https://www.researchgate.net/publication/342714871_A_Review_on_Informed_Search_Algorithms_for_Video_Games_Pathfinding.

[5] "CSS" https://en.wikipedia.org/wiki/CSS.

[6] "HTML" https://en.wikipedia.org/wiki/HTML.

[7] "Microsoft Visual Studio" https://en.wikipedia.org/wiki/HTML.

[8] "JavaScript" https://en.wikipedia.org/wiki/JavaScript.

[9] "JavaScript" https://www.geeksforgeeks.org/introduction-to-javascript.

[10] "React" https://en.wikipedia.org/wiki/React.

[11] "React.js (Introduction and Working)" https://www.geeksforgeeks.org/react-js-introductionworking.

[12] "Node.js" https://en.wikipedia.org/wiki/Node.js.

[13] “Breadth-First Search (BFS).” https://brilliant.org/wiki/breadth-first-search-bfs.

Science Engineering and Technology (SET) Conference - 2021

Realistic Rendering System Using GAN

Rajiv Ranjan Sah[1], Sailesh Kafle[2], Sagar Timalsina[3], Ukesh Thapa[4], Sujata Dahal[5]

[1,2,3,4]*Students of Department of Electronics and Computer Engineering, Advanced College of Engineering and Management, Kupondole, Lalitpur*

[5]*Lecturer at Department of Electronics and Computer Engineering Advanced College of Engineering and Management, Kupondole, Lalitpur*

f9rajiv@gmail.com, saileshkafle47@gmail.com[2], timalsinasagar2@gmail.com[3], yukeshthapa8@gmail.com[4], sujata.dahal@acem.edu.np[5]

Abstract

Even though technology has advanced, the realistic rendering of computer images has remained manual in today's society. Movies have progressed from the primitive black-and-white film era to the contemporary digital age as science and technology have advanced. There is a lengthy procedure that must be followed to bring the old movies back in life with a colorful and realistic approach. The only possible way is to use a post-processing software which is highly time consuming and requires great skills, patience, and aesthetics from the operator. In recent years, the extensive use of machine learning and neural networks has made it possible for computers to intelligently process images. In our research work, we attempt to use the generative adversarial networks principle to process pictures and videos to realize the automatic rendering of old films and pictures. Our system basically realizes the re-color rendering of black and white video frames, and the rendering results are more reasonable, furthermore, the color configuration confirms to people's normal aesthetic standard.

Keywords: *Generative Adversarial Networks; Deep Learning; Convolutional Neural Network; Image recoloring*

1. Introduction

With the increasing sophistication of computer graphics since the 1970s, Rendering or image synthesis has become a more distinct subject in the graphics pipeline, giving models and animation their final appearance. Rendering is basically the process of generating a photorealistic or non-photorealistic image from a 2D or 3D model by means of a computer program. However, rendering old films and pictures is not quite easy and requires teams to rely on post-processing software that take a lot of labor costs. The re-rendering of old documentary movies often causes the special effects team to spend months or even years to complete.

Although, in recent years, the extensive use of machine learning and neural networks has made it possible for computers to intelligently process images. Our system adopts generative adversarial networks models and combines with the video processing function to realize the classic black-and-white movie or the automatic coloring of the photos, and solves the problem that requires a lot of human

interaction in the current dyeing process. A generative adversarial network (GAN) [1] is a class of machine learning frameworks designed by Ian Goodfellow and his colleagues in 2014.Since 2014, the development of GAN has been in full swing, and related achievements have continued to emerge. The basic principle behind GAN is that two neural networks contest with each other in a game to create or generate variations in the data. In our research work, we attempt to use this network to make a realistic rendering system for old pictures and videos.

In the last few years, especially thanks to the recent advancements in the field of Deep Learning [10], Machine Learning has drawn a lot of attention. One of the main driving factors of the machine learning hype is related to the fact that it offers a unified framework for introducing intelligent decision-making into many domains. That's the main motivating factor in choosing our research work. Especially, the machine learning framework that our research work is based on is fairly new. As it was only introduced in 2014, there hasn't been much work and deployment of the GAN in the real world, most of which is still in the research phase. Our research work not only helps to render old footage and pictures but give a new perspective of design to the engineer's artists and sculptures too.

The ability of a model to process images has been gradually investigated in recent years. The expressive potential of colorless video can be substantially enhanced by image colorization. In terms of film coloring, post-production teams in various countries must rely on post-processing tools such as PR (Adobe Premiere), AE (Adobe After Effects), and AE (Adobe After Effects) (Adobe After Effects) and DaVinci Resolve. The rerendering of old documentary films might take months or even years for the special effects team to finish. Our system uses generative adversarial networks models in combination with OpenCV's [14] video processing function to create a classic black-and-white movie or automatic photo coloring, and it tackles the problem of the present dying process requiring a lot of human input.

The main objectives of the research work is to generate realistic rendered images and videos. Our research and study are mostly focused on automating the rendering of images and films. Until date, these works have relied on post-production technologies such as Adobe Premiere, Adobe After Effects, and DaVinci Resolve.

These software's necessitate highly trained operators and incur significant labor costs. Our research work contributes to the solution of such issue. In addition, users will gain a unique viewpoint on automatic rendering. Our research work also contributes to the advancement of previous research on the generative adversarial networks by bringing fresh GAN-implemented work into the real world.

2. Literature Review

The automatic rendering of images and videos using machine learning frameworks is a relatively new field of research. Image synthesis is an important problem in computer vision. There has been remarkable progress in this direction with the emergence of Generative Adversarial Networks. GANs have achieved great success in various image generation tasks, including image-to-image translation, image super resolution and text-to image synthesis.

A generative adversarial network is a class of machine learning frameworks designed by Ian Goodfellow and his colleagues in 2014. In 2017, a GAN was used for image enhancement focusing on realistic textures rather than pixel-accuracy, producing a higher image quality at high magnification. In 2017, the first faces were generated. These were exhibited in February 2018 at the Grand Palais. Faces generated by Style GAN [16] in 2019 drew comparisons with deep fakes.

Colorization Using Convnet [17] and GAN is done by Standford student which is similar work as realistic rendering system using GAN. This system was able to predict the color to the greyscale image where they have used the manga. Enhancing photorealism [18] enhancement by Stephan R. Richter, Hassan Abu Alhaija and Vladlen koltun which was released in 2020. This system was able to render the video from the GTA-V.

In our research work we use the Generative Adversarial Network (GAN) which allows attention-driven, longrange dependency modeling for image generation tasks. During the research phase of our research work, we studied various articles about GAN and took reference from the research paper of Yongcheng Cui,
Wenyong Wang titled “Colorless Video Rendering System” [5].

3. Methodology

The paper proposes the system to render the images and videos using Generative Adversarial Network (GAN). The system has been developed in three stages: Dataset Preparation, Image Pre-processing, Generative Adversarial Network Architecture, Compiling and Training GAN.

3.1 Dataset Preparation

We have used COCO dataset as dataset for the model to be trained in the variety of images in order to make system more versatile in prediction of the color of image. COCO is a database organized according to the WordNet hierarchy, where each node of the hierarchy is depicted by hundreds to thousands of images. It contains:

Training set: 14,000 pictures,

Validation set: 2,000 Pictures,

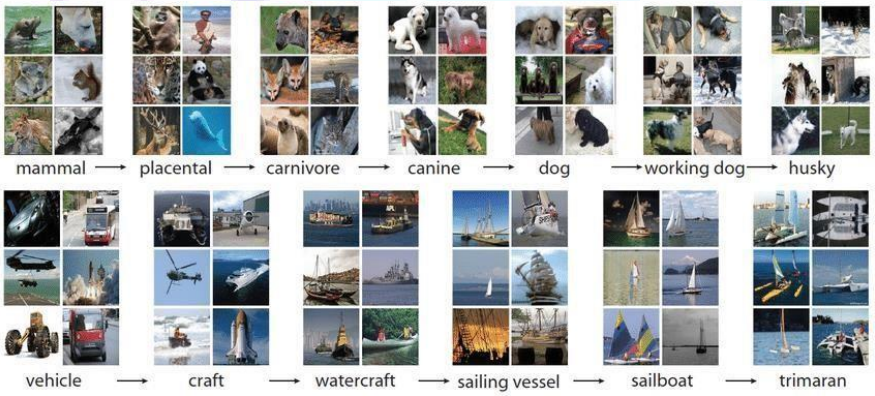

Figure 1. COCO Dataset

3.2 Image Pre-processing

The dataset should be processed before feeding it into the neural network. We resized images to uniform (256 x 256) resolution provided by Pytorch [15]. Resizing is necessary for translation of images to images any size image input to the system.

We have translated images from RBG (red green blue) color values to LAB colors values. Unlike RBG, which merges red, blue and green color values to create the color image, LAB consists of a light sensitivity channel and two-color channels. The L channel contains information for the light sensitivity of a photo and is equivalent to a black and white version. A and B are the color channels where A controls the green-red tradeoff and B controls the blue-yellow tradeoff.

When using L*a*b, we can give the L channel to model (which is the greyscale image) and want it to predict the other two channels and after its prediction, we concatenate all the channels and we get our colorful image.

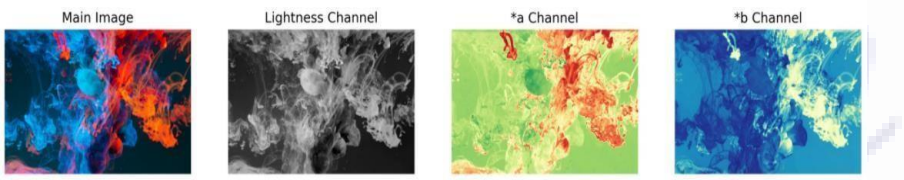

Figure 2. LAB color channels

3.3 Generative Adversarial Network Architecture

GAN are generative models that learn a mapping from random noise vector z to output image y, G: $z \rightarrow y$. In contrast, conditional GANs learn a mapping from observed image x and random noise vector z, to
y, G: $\{x, z\} \rightarrow y$. The generator G is trained produce outputs that cannot be distinguished from 'real' images by an adversarial trained discriminator, D, which is trained to do as well as detecting 'Fake' image by generator. Building neural network was a great challenge because in GAN we have two different type of neural network which are playing the game of the adversarial game to dominate one another so special consideration was done while building each neural network. Otherwise, prediction of color won't be as accepted from the generator and it may lead to the instability in training the two neural networks.

3.3.1 Generator Network

In this network we have used U-Net[6] as generator for system. The generator model takes a grayscale image (1-channel image) and produces a 2-channel image. In U-Net we have add down-sampling and upsampling modules to the left and right of that middle module at every iteration until it reaches the input module and output module. It is going 8 layers down, so if the inputs start with (256X256) image, in the middle of the U-Net we got (1X1) images and then it was up-sampled to produce a (256X256) image.

In model, we have used 8 different (64X64) filters, 2 strides, (4x4) kernel size and padding were set to 1 with no bias. In down convolutions we have used leakyReLU which negative slope is set to **0.2** and Batch Normalization are used for stabilization of the layers. In up convolution we have used ReLu as activation and Batch Normalization.

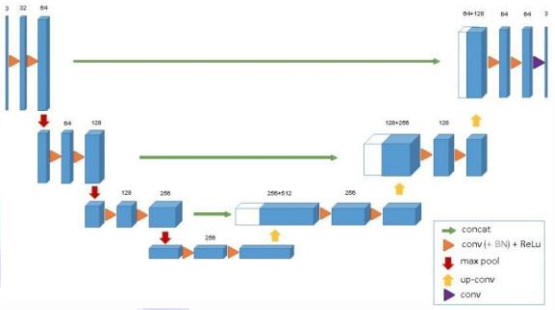

Figure 3. U-NET Architecture

3.3.2 Discriminator Network

We have used convolutional 'PatchGAN'[6] classifier in the discriminator. In a patch discriminator, it only penalizes structure at the scales of patches. This discriminator tries to classify if each N x N patch in an image is real or fake. We run this discriminator convolutionally across the image, averaging all responses to provide the ultimate output of discriminator. We have designed this model by stacking blocks of ConvBatch-NormLeakyReLU.

The model's output shape is (30x30) but it does not mean that patches are (30x30). The actual patch size is obtained when you compute the receptive field of each of these 900 output numbers which in our case will be (70x70).

3.3.3 ReLU Activation

Rectified Linear Unit (ReLU) rectifies the linearities in the non-linear images. Relu boots up the training process so as to converge to accurate predictions. The graphical representation of ReLU in figure below demonstrates how the linearity is removed from the image. The negative values are pruned by the rectifier function and only the non-linear details are preserved.

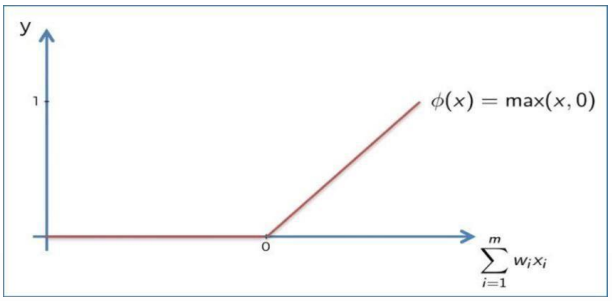

Figure 4. Relu Activation function

3.3.4 Leaky ReLU Activation

Leaky Rectified Linear unit or Leaky ReLU, is a type of activation function based on ReLU, but it has a small slope for negative values instead of a flat slope. This type of activation function is popular in tasks where we may suffer from sparse gradients.

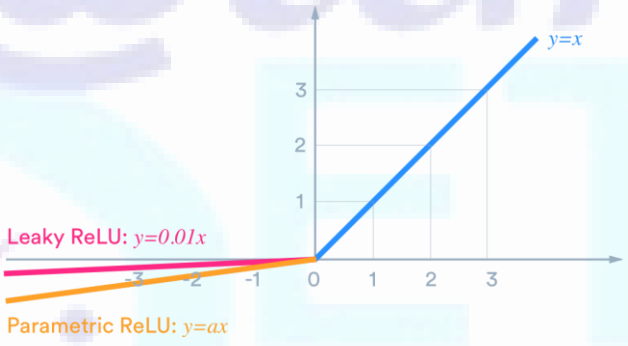

Figure 5. Leaky ReLU Activation Function

3.4 Compiling and Training CNN

The compilation of the GAN architecture is done designating the following parameters:

3.4.1 Loss Function

The greyscale image which both generator and discriminator see is the condition that we have provide to both models in our GAN and expect that they take this condition consideration.

$$L_{cGAN}(G, D) = \sum_{x,y}[logD((x, y)] + \sum_{x,z}[\log(1 - D(x, G(x, z)))] \qquad (i)$$

Here, x is considered as greyscale image, z as the input noise for the generator, and y as the 2-channel output we want from the generator. G is the generator model and D is the discriminator. The loss for conditional GAN shown in above equation.

The above loss function helps to produce good-looking colorful images that seem real, but to further help the model we have introduced L1 loss or mean absolute error of the predicted colors compared with the actual colors.

$$L_{L1}(G) = \sum_{x,y,z} [\|y - G(x,z)\|_1] \qquad (ii)$$

As only with the use of L1 loss alone leads the model to be conservative though it will colorize the images and most of the time uses colors like 'gray' or 'brown' because when it doubts which color is the best, it takes the average and uses these colors to reduce the L1 loss as much as possible. So, we have used L1 loss over L2 loss or mean squared error because it reduces that effect of producing gray images. So, the combine loss function will be:

$$G = \arg\, min_G\, max_D\, L_{cGAN}(G, D) + \lambda L_{L1}(G) \qquad (iii)$$

Where λ is a coefficient to balance the contribution of the two losses to the final loss.

3.4.2 Optimizer

We experimented with our system on adam, adagrad and adadelta optimizers. Adam optimizer had big time complexity in our system. Furthermore, in adagrad continuous decay of the learning rates throughout the training process was a major problem. Adadelta adapts the learning rate dynamically using only the first order information. So, we used adadelta optimizer which is the adaptive leaming rate method surpassing adam and adagrad optimizer.

4. Experiments and Results

We experimented with our model by using different numbers of hidden nodes.

4.1 Experiment with different number of hidden nodes

The number of hidden nodes is to be computed from the experiments. We took 5 sets of hidden nodes with 200, 400 and 700 nodes, running for 40 epochs. The loss decreased with an increase in the number of hidden nodes. There was no huge difference in using 200 and 700 number nodes, so we decided to take 700 number of hidden nodes for our neural network design. The results are demonstrated in the following chart.

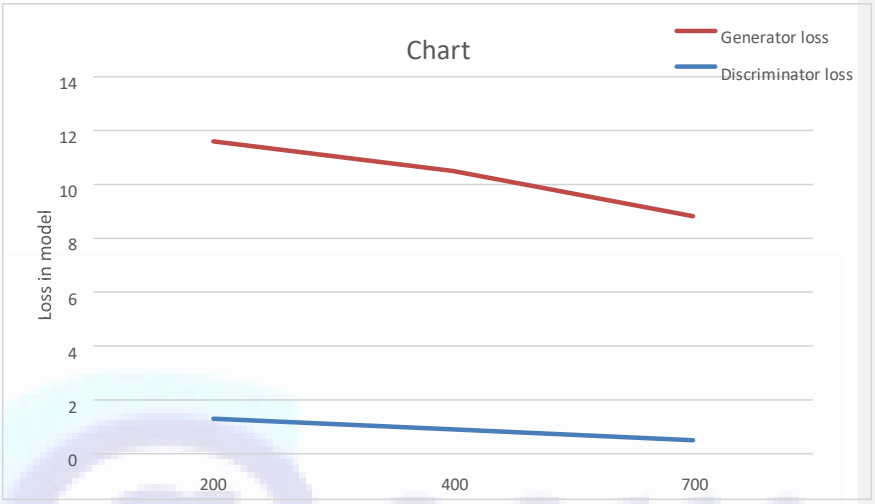

Chart 1. Change in loss with increasing number of hidden nodes

4.2 Output

After the model generation, we tested our system for the 2 different videos . In the scenario, the videos rendered were almost correct (fig 6) i.e. the GAN model rendered the video. The frames of the videos are shown below.

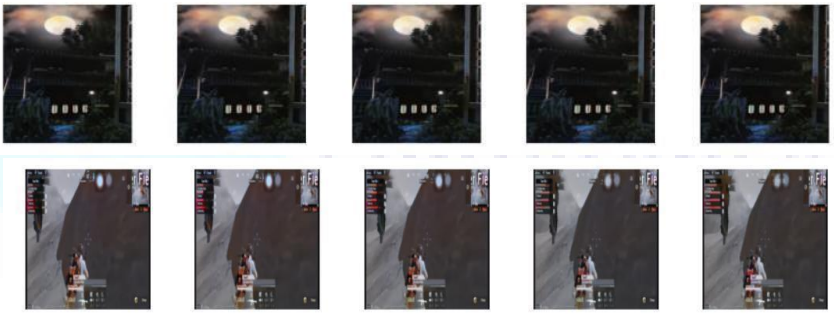

Figure 6. Rendering frames

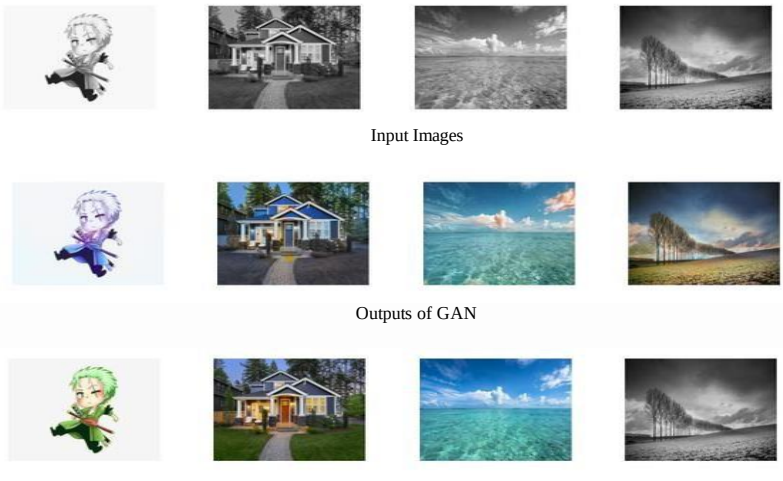

Figure 7. Rendering of Grayscale Images on Test Set

Fig 6 and Fig 7 shows some sample results from the test set of the task of colorizing grayscale images and videos frame. It is noticeable that quality of the images generated by GAN is even brighter than the ground truth image.

Fig 7 shows some sample results from the test set of the task of colorizing edge-only images. With less input information, the generated images, which are blurry, are inferior to those from the grayscale images.

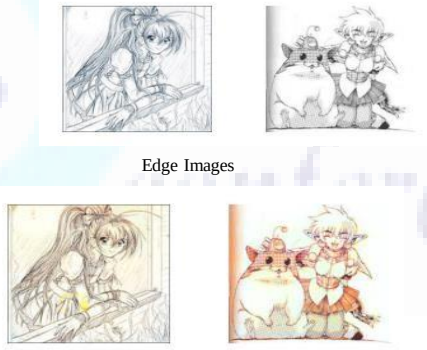

Figure 8. Rendering of Edge Images on Test Set

To evaluate the performance of our models quantitatively, we calculate the average L1 and L2 distance (per pixel-channel) between the generated images and the ground truth images on our test set. The results are shown in Table 1. Two observations can be made from the table: 1) GAN model generates

images closer to ground truth in both L1 and L2 distance metrics. 2) For both models, using grayscale images as input yields lower distance differences than using edge-only images as input. This is not surprising because grayscale images contain more information than edge-only images.

Table 1. Average L1 & L2 distance between the generated images on test set and ground truth images

Distance	Grayscale	Edge
L1	41.25	83.22
L2	947.29	4720.77

5. Conclusion

The results show that the system basically realizes the re-color rendering of black and white video frames, and the rendering results are more reasonable, furthermore, the color configuration confirms to people's normal aesthetic standard. The synthesized video frame provides a more sufficient information and has better viewing quality. Moreover, the coloring of black-and-white documentaries decades ago restored the world scene before the color camera Invented. From this point of view, the experiment has further academic research values.

However, this experiment still has shortcoming. For example: if the video frames are in same scene, the rendering depth is different and still some part of the object in frames are not able to colorized, it's due to dataset we have trained is less. In addition, the color stability of the generated video is also related to the resolution and sharpness of the image data, so this experiments still needs further research. The final model of our system still ensued some inaccurate results. This inaccuracy can be improved by adjusting the different parameters like using the high resolution and sharp images as inputs to the model, training for higher number of epochs i.e., beyond 100 and increasing the dataset i.e., using imagenet dataset.

We recommend the following future research activities to direct our research work implementation using the emerging Rectified Adam Optimizer (RAdam), implementation of self-attention layer to the model, research to encompass different other field like rendering 3D model of houses, city, machines for engineers, rendering on the virtual reality, augmented reality etc.

References

[1] J. Goodfellow, J. Pouget-Abadie, M. Mirza, B. Xu, D. Warde-Farley, S. Ozair (2014). Generative adversarial nets.

[2] Spectral Normalization For Generative Adversarial Networks. https://arxiv.org/pdf /1802.05957v1.pdf [3] Photo-Realistic Single Image Super-Resolution Using a Generative Adversarial Network. https://arxiv.org/abs/1609.04802

[4] Deep Multi-Scale Video Prediction Beyond Mean Square Error. https://arxiv.org/pdf /1511.05440.pdf [5] Y. Cui and W. Wang (2019). Colorless Video Rendering System via Generative Adversarial Networks. IEEE International Conference on Artificial Intelligence and Computer Applications (ICAICA), 2019, pp 464-467, doi: 10.1109/ICAICA.2019.8873434.

[6] Olaf Ronneberger, Philipp Fischer, and Thomas Brox (2015). U-Net: Convolutional Networks for Biomedical Image Segmentation.

[7] H Zhang., I. Goodfellow, D. Metaxas and A. Odena (2018). Self-Attention Generative Adversarial Networks.

[8] Bengio, Y. (2009). Learning Deep Architectures for AI. Foundations and Trends® in Machine Learning, *2*(1), 1-127 .

[9] Chollet, F. (2017). Deep Learning with Python. Manning Publications.

[10] Courville, I. G. (2016). Deep Learning. MIT Press. Retrieved from http://www.deeplearningbook.org.

[11] Jha, G. (2019). Artificial Neural Networks and Its Applications.

[12] Keiron Teilo O'Shea, R. N. (2015). An Introduction to Convolutional Neural Networks. ArXiv eprints.

[13] Li Deng, D. Y. (2014). Deep Learning: Methods and Applications. Foundations and Trends® in Signal Processing, 7(3-4), 197 - 387. doi:10.1561/2000000039

[14] Culjak, D. Abram, T. Pribanic, H. Dzapo and M. Cifrek (2012). A brief introduction to OpenCV.2012 Proceedings of the 35th International Convention MIPRO, 2012, pp. 17251730.I. Culjak, D. Abram, T. Pribanic, H. Dzapo and M. Cifrek, "A brief introduction to OpenCV," 2012 Proceedings of the 35th International Convention MIPRO, 2012, pp. 17251730

[15] Pytorch. https://pytorch.org/docs/stable/index.html

[16] Tero Karras, Samuli Laine, Timo Aila(2018). A Style-Based Generator Architecture for Generative Adversarial Networks

[17] Colorization Using ConvNet and GAN. http://cs231n.stanford.edu/reports/2017/pdfs/302.pdf [18] Enhancing photorealism enhancement. http://vladlen.info/papers/EPE.pdf

Part III: Software Engineering

Research on the role of app localization in Universal Usability and its implementation in eSewa app with UI enhancement using Donald Norman's design principles

Sarayu Gautam[1], Sailesh Dahal[2], Ashish Subedi[3]

[123] *Department of Computer Science and Engineering, Kathmandu University, Dhulikhel, Nepal*

sarayugautam1@gmail.com[1], saileshbro@gmail.com[2], ashishsubedi10@gmail.com[3]

Abstract

The role of localization and implementation of design principles in the universal usability of mobile applications is undeniable. This research paper aims to consolidate previous statement through analysis of UI of e-Sewa mobile app based on HCI principles and by implementing localization on its prototype. The major objective of our research was to enhance the usability of the contemporary Nepali application (eSewa). The primary HCI principles and tools used in the implementation of our research are Donald Norman's design principles, survey, Prototype, User-Persona, Ethnography, Schneiderman's Eight Golden Rules, Heuristic evaluation, and Cognitive walkthrough. After the post-survey of the developed application, it was found that all demographic groups felt comfortable using the localized version of eSewa compared to the original one. Also, the use of design principles while designing UIs immensely improved the experience of using applications by the users. A flutter application demonstrating the UI of eSewa was developed based on usability techniques and implementation of localization in Nepali language.

Commented [U1]: need to put result(s) clearly. comparative study with other published papers

Keywords: *Human-Computer Interaction, Localization, eSewa, Universal Usability, Mobile Application, Design Principles*

1. Introduction

The older generation Nepalese sometimes struggle to use mobile applications, even mobile phones, and such technological devices in general. In delving deeper into the reason behind this struggle, apart from lack of technical knowledge, we found that the language barrier is the main problem. Most of the elders are more comfortable in talking and using the Nepali language than English but most of the applications and websites are mainly present only in the English language. In researching more about this topic, we found that this is a universal problem, and mobile applications, as well as websites and web apps all over the world, are localizing their products to include all demography to use their applications with ease. Now the unlocalized product is a major hindrance to the continued growth of your brand, and avoiding this entirely would eventually, cause your application to stagnate. It would be wonderful if users across the world can access an application without the limitation of this barrier. And no doubt, localization of applications is key to solve this problem.

This conclusion was not satisfactory. We wanted to explore how much impact localization makes on

the universal usability of an application. Does localization is the ultimate answer to usability problems or does the user experience need to be enhanced using design principles? Following these queries, we conducted this research and took a popular existing application eSewa [1] to localize it in the Nepali language and enhance its UI based on design principles.

A literature review was conducted as the research progressed. A paper concluded that differences can occur as a result of cultural differences related to different cultural user groups, with differing groups potentially reacting differently to unlocalized commands [2]. The next paper dealt with the project - localization of a visual programming environment in bidirectional languages [3]. Localization of that application increased the user base by 10 folds which were targeted to children having different native languages which demonstrated the huge role that localization plays in universal usability and HCI. Facebook has gained its massive user base due to its availability in multiple languages and has shown the importance of language in HCI [4]. Wikipedia is provided in both local as well as international languages which have helped people across the globe to easily access the information [5]. As a demonstration project, we decided to translate a current application in Nepali similar to what Hamro Patro [6] and Khalti [7] applications had done.

The hypothesis of our research postulated that implementation of localization and design principles in an application increases the number of people using that app, which in turn increases the marketing, popularity and induces more people to use the app. We approached this hypothesis by implementing both localization as well as design principles in the eSewa application UI that we developed. We used usability metrics to ensure our application adhered to the concept of universal usability. Also, we used Donald Norman's design principles [8] and Schneiderman's 8 golden rules [9] of UI design during our design process and later on evaluated it with multiple evaluation techniques like heuristic evaluation and cognitive walkthrough. The result obtained is a flutter application to depict the localized and redesigned eSewa UI. By creating the user persona and conducting ethnographic observation on our target audience, we tested the developed UI. Multiple surveys were conducted during the development phase as well as post-development. Through all these evaluations, analyses, and survey it was found that most users were comfortable with the localized version of the application, and also incorporating design principles in the UI design greatly improved their experience. The conclusion we deduced from this research is that localization plays a great role in universal usability (although we have only implemented the app in the Nepali language for now) and using design principles to design the UI of the application greatly improves its user experience.

The result that we wanted to obtain was a redesigned and localized eSewa UI which solved the barrier of language between the application and all the demographics who use it and provide the users with the best user experience while using the application.

2. Methods and materials

The result that we wanted to obtain was a redesigned and localized eSewa UI which solved the barrier of language between the application and all the demographics who use it and provide the users with the best user experience while using the application.

2.1. Survey

For achieving this result, first of all, brainstorming was needed to prepare the pre-development survey questions. This survey was conducted to know about the satisfaction of eSewa applications with the users in the current scenario and to validate our problem statement. We prepared the survey questions in English. The purpose of our research needed to include every age group of the target audience since the target audience using any sort of application ranges from very young to even old age groups. We were alerted by the result of the survey as most of the users attending the form belonged to the age group of 21-30.

The distribution of people filling the survey was unequal which was later concluded to be due to the language barrier. While English is easily understandable by young age groups, older age groups have a difficult time grasping every word written in English although they might know how to use an app (in this case filling the survey form). Although we wanted to include responses from different countries, we lacked resources to translate the form into different languages. Hence, we decided to translate the form into the Nepali language to see whether there will be any changes in the response. And we did see the change. There was participation from almost every age group including the older ages.

2.2. Digital Prototype and its Survey

Revamping the UI of e-Sewa dealt with color combinations and visual factors. Hence, we used a digital prototype in contrast to a paper prototype. The prototype tool was needed as a visual representation of what we are trying to achieve with eSewa. We have implemented Donald Norman's 6 design principles and Schneiderman's 8 golden rules while constructing our prototype and have reflected the same thing through UI.

Figure 1. Prototype sample of eSewa homepage

The survey of our prototype was conducted on tech-savvy eSewa users having enough knowledge of design principles so that they could separate bad design changes from good ones and provide constructive feedback on how we can improve. Nearly three-quarters of people filling the survey agreed to eSewa being available in Nepal as a good step towards the usability of this application. And though more than three-quarters of responders were satisfied with the current UX of eSewa, when we presented them with our improved prototype that incorporated design

principles, almost all of them agreed that the prototype version of UI was better in terms of usability.

2.3. User Persona

The ideal user of an eSewa application is anyone who wants to have a utility application carry out most of the monetary transactions without having to be physically present to pay the bills. This mostly includes teenagers, young adults, adults, and early old age people.

The general behavior pattern exhibited by current users are:

- Financially responsible
- Understanding of time value of money
- Good time management skills
- Performs frequent monetary transactions

The ideal user of an eSewa application is anyone who wants to have a utility application carry out most of the monetary transactions without having to be physically present to pay the bills. This mostly includes teenagers, young adults, adults, and early old age people. One of the issues they faced within given context was that no localization feature was present causing majority of target audience to stop using the application. The users were oblivious to multiple features provided by e-Sewa which were not properly accessible. Also, the UI/UX of contemporary utility applications did not address the need of people.

2.4. Ethnography

The observed user was a male of age 60. He was not able to utilize all the features provided by the current eSewa application like load /transfer and sending money with ease along with other minor functions. He could not find the option to buy the movie ticket through the application which we had suggested he do before observation. He wanted to pay his utility bills which, as he mostly used eSewa for that purpose, were conducted with ease. Although he admitted at a short interview after the observation that it had taken quite a while for him to figure the feature when he had just started using the application. He admitted that he wanted the application to be in the Nepali language.

2.5. UI design using Flutter and Localization in Nepali

After designing and finalizing our prototype, we moved on to the UI development part. We used flutter which is a front-end framework for building an android application to mimic the eSewa UI containing localization and design enhancements. We were able to demonstrate most of the major pages where design principles were applied. We translated the English strings into Nepali through google translate and used them as localized strings. The localization we performed in a static localization where dynamic contents are not changed.

2.6. Donald Norman's 6 design principles

From Norman's principle, considering the visibility, we decided to change the current vertical scrolling to a horizontal one.

Then for consistency, we focused on having consistent button size, spacing, color, and font throughout the app.

Including intuitive iconography and most importantly, integrating the localization feature, we tried to enhance the affordance of the eSewa application.

Figure 2. Consistency in button size, contrast between background and button to enhance visibility

The circular progress indicator, shimmer, and ripple effect in the button act as the feedback in the UI of e-Sewa that we developed.

To ensure the constraint principle, we added * signs for the required field in the form. Form validation techniques were also included. The users cannot go inside and use the application without agreeing to the terms and conditions.

2.7. Schneiderman's Eight Golden Rules

Using Schneiderman's golden rules. For offering informative feedback, we used toasts for success and error messages.

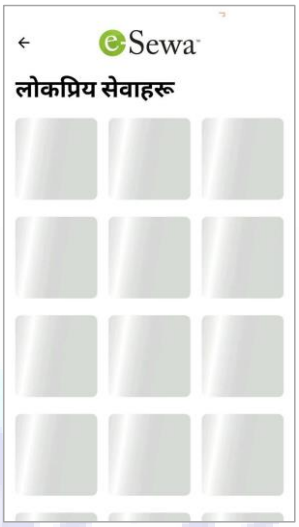

Figure 3. Shimmer effect as feedback of content loading

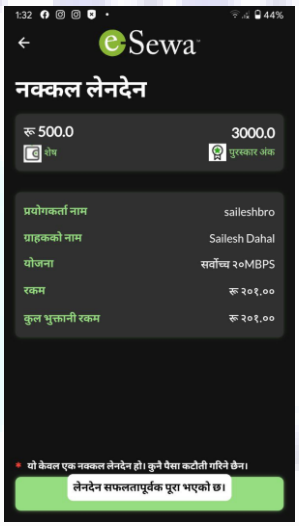

Figure 4. Feedback on successful transaction

Also, we integrated form validation techniques to offer simple error handling. In UI, we designed a timer-based transaction cancellation feature to permit an easy reversal of action.

To support the internal locus of control, we included theme changing and localization features which is the major part of our project.

Figure 5. Settings page for theme changing, localization, and much more

Figure 6. Transaction cancellation feature after clicking on start transaction

Figure 7. Theme changing feature

To reduce the short-term memory load, a stepwise guidance feature is provided.

2.8. UI design survey

The UI design was followed by a survey on the developed APK. We sent this APK to the same people who had filled our prototype survey.

We requested the respondents to install it on their device, check it out, and fill the form with their honest review. Almost all the respondents were frequent users of eSewa which made it more effective to work on their review.

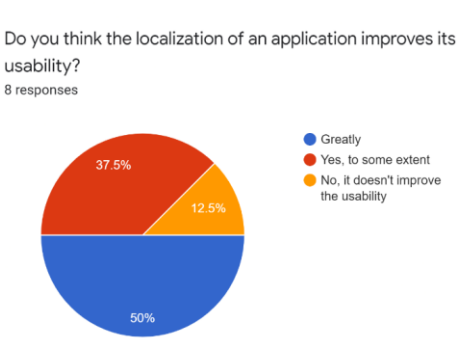

Figure 8. Usability of the application after localizing

More than three-fourths of the respondents agreed that localization made it easy to understand the instructions provided in the application. They also confirmed that localization in Nepali was a

necessary step in including a wider population to use the eSewa application.

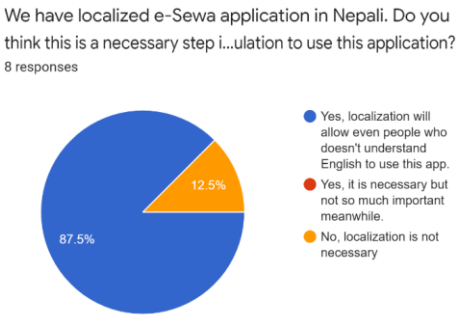

Figure 9. Positive response on the localization of eSewa

2.9. Heuristic Evaluation

Finally, after analyzing the feedback from the prototype and developing UI following the design principles, we requested Mr. Mala Deep Upadhaya to conduct a Heuristic evaluation based on Jacob Neilson's heuristics [10], considering him as an expert, and conclusions were thoroughly documented.

2.10. Cognitive Walkthrough

After Heuristic Evaluation, we performed Cognitive Walkthrough in the UI application that we developed considering the task of paying for a movie ticket of QFX cinemas. We chose this task because we had found it was hard for novice users to find and perform this transaction.

Commented [U2]: rewrite and rearrange needed

3. Findings

3.1. Findings from the survey

From the two surveys taken to justify our problem statement, we concluded that the participants from the first survey are not concerned about the presence of localization in an application mostly because they are comfortable and are well versed in the English language.

Most of them wanted only some of the apps they use to be available in their native language and other significant groups say that it doesn't impact them. We can somehow conclude from the data that there is no noteworthy opposition to the use of localization in apps.

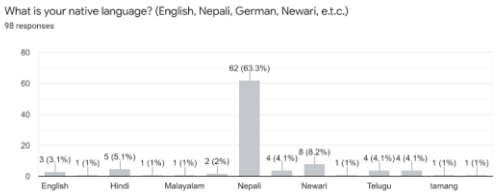

Figure 10. Graph showing Nepali language as the most used language for communication in Nepal

Participants from the second survey would like to use applications available in their native language. And both surveyors agree that applications available in different languages are easy to use.

The participants of both survey groups are positive that governmental applications, as well as utility applications, should be available in different languages to facilitate every user who uses them.

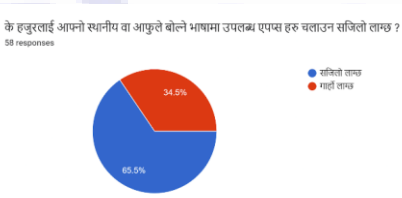

Figure 11. Chart showing the preference of people to use apple in their native language

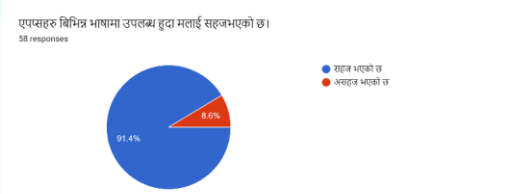

Figure 12. Chart showing that localization makes use of apps easier for most of the population

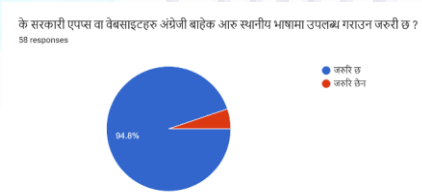

Figure 13. Chart showing that most people prefer using governmental and utility applications in their native language

Though some contrast can be found on surveys about each user, everyone agrees with the fact that localization makes use of applications easier, and localized applications can reach a wide audience. From this survey, it can be inferred that some people found it difficult to use applications available in the native language. Even this problem can be addressed by including localization features in the app.

From the prototype survey, we had included images of the prototype where we had maintained consistency in button size, images, and typography. More than half of the respondents agreed that the prototype version was better than the original eSewa UI where consistency wasn't given priority.

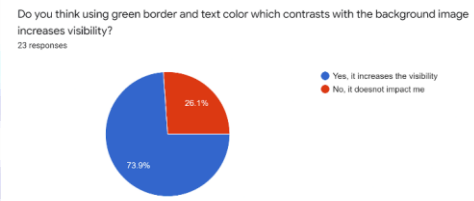

Figure 14. Chart showing that visibility has been improved in the prototype by contrasting background image and button

All of the respondents agreed that compared to the original eSewa UI where the submit button was kept on the top right of the screen, the prototype version having the same button on the bottom right was more user-friendly.

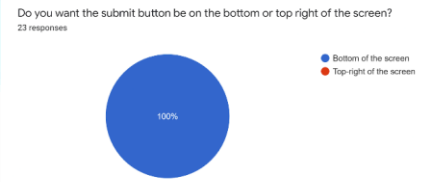

Figure 15. Chart displaying full agreement on the placement of submit button on the bottom right of the screen to reduce thumb movement

More than three-fourths of respondents conceded that the prototype version of the Login and Sign-up pages is more consistent than that of the original version.

The same number of respondents admitted that layouts in the prototype have a clear distinction between clickable and non-clickable components compared to the original one.

Also, more than half of the respondents preferred the prototype version of the Home Page of the eSewa application and also agreed to the prototype version as being a better way of showing that there is a provision of cashback feature (considering the spacing).

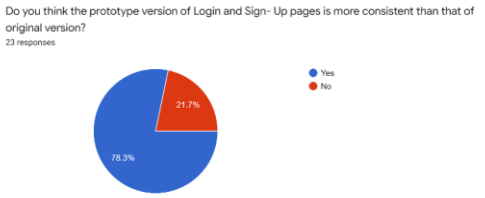

Figure 16. Chart showing the preference of people to prototype version compared to original eSewa UI considering the consistency

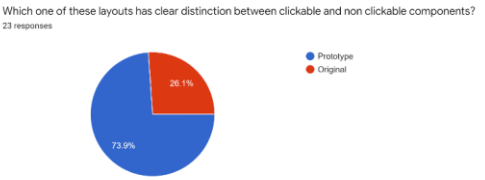

Figure 17. Chart showing the preference of people to prototype version compared to original eSewa UI considering the clear distinction between CTAs

The responses were extremely helpful as they shaped our final thoughts on building UI and also guided us on real user needs.

3.2. Findings from Heuristic Evaluation

Every feature that this app provides is present on its front page and bottom navigation bar so that users don't have a hard time knowing about the current status of the system.

As eSewa is a dynamic app that involves monetary transactions, by using a cashback system and reward points, the match between the system and the real world is made. Also, there is the inclusion of intuitive iconography for referencing various characteristics.

Figure 18. Cashback is displayed as a bubble to reduce extra spaces

On eSewa UI, the User control and freedom metric are assured by providing quick navigation at the bottom of the page so that users can go back to the user control state from where they come from. Users can also access any feature of this app after signing up. They can communicate with the content by loading, receiving, transferring, and paying cash whenever they want to.

For all pages, eSewa has a consistent style. Also, this role is enhanced in UI by maintaining consistency across the app in button size, spacing, color, and font.

Through the use of validation techniques in the form, the Error prevention analysis criterion is met. E.g., a 10-digit number must be entered in the form field of the phone number. In the form, there are also * signs added for the required field. For content that is limited to being selected from the given choice, there are also dropdown menus kept in place.

After visiting eSewa more than once, it is a little bit harder to recognize where a particular feature is, for instance buying a movie ticket.

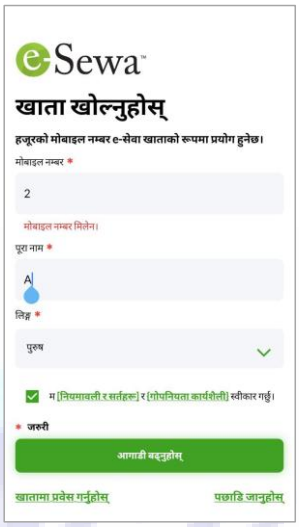

Figure 19. eSewa signup page using form validation and * for required field

Users need to scroll for quite an amount of time before reaching some features and this is a tedious job for memory. So, all major features have been incorporated in the front page of the application which can be accessed without scrolling to reduce the cognitive load.

Figure 20. Horizontal scroll for minimizing scroll and enhancing visibility

eSewa has a flexible UI because it enables its users to follow any track they want when visiting the app without limiting them to one specific path. Each consumer can now easily benefit from the features offered by eSewa, whether they are comfortable in the Nepali or English language, as the localization feature has been introduced.

Figure 21. Implementation of localization feature

The design of eSewa UI, for the most part, is minimalistic. The arrangement of text and font sizes is also aesthetic. The design is plain and elegant, matching this application's function as a digital wallet.

3.3. Findings from Cognitive Walkthrough

To get to the movie payment option in our enhanced eSewa UI, firstly users will have to log in to get inside the application. Before getting to the login there are onboarding pages that provide summarized guidelines on what the app is about. After login, the first instinctive way is to explore the home page and hence we have integrated all important features in this page. The user will firstly search in the top services section and then on other services sections. They will horizontally scroll through other services sections and search for the movies option. When they don't find it there, they will move to all categories and with one horizontal swipe, they will see the movies section. When clicked it will lead to all the cinemas that offer online ticket services. Like this, the user will try and achieve the right outcome through minimal steps compared to the original UI of eSewa where the user had to vertically scroll and check for every category before moving on to the next once before finally reaching the movies section.

After conducting this walkthrough, it was concluded that the user noticed correct action is available to them and associate the correct action with the outcome they expected to achieve. Also, they realized that if the correct action is performed, they can see that progress is being made towards their intended outcome.

4. Discussion

Commented [U3]: rewrite and rearrange needed

4.1. Discussion on the market value of localization

The concept of localization has been in existence since the 1980s but its concept has been booming in recent years. Since the market is getting stagnant, developers are targeting their applications globally. However, in the context of our country, only a few popular apps such as Hamro Patro, Hamro Keyboard [11] are localized. Most older generation people do have difficulties when it comes to using non-localized apps; localizing helps those users to use these apps easily and

comfortably. So, the solution we present seems innovative and viable for developers developing apps for our country.

4.2. Discussion on analysis of Ethnographic observation

Apart from expert users, people mostly use eSewa for loading/transferring and sending money. More vertical scrolling needs to be done to reach different features and also there is a view-more link to access more hidden features. This can be cumbersome to many people.

From the discussion, the common and noteworthy pros of our project were pointed out to be:

- Applications will be usable for people who are not fluent in English.
- Provides for better communication amongst multilingual people and serves the concept of universal usability
- The localization of app is sure to increase the number of users using e-Sewa as some users might not be comfortable using apps in a language other than their native tongue.

The cons of this project and probable ways to address them were also discussed:

- Local slang and colloquialisms cannot be translated word to word which can be mitigated by avoiding vague words in an application.
- If there is a loss of information and meaninglessness during translation, a dedicated team of professional translators can be put to work while developing applications.
- If people are uncertain about how much localization is appropriate, and to what extent we can localize only the static content for time being as we know that it is not possible to localize all of the dynamic contents.
- The impact of Localization boils down to the persona of users who use the application hence we need to provide them the option of choosing between different languages and not localize to a specific local language.

5. Conclusion

To recapitulate, the review clearly shows that localization is crucial if all demography is to be included to use the application. Universal usability means that the product should be usable by everyone despite their condition if they belong to the target group. For instance, if a person doesn't know the English language and doesn't want to, he should not be excluded from using the application they want. It is the responsibility of that application to make it suitable for everyone using it. The problem that we've chosen is that of implementing localization. Also implementing design principles in UI greatly affects the user experience and is directly related to users enjoying the application more. The key points that arose from the final survey and usability testing with the participants were that they all very much preferred the new design as it was: easy to use thanks to localization, nicely presented, and had good visual aspects that were clear and recognizable and the result indicated that the new design is friendlier to all kinds of user groups underlining the concept of universal usability. Their response showed that they are interested in using the redesigned app as it achieves specified goals with effectiveness, efficiency, and satisfaction in a relevant context, mainly related to the language barrier.

Acknowledgment

This work was supported by the Department of Computer Science and Engineering, Kathmandu University, Dhulikhel, Kavre, Nepal in 2020.

References

[1] eSewa, "eSewa | Digital wallet in Nepal for Online payment services," 29 11 2020. [Online]. Available: https://esewa.com.np/. [Accessed 30 11 2020].

[2] A. Smith, L. Bannon and J. Gulliksen, "Localising HCI Practice for Local Needs," *Proceedings of the 2010 International Conference on Interaction Design & International Development*, pp. 114-123, 2010.

[3] A. M. A. Awwad, "Localization to Bidirectional Languages for a Visual Programming Environment on Smartphones," *International Journal of Computer Science Issues*, vol. 14, no. 3, May 2017.

[4] Quora, "How The Growth Team Helped Facebook Reach 500 Million Users," 15 9 2014. [Online]. Available: https://www.forbes.com/sites/quora/2014/09/15/how-the-growth-team-helped-facebook-reach-500-million-users/?sh=13bf96d17058. [Accessed 30 11 2020].

[5] Wikipedia, "List of Wikipedias - Meta," 30 11 2020. [Online]. Available: https://meta.wikimedia.org/wiki/List_of_Wikipedias. [Accessed 30 11 2020].

[6] Google, "Hamro Patro : The Best Nepali Patro NP - Apps on Google Play," 30 11 2020. [Online]. Available: https://play.google.com/store/apps/details?id=com.hamropatro&hl=en&gl=US. [Accessed 30 11 2020].

[7] Google, "Khalti Digital Wallet (Nepal) - Apps on Google Play," 30 11 2020. [Online]. Available: https://play.google.com/store/apps/details?id=com.khalti&hl=en_US&gl=US. [Accessed 30 11 2020].

[8] Enginess Insights, "The 6 Principles Of Design, a la Donald Norman | Enginess Insights," 30 11 2020. [Online]. Available: https://www.enginess.io/insights/6-principles-design-la-donald-norman. [Accessed 30 11 2020].

[9] University of Texas, "Shneiderman's Eight Golden Rules of Interface Design," 15 5 2004. [Online]. Available: https://faculty.washington.edu/jtenenbg/courses/360/f04/sessions/schneidermanGoldenRules.html. [Accessed 30 11 2020].

[10] J. Nielsen, "10 Usability Heuristics for User Interface Design," 24 5 1994. [Online]. Available: https://www.nngroup.com/articles/ten-usability-heuristics/. [Accessed 30 11 2020].

[11] Google, "Hamro Nepali Keyboard - Apps on Google Play," 30 11 2020. [Online]. Available: https://play.google.com/store/apps/details?id=com.hamrokeyboard&hl=en_US&gl=US. [Accessed 30 11 2020].

Selection of Appropriate Requirement Prioritization Technique for Various Software Domains.

Sameer Sitoula

MTech in Software Engineering (Ramaiah Institute of Technology, Bangalore, India)

Lecturer, Department of Computer and Electronic Engineering, Advanced College of Engineering and Management

Sameer.sitoula@acem.edu.np/sameersitaula67@gmail.com

Abstract

Software is ending up the dynamically progressively basic need of everyday life. Building up the product that addresses stakeholders' issues is a definitive objective in the present condition. As the quality of software increments so does the requirements. Numerous requirements ought to be satisfied in the given time frame then again, a few necessities need to be viewed as first to diminish the risk. Consequently, legitimate assembling and prioritizing requirements may prompt the progressive improvement of the product. This technique is regarded as one of the most essential tactics in the requirement engineering process. The weight on time-to-advertise and having the capacity to anticipate the progressive arrival of the product item has presented numerous difficulties to the software engineering process. Budgetary confinements and time-to-showcase due dates regularly force stakeholders to mindfully prioritize requirements. It is used to define the ordering or scheduling for executing requirements primarily based on the priority or importance of the stakeholder's viewpoint. Various researchers have led to many requirement prioritization strategies, and there is no single approach of requirement prioritization that can be used for all project types. In this paper, the overview of selecting appropriate requirements prioritization techniques using the most famous strategies and their comparison against each other will be discussed.

Keywords: *Legitimate, Confinements. Dynamically, Progressively, Prioritizing, Requirement, Stakeholder*

1 Introduction

1.1 Motivation

Requirement prioritization is considered one of the most significant activities in the process to construct software project and deliver the good system as the customer need [1]. Most projects include many software requirements which are to be prioritized according to the limited resources in terms of time, budget, and customer satisfaction which is the major purpose in software development [2]. This demand in requirement prioritization has motivated us to integrate the right requirement prioritization technique for the given software domain. The main motive is to rectify the best and urgent requirements which can be feasible for both client and the firm. It must support the product that can be formed with limited resources if required urgently.

1.2 Literature Review

- Programming is ending up continuously an increasingly necessary piece of everyday life. Building up the product that address partners' issue is a definitive objective in the present condition. As the multifaceted nature of programming increments so does the prerequisites. Numerous prerequisites ought to be satisfied in the given time length then again, a few necessities ought to be viewed as first to diminish the dangers. Consequently, appropriate assembling and organizing prerequisites may prompt the progressive improvement of the product. In writing, there are several strategies that center around the prerequisite prioritization issue. This paper exhibits the relative investigation of different prerequisite prioritization methods [3].

- Requirement prioritization is considered as a standout amongst the most imperative exercises in the prerequisite building process. This paper gives an outline of the prerequisite's prioritization exercises and procedures. It additionally introduces how information mining and machine learning strategies have been utilized to organize the product venture necessities. A correlation between these methods is additionally introduced [3].
- Requirement prioritization assumes an imperative job in the necessity building process, especially, concerning basic assignments like necessities transaction and programming discharge arranging. Choosing the correct arrangement of necessities for an item discharge to a great extent relies upon how effectively the prerequisite competitors are organized. There are distinctive prerequisite prioritization strategies accessible which are more expounded than others. This paper investigates nine unique systems of prerequisite prioritization specifically Analytical Hierarchy Process (AHP), Hierarchy AHP, Minimal Spanning Tree, Bubble Sort, Binary Search Tree (BST), Priority Group, Planning Game (PG), 100 points technique, and Planning Game joined with AHP (PGcAHP) and afterward placed them into a controlled analysis, to discover the best one. The assessment was done based on a few criteria like convenience, sureness, the precision of the result, technique's capacity to scale up to a lot more necessities, required number of correlations, and expected time to settle on a choice. Examination of the information from the test shows that the explanatory progressive system procedure to be a promising applicant, even though it might be dangerous to scale up. Nonetheless, the outcome plainly shows that the Planning Game (PG) yields exact outcomes, can scale up, requires a minimum measure of time, the most straightforward technique to utilize, etc. Consequently, the finding of the examination is, the Planning Game (PG) technique should be the best strategy for organizing prerequisites [4].

2 Requirement Prioritization

2.1 Why Prioritize in accordance to the Stakeholder?

As all the requirements related to more than release are based on customer needs the software engineers do not know which requirements have higher priority and which are not. Thus, various stakeholders participate in the system development to prioritize the requirements in the right way according to their importance, therefore, those requirements can be ordered in execution.

2.1 Types of Requirement Prioritization

2.1.1 High priority requirements

High priority requirements may be processes that help the business increase revenue or mitigate risks

2.1.2 Lower priority requirements

Lower priority requirements are those that provide minimal impact to organisational outputs or end user experience.

2.2 What requirements to prioritize?

Start by prioritizing the business requirements or objectives of the project. Once that's done, you should be able to determine which stakeholder's requirements are most urgent, only the stakeholder's requirement that supports a business requirement should be in scope. The project team should address the other requirements in order or urgency. This will dictate the order of implementation and ensure that the product is valuable even if some requirements have to be left out due to time and money constraints.

3 Requirement Prioritization Techniques

Software advancement or some other venture confronting different prerequisites, budgetary imperatives, and tight due dates frequently require the need to organize stakeholder's requirements. Sooner or later, it's generally important to settle on choices on which set of requirements should be executed first and which ones can be postponed till a later discharge.
Various strategies on the most proficient method for requirement prioritization have been produced. While some work best on few prerequisites, others are more qualified for extremely complex activities with numerous chiefs and factors. This rundown of requirement prioritization systems gives a review of regular strategies that can be utilized in organizing necessities.

3.1 Hundred Dollar Technique

This straightforward technique is valuable anyplace various partners need to justly cast a ballot on which prerequisites are the most imperative [5]. All partners get a reasonable 100 dollars, which they can disperse among the necessities. All things considered, the partner may give each of the 100 dollars to a solitary necessity, or the individual may disperse the focuses all the more equally [5]. The higher the sum allotted to every necessity, the higher the need of the prerequisite. Toward the end, the all-out is checked and the requirements are arranged dependent on the quantity of points received [5].

This method should possibly be utilized when you have a little gathering of prerequisites to organize and when you have a similar arrangement of necessities to keep respondents from impacting their outcomes by allocating more dollars to their most loved necessity. With this system, in any case, it tends to be hard to monitor what amount has been allotted and what sum is left to discard.

3.2 Ranking Technique

This one is the most popular among all other requirement prioritization techniques because it is simple to understand and deliver [5]. In this technique, we fix some scale rules ranging from 1 to n and rank the importance of the software [6]. As '1' will be the most important, '2' being the second important and 'n' is the least important among all. This method is supposed to be working perfectly and best when we are dealing or managing with a single stakeholder or a solitary partner as it is very difficult to align the outlook of various stakeholders on what the need of prerequisite ought to be and hence taking the normal can in any case, however, deliver the issue in some extent.

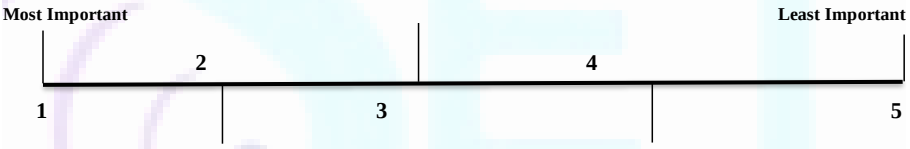

Fig 3.2.1 Ranking based on Importance

Using Pathao Foods as an example, here's is the explanation of how Ranking Technique is used to categorize the services in numerical form

Fig 3.2.2 Numerical assignment of services

Fig 3.2.3 Ranking based on priority

3.3 Numerical Assignment Technique

This method is also known as the grouping technique. This technique is formed on gathering prerequisites into various prime concern categories with each gathering speaking to something which stakeholders can connect to [5]. Business analyst responsibility is to group the requirement in various prime concern or priority level groups with each group comprises what stakeholders connect to [6].

Requirements can be grouped into three categories: -

1. **Critical priority.**
2. **Moderate priority &**
3. **Optional priority.**

Thus, the simple explanation of these three categories can be slated as follows: -

1. **Critical priority**
   It is the most important or compulsory if we wish to describe their importance.
   On a scale of 1 to 10, we can give them as 10 in a matter of importance.
2. **Moderate priority**
   It is less important or has less priority what stakeholders could ask for.
   On a scale of 1 to 10, we can give them 5 or 6 in a matter of importance.
3. **Optional priority**
   Lessor not important requirements come under this optional priority.
   Either present or not present does not affect the business model.

3.4 Bubble Sort Technique

Bubble sort is a straightforward arranging calculation which over and again navigates through the rundown, thinks about the two numbers or information, and changes their requesting if they are wrongly requested. Here, likewise, we do a similar thing, that is on the off chance that we discover one necessity must be positioned higher than the other, we change their request or swap them as needs be.
The means required to organize prerequisites with bubble sort strategy are as follows:

1. Outline the requirements in a vertical column [6].
2. Look at the best two necessities from the segment with one another to figure out which is the most imperative. On the off chance that the lower prerequisite could easily compare to the best one, swap their positions [6].
3. Repeat this pairwise comparison and swapping for the second and third requirement, then the third and fourth requirement, and so on until the bottom of the column is reached [6].
4. If any of the prerequisites have been moved amid stages 2 and 3, rehash the procedure for the entire section beginning again from the main two necessities (stage 2). Continue

rehashing this until the point when no necessities are swapped amid a total go through the section, which implies that the prerequisites are currently in need arrange [6].

Thus, the result of the procedure is a positioned segment of necessities where the most critical prerequisite is at the highest point of the section and the minimum essential one is at the base.

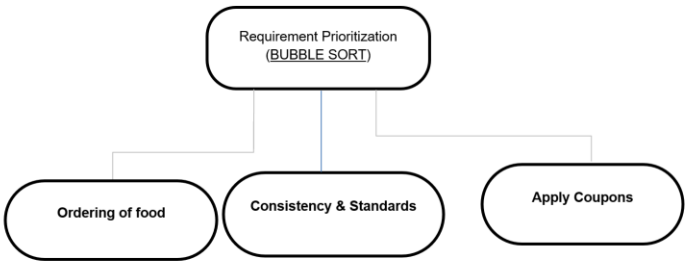

Fig 3.4.1 Bubble Sort Technique

3.5 MOSCOW Technique

The MOSCOW strategy is a prioritization system utilized in the board, business examination, venture the executives, and programming advancement to achieve a typical comprehension with partners on the significance they put on the conveyance of every necessity; it is otherwise called MOSCOW prioritization or MOSCOW study [7]. All necessities are critical; however, they are organized to convey the best and quickest business benefits early. Engineers will at first endeavor to convey all the Must have, should have, and could have necessities however they Should and Could prerequisites will be the first to be expelled if the conveyance timescale looks undermined.

The classifications are ordinarily comprehended as:

i.) Must have

Necessities marked as Must have been basic to the present conveyance time box with the goal for it to be a triumph. Characterizes a necessity that must be fulfilled for the last answer to be satisfactory [8]. On the off chance that even one Must have prerequisite is excluded, the undertaking conveyance ought to be viewed as a disappointment (note: necessities can be downsized from Must have, by concurrence with every pertinent partner; for instance, when new prerequisites are considered progressively essential). MUST can likewise be viewed as an abbreviation for the Minimum Usable Subset [7].

ii.) Should have

Prerequisites named as Should have been vital however redundant for transfer in the present carrying case [7]. This is a high-need necessity that ought to be incorporated if conceivable, inside the conveyance period [8]. While should have prerequisites can be as imperative as Must have, they are frequently not as time-basic or there might be another approach to fulfill the necessity, so it tends to be kept down until a future conveyance time box.

iii.) Could have

This is an attractive or pleasant to-have prerequisite (time and assets allowing) yet the arrangement will at present be acknowledged whether the user is excluded [8]. Prerequisites marked as Could have been attractive however a bit much and could enhance client experience or consumer loyalty for little advancement cost. These will normally be incorporated if time and assets allow.

iv.) Won't have

This speaks to a necessity that partners need to have, however have concurred won't be executed in the present rendition of the framework. Prerequisites marked as Won't have been concurred by partners as the slightest basic, most minimal restitution things, or not proper around then [7]. That is, they have chosen it will be put off till the following round of advancements [8]. Won't have prerequisites are either dropped or re-examined for consideration in a later time box. (Note: periodically the term Would get a kick out of the chance to have been utilized; in any case, that use is mistaken, as this last need is plainly expressing something is outside the extent of conveyance).

4 Selection of Appropriate Requirement Prioritization Techniques

The determination of a fitting prioritization technique from a given arrangement of different prioritization strategies {M1, M2…. Mn} is guided by contrasting their profile and particular characteristics {C1, C2….. Cn} against an ideal profile of an explicit programming application as far as given criteria. Here various prioritization methods {M1, M2 …. Mn} are the ones discussed above and characteristics {C1, C2 …. Cn} are size of the project, ease of implementation, speed, complexity, etc. [9],

- Convert fluffy qualities indicated to its comparing fresh qualities utilizing defuzzification strategy. This grid of every single fresh esteem can be named as: R = [rij] i.e.

	C1	C2	..	..	CN
P1	r11	r12	..	..	r1n
P2	r21	..	..	..	r2n
..	..	..	..	..	..
PM	rm1	rm2	..	..	rmn

where all entries of this matrix R expresses degree to which characteristic Cj is satisfied by method Pi(i=1..m) and (j=1..n).

- Normalize the estimations of grid R by partitioning each estimation of this lattice by the most extreme estimation of the framework. All passages of this network are genuine numbers in [0,1].

N = R/MAX

where max is the most extreme estimation of the matrix.

- Recognize an application for which an appropriate technique is wanted. This application is limited by various criteria. Allot the fitting weight that ranges from 0 (not imperative or pertinent) to 5 (significant) to these criteria.

$$W = \begin{pmatrix} W1 \\ W2 \\ .. \\ Wn \end{pmatrix}$$

5 Case Study

So as to outline the proposed system, a test investigation of the Travel Management Planning Website was performed. The point of the investigation was to choose the proper prioritization technique for the site. Five prioritization strategies to be specific Ranking Technique, Numerical Assignment Technique, MOSCOW Technique, Bubble Sort Technique, and Hundred Dollar Method and five qualities, for example, Ease of utilization, Size of the undertaking, Fuzziness, Multi-criteria, and multi-individual were chosen to improve the examination. Three area specialists were asked to give their proposal about the degree to which trademark Cj is controlled by technique Pi utilizing semantic terms. Defuzzification was utilized to change over the etymological terms to fresh qualities and results are appearing in network R [2].

$$R = \begin{array}{c|ccccc} & C1 & C2 & C3 & C4 & C5 \\ P1 & 4 & 2 & 0 & 0 & 4 \\ P2 & 4 & 3 & 0 & 5 & 0 \\ P3 & 3 & 3 & 5 & 5 & 4 \\ P4 & 3 & 3 & 0 & 5 & 2 \\ P5 & 2 & 5 & 0 & 5 & 2 \end{array}$$

To obtain Rn normalize the matrix R.

$$Rn = \begin{array}{c} \\ P1 \\ P2 \\ P3 \\ P4 \\ P5 \end{array} \begin{pmatrix} C1 & C2 & C3 & C4 & C5 \\ 0.8 & 0.4 & 0 & 0 & 0.8 \\ 0.8 & 0.6 & 0 & 1 & 0 \\ 0.6 & 0.6 & 1 & 1 & 0.8 \\ 0.6 & 0.6 & 0 & 1 & 0.4 \\ 0.4 & 1 & 0 & 1 & 0.4 \end{pmatrix}$$

Three stakeholders including Project Manager, System Engineer and Website Maintainer were asked for to give their prerequisites for the site as wanted criteria. These criteria were appointed loads in the size of 0 to 5 to acquire the matrix W.

$$W = \begin{pmatrix} 3 \\ 3 \\ 2 \\ 4 \\ 5 \end{pmatrix}$$

To obtain the matrix Wn normalise the matrix W

$$Wn = \begin{pmatrix} 0.6 \\ 0.6 \\ 0.4 \\ 0.8 \\ 1 \end{pmatrix}$$

Multiply Rn and Wn to get the resultant matrix S.

$$S = \begin{pmatrix} 1.52 \\ 1.64 \\ 2.72 \\ 1.92 \\ 2.04 \end{pmatrix}$$

Table 5.1 Final Result

Methods	Ranking	Numerical	MOSCOW	Bubble Sort	Hundred Dollar
Values	1.52	1.64	2.72	1.92	2.04

It shows that MOSCOW Technique is found most suitable followed by Hundred Dollar, Bubble Sort and Numerical Assignment. Ranking Method was found least suitable for the website.

6 Conclusion

Nearly all existing prioritization techniques need to be more continuous, scalable, clearly implemented, and integrated with the software development life cycle. Based on the outcome we achieved MOSCOW technique is found to be the most prominent and effective prioritization technique of all. This technique differs from one domain to another and entirely dependent on what is our urgent and critical requirement

So, which prioritization technique is best? The one that fits your needs the most and accomplishes your goals in the least amount of time and with a minimal number of resources. Once you have an idea of which techniques are applicable to your project, you can evaluate them in real life to see how well they perform.

References

[1] H. Ahuja, Sujata and G. N. Purohit, "Understanding requirement prioritization techniques," in *IEEE*, Delhi, India, 2016.

[2] H. Ahuja, Sujata and G. N. Purohit, "Understanding requirement prioritization techniques," in *IEEE*, Delhi, India, 2016.

[3] R. Qaddoura, A. Abu-Srhan, M. H. Qasem and A. Hudaib, "Requirement Prioritization Technique Review and Analysis," in *IEEE*, 2018.

[4] A. A. M. S. M. N. H. M. J. A. Mohammad Shabbir Hasan, "An Evaluation of Software Requirement Prioritization Techniques," *research gate*, vol. 8, pp. 83-94, 2010.

[5] S. Famuyide, "businessanalystlearning.com," Business Analyst Learning, 16 8 2016. [Online]. Available: https://businessanalystlearnings.com/blog/2016/8/18/a-list-of-requirements-prioritization-techniques-you-should-know-about. [Accessed 15 7 2021].

[6] V. Mikko, "A Comparison of Nine Basic Techniques for Requirements Prioritization," *semanticscholar.org*, 2010.

[7] Wikipedia, "en.wikipedia.org," Wikipedia, 2016. [Online]. Available: https://en.wikipedia.org/wiki/MoSCoW_method. [Accessed 5 July 2021].

[8] S. Famuyide, "businessanalystlearning.com," Business Analyst Learning, 5 3 2013. [Online]. Available: https://businessanalystlearnings.com/ba-techniques/2013/3/5/moscow-technique-requirements-prioritization. [Accessed 11 6 2021].

[9] P. B. Vineet Arora, "A Novel Approach to Select an Appropriate Requirements," *semanticscholar.org*, 2013.

Part IV: Hydrology and Hydropower

Best performing CMIP6 GCMs and Bias Correction Method for Projection of Precipitation in Kankai River Basin, Nepal

Manoj Lamichhane

Author, Project Coordinator and a Lecturer of the Department of Civil Engineering, Advanced College of Engineering and Management, Kalanki, Kathmandu

manoj@acem.edu.np

Abstract

The choice of representative Global Circulation Models (GCMs) and an acceptable bias correction method is critical in assessing future precipitation and temperature using climate models. This study determines the representative GCMs and appropriate bias correction method for projection of future precipitation which minimizes the biases while downscaling precipitation data in regional scale from global models. The performance of 10 different raw GCMs from the Coupled Model Intercomparison Project Phase 6 (CMIP6) to simulate precipitation in Nepal's Kankai River Basin is assessed in this study. To evaluate the GCMs using historical observations, three statistical performance metrics are used: Nash-Sutcliffe efficiency (NASH), Percentage Bias (PBIAS) and Root Mean square Error (RMSE). According to the findings, ***ACCESS-ESM1-5, MPI-ESM1-2-LR****,* ***BCC-CSM2-MR*** *and* ***ESM2-MM*** *are the best models for forecasting precipitation events. Similarly, thirteen bias correction methods were applied on selected representative GCMs and result revealed that Bernoulli's Weibull method is best bias correction method for bias correction of precipitation in this region. The result of this study may be useful for assessing future hydro-meteorology of Kankai River Basin and surrounding basins having similar meteorological characteristics.*

Keywords: *Climate Change, Global Circulation Model (GCM), Bias Correction, Kankai River Basin*

CHAPTER 1: INTRODUCTION

General circulation models (GCMs) are models that create meteorological variables such as precipitation (rainfall), temperature, wind speed, relative humidity, solar radiation, and so on. The elementary equations of thermodynamics, mass, and momentum (Nunez & McGregor, 2007) are used to construct these meteorological variables. For various Green House Gas (GHG) emission scenarios, climate statistics are derived as time series future data. Individual GCM climate variables, on the other hand, frequently disagree with observed time series. GCMs are typically employed as part of a multi-model analysis to generate climatic statistics (Helfer et al., 2012). Several institutes and organizations, led by the Intergovernmental Panel on Climate Change (IPCC), investigated the impact of climate change on numerous climate variables, resulting in GCM gridded data with resolutions ranging from 100 to 300 km grid size.

Climate change is a major factor affecting the Himalayan areas' long-term viability (Hopmans & Maurer, n.d.). Because extensive sections of the Himalayan region are covered by snow and glaciers,

they are particularly vulnerable to global warming (Maskey et al., 2011). Warming is more pronounced in these areas than in lower elevation areas, and they are especially vulnerable to global change and variability (Buytaert et al., 2010). Agriculture, which is tied to monsoon rainfall and winter temperatures, is a major contributor to the economies of South Asian countries. The summer monsoon provides more than 80% of the water in the region (Goswami, 2012), while significant areas in the north and northwest also receive winter precipitation (Dimri et al., 2015).

In the majority of Nepalese river basins, precipitation is the primary driver of streamflow. A realistic estimate of future climate (temperature and precipitation) is a necessary first step in predicting future water supply. Studies have been conducted to forecast future climate in particular basins and its potential effects on hydrology. Rajbhandari et al., (2016) used RCP4.5 and RCP8.5 to estimate precipitation and temperature patterns in the Koshi river basin for the years 2021–2050. The impact of climate change on the snow hydrology of the Koshi river basin was investigated by A. Khadka et al. (2016). The influence of climate change on water availability in the Bagmati basin was also calculated by Dahal et al. (2016). According to this research, climate change would cause significant changes in the hydrology of the local basin in the long run under several future scenarios.

GCMs are the key tools for projecting future climate patterns and researching changes in precipitation and temperature trends because they represent the innumerable atmospheric processes that make up the global climate system. In Phase 6 of the Coupled Model Intercomparison Project, the many GCMs are continuously updated to allow the output to be used for diverse climate change studies (CMIP6). However, many questions remain unsolved, such as 'Which GCM is the most appropriate?' or 'How should a decent GCM be selected?', making it difficult for the majority of GCM users to choose the most appropriate one for their research (Lin et al., 2017).

The assessment of GCMs before to their use in climate change studies is critical. Over time, the performance of climate models varies from place to place and model to model (IPCC, 2013). In hydrological modeling research, evaluating the efficacy of GCMs aids in simulating numerous hydro-climatic factors. Many research have suggested using simple and substantial statistical performance metrics to evaluate GCMs (Preethi et al., 2009). Other research suggests that skill score and other performance indicators such as the correlation coefficient (CC), normalized root-mean-square deviation (NRMSD), and root-mean-square error (RMSE) are useful (MacAdam et al., 2010). Selected climatic models may still have systematic errors, necessitating some type of modification to the models' estimates. To account for this, bias correction, which is simply the process of rectification of climate model output in order to improve their performance based on observable data, should be carried out.

CHAPTER 2: STUDY AREA

Kankai Basin is located in eastern part of Nepal. The latitude and longitude for the selected study area lies between 26^0 41' to 27^0 07' N and 87^0 44' to 88^0 09' E respectively. Kankai is the major river in the basin originating from the border of Ilam and Panchthar district. It is rain fed Perennial River. The catchment area of the Kankai basin is 1165 square kilometer. The elevation of the catchment area varies from 130 m to 3535 m above mean sea Level. The Kankai basin in the map of Nepal has been shown in Figure below and the drainage networks in the study area has been shown in Figure 1 Kankai Basin attached together.

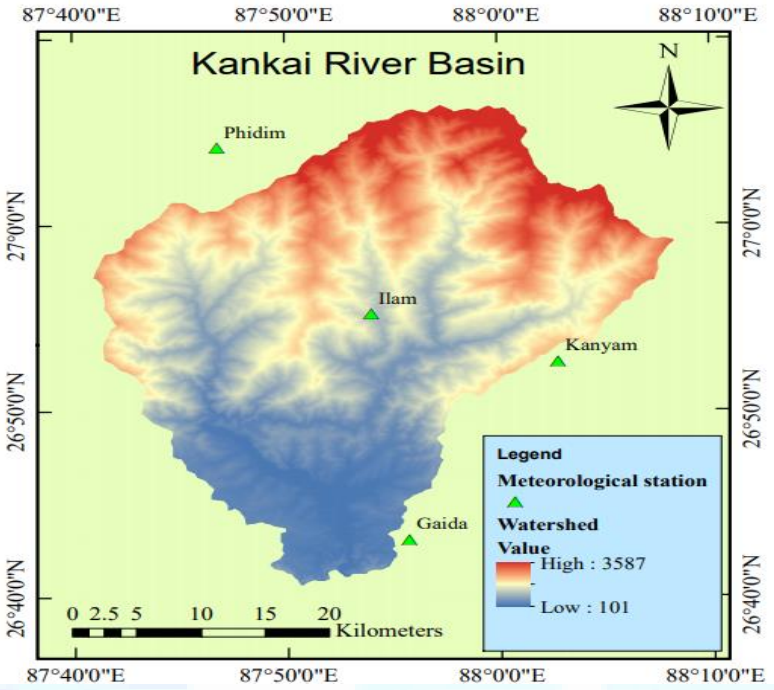

Figure 2.1: Study area

CHAPTER 3: METHODOLOGY

The step-by-step procedure for selecting the best GCMs and bias correction method for precipitation is illustrated in

Figure 0.1., there are four major stages for selecting the best GCMs and bias correction method.

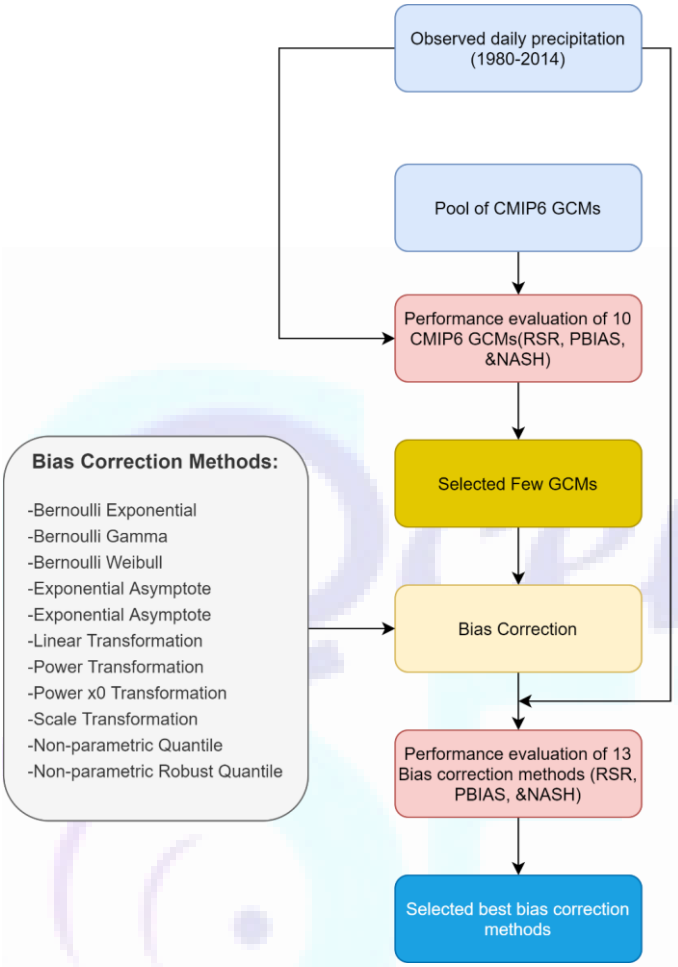

Figure 0.1: Methodological flow chart

First stage was performance evaluation of raw historical GCMs by comparing them with observed historical data. Then the rating was given to each GCMs and highest rated four GCMs were selected for further bias correction. Then the selected four GCMs were bias corrected using thirteen bias correction methods and again rating was given to each method by calculating their performance by comparing bias corrected historical data with observed data collected from DHM. Then the highest rated bias correction method was considered as best bias correction method for this study area. The details of these methods are described in following sections.

2.1 Performance evaluation of Raw GCMs

The performance metrics of each model for four stations were computed and converted into arbitrary performance ratings based on the average of combined ratings of all metrics across all selected stations. From the pool of 10 GCMs, the GCMs were ranked and the best performed 4 GCMs were selected. Using the four earlier mentioned performance metrics (i.e., RSR, R^2, PBIAS and NSE), the rating of the individual GCMs for each station were calculated and their ranks were assigned based on the average rating. Then the best performed GCMs were selected for further bias correction.

Table 0.1: Performance Ratings for Initial Selection of GCMs (Moriasi et al., 2007)

Performance	NSE	RMSE	PBIAS	Rating
Very Good	0.75<NSE<=1.00	0.00<RMSE<=0.50	PBIAS< 10	**5**
Good	0.65<NSE<=0.75	0.50<RMSE<=0.60	10 <= PBIAS <15	**4**
Satisfactory	0.50<NSE<=0.65	0.60<RMSE<=0.70	15 <= PBIAS <25	**3**
Unsatisfactory	0.4<NSE<=0.5	0.70<RMSE<=0.80	25 <= PBIAS <35	**2**
Poor	NSE<=0.4	RMSE>0.80	PBIAS>=35	**1**

2.2 Bias Correction

The precipitation projections using climate model do not always match the statistical characteristics of the observed time series in the control period. To reduce such inaccuracies, bias correction approaches are applied. The selected GCMs are statistically downscaled and bias corrected using the following methods:

i. Bernoulli Exponential

It is a mixture of the Bernoulli and the exponential distribution. The mixture is analogous to the one described for the Bernoulli gamma distribution.

ii. Bernoulli Gamma

Non-zero values follow the Gamma distribution with shape and scale parameters. The probability density function (PDF) is defined as:

$$g(x) = \begin{cases} \pi * \gamma(x) & if\ x > 0 \\ 1 - \pi & if\ x \leq 0 \end{cases}$$

where, $\gamma(x)$ is the probability density function of the gamma distribution and π is probability of a non-zero event.

The cumulative distribution function (CDF) is defined as:

$$G(x) = \begin{cases} 1 - \pi + \pi * \Gamma(x) & if\ x > 0 \\ 1 - \pi & if\ x \leq 0 \end{cases}$$

where, $\Gamma(x)$ is the cumulative distribution function of the gamma distribution.

The quantile function (inverse of the CDF) is defined as:

$$G^{-1}(p) = \begin{cases} \Gamma^{-1}\left(\frac{p-1+\pi}{\pi}\right) & if\ \pi > 1-p \\ 0 & if\ \pi \leq 1-\mathrm{p} \end{cases}$$

where, Γ^{-1}(p) is the inverse CDF of the gamma distribution and p is a probability.

iii. Bernoulli Weibull

It is a mixture of Bernoulli and Weibull distribution. This mixture is also analogous to the one described for the berngamma distribution.

iv. Bernoulli Log-normal

It is a mixture of Bernoulli and Log-normal distribution. This mixture is also analogous to the one described for the Bernoulli gamma distribution.

v. Exponential Asymptote

vi. Exponential Asymptote x0

vii. Linear Transformation

viii. Power Transformation

ix. Power x0 Transformation

x. Scale Transformation

xi. Non-parametric Quantile Mapping

xii. Non-parametric Robust Quantile Mapping

The values of the quantile–quantile relationship is derived form of observed and model time series for regularly spaced quantiles using local linear least square regression, and performs quantile mapping by interpolation of the empirical quantiles (Tong et al., 2020). Linear and monotonic tri-cube interpolation are commonly used.

xiii. Smoothing Spline

The smoothing spline is only fits to the fraction of the CDF corresponding to observed wet days and modelled values below this are set to zero. The smoothing parameter of the spline is identified by means of generalized cross-validation.

Selection of bias correction method is done by comparing the performance of precipitation and temperature projection made by the GCMs with the baseline observed data from 1980 to 2014. For quantifying the performance, the performance used are Nash-Sutcliffe efficiency (NSE), root mean square error (RMSE) and percentage bias (PBIAS).

Table 0.2: Performance Ratings for Bias correction method (Moriasi et al., 2007)

Performance	NSE	RMSE	PBIAS	Rating
Very Good	0.85<R2<=1.00	0.00<RMSE<=0.25	PBIAS< 5	**8**
	0.75<R2<=0.85	0.25<RMSE<=0.50	5 <= PBIAS <10	**7**
Good	0.70<R2<=0.75	0.55<RMSE<=0.60	10 <= PBIAS <12.5	**6**
	0.65<R2<=0.70	0.50<RMSE<=0.55	12.5 <= PBIAS <15	**5**
Satisfactory	0.57<NSE<=0.65	0.65<RMSE<=0.70	15 <= PBIAS <20	**4**
	0.50<NSE<=0.57	0.60<RMSE<=0.65	20 <= PBIAS <25	**3**
Unsatisfactory	0.4<NSE<=0.5	0.70<RMSE<=0.80	25 <= PBIAS <35	**2**
Poor	NSE<=0.4	RMSE>0.80	PBIAS>=35	**1**

CHAPTER 4: Data Collection

4.1 CMIP6 raw GCMs data

CMIP6-GCMs model outputs were collected from World Climate Research Programme (WCRP) website (https://esgfnode.llnl.gov/search/cmip6/). Daily precipitation was available only for these 10 GCMs. Those CMIP6-GCMs (along with their spatial resolutions) as given in Table 0:1.

Table 0:1: CMIP-6 GCMs model output

S.no	Model name	Latitude resolution	Longitude resolution	Research center
1	ACCESS-CM2	1.5	1.875	Australian Community Climate and Earth System Simulator (ACCESS)
2	ACCESS-ESMI-5	1.5	1.875	Australian Community Climate and Earth System Simulator (ACCESS)
3	BCC-CSM2-MR	1.1215	1.125	Beijing Climate Center (BCC)
4	EC-Earth3-Veg	0.7018	0.7031	European Community Earth (EC-Earth)
5	EC-Earth3	0.7018	0.7031	European Community Earth (EC-Earth)
6	MRI-ESM2-0	1.1215	1.125	Meteorological Research Institute (MRI)
7	MPI-ESMI-2-LR	1.8653	1.875	Max planck Institute for Meteorology (MPI)
8	MPI-ESMI-2-HR	0.9351	0.9375	Max planck Institute for Meteorology (MPI)
9	NorESM2-MM	0.9424	1.25	Norwegian Climate Center
10	INM-CM4-8	1.5	2	Institute for Numerical Mathematics (INM)

4.2 Meteorological data

Meteorological data was collected from Department of Hydrology and Meteorology (DHM) from 1980-2014. There are four meteorological stations inside and near the outside of Kankai river basin.

Table 0.2: Meteorological stations of study area

S.N.	Station Name	Index No.	District	Latitude	Longitude	Elevation (m)
1	GAIDA	1421	Jhapa	26°35’	87°54’	143
2	ILAM	1407	Ilam	26°55’	87°54’	1300
3	KANYAM	1416	Ilam	26°52’	88°04’	1678
4	PHIDIM	1419	Panchther	27°09’	87°045’	1205

CHAPTER 5: RESULT AND DISCUSSION

5.1 Selected GCMs from Pool of GCMs

The final average rating of each GCMs is shown in Figure 0.1. Results showed that ACCESS-ESM1-5, MPI-ESM1-2-LR, BCC-CSM2-MR, NorESM2-MM are the models with generally higher ratings for the Precipitation. The above-mentioned GCMs were selected for further bias correction.

The precipitation forecasts produced by several GCMs showed significant diversity. Each GCM has its own set of strengths and shortcomings; some are better in tropical areas than others in mountainous areas. It is critical to choose the model that works well in the desired area. As shown by the performance metrics, the performance of GCMs under various climatic indices varies depending on the model employed.

Table 0.1: Average Performance Rating of Pool of GCMs for Precipitation

S.N.	GCM Name	Average Performance Rating
1	**ACCESS-ESM1-5**	**2.7**
2	ACCESS-CM2	1.9
3	**MPI-ESM1-2-LR**	**2.9**
4	MIROC6	2.1
5	MRI-ESM2-0	2.1
6	**BCC-CSM2-MR**	**2.3**
7	INM.INM-CM4-8	1.4
8	INM-CM5-0	1.8
9	**NorESM2-MM**	**2.6**
10	CMCC-CM2-SR5	1.5

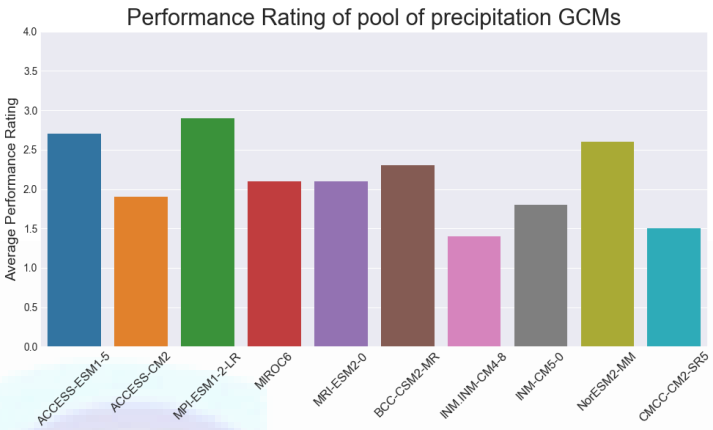

Figure 0.1: Average Performance Rating of Pool of GCMs for Precipitation

5.2 Selected best performed bias correction method

At first, the bias correction of precipitation of the historical period was done. The historical rainfall data from ACCESS-ESM1-5, BCC-CSM2-MR, MPI-ESM1-2-LR, and NorESM2-MM were bias-corrected for the four observed stations.

For precipitation, bias correction was done by thirteen methods, and selection of the best bias correction method was done by using performance rating of past data. For quantifying the performance, the performance used are Nash-Sutcliffe efficiency (NSE), root mean square error (RMSE) and percentage bias (PBIAS) and coefficient of determination(R2). Based on the average of combined ratings of all metrics overall selected stations using all 13 bias correction methods on a pool of 4 GCMs, the best performing bias correction method for precipitation was as Bernoulli Weibull method.

Table 0.2: Performance rating of bias correction method

Bias correction method	**Performance Rating**
Bernoulli Exponential	2.2
Bernoulli Gamma	3.2
Bernoulli Weibull	**3.4**
Bernoulli Log-normal	2.5
Exponential Asymptote	2.8
Exponential Asymptote x0	2.9
Linear Transformation	2.7
Power Transformation	3.1

Power x0 Transformation	3.1
Scale Transformation	2.4
Non-parametric Quantile Mapping	3.0
Non-parametric Robust Quantile Mapping	3.0
Smoothing Spline	3.1

5.3 Raw data verses bias corrected data

Mean monthly values of GCM simulations before and after correction against observed values are presented in this section. The time range used for averaging out monthly values is 1980–2014. However, it should be noted that the correction functions for bias correction techniques were generated using the historical time range from 1980 to 2014.

Climate models usually supply differing precipitation magnitude in the control period compared to observed. The GCMs show significant variability and bias throughout the year compared to the observed mean monthly rainfall. However, the variability seems to be comparatively lower during the pre-monsoon and post-monsoon periods and higher during the monsoon. It can also be noted that the GCMs generally overestimate precipitation, even more so at higher elevations (stations 1407, 1419) compared to lower elevations (stations 1421, 1416).

The monthly precipitation GCMs before and after bias correction with observed data at station Ilam (Higher altitude station) is shown in Figure 0.2. Bernoulli's Webull method was used for the bias correction of rainfall data. Bias correction of GCM simulated rainfall data showed correction in the mean as well as improvement in the RMSE, NSE and R^2. For all selected GCMs the mean precipitation before and after correction were nearly equal for each month. Bias correction of GCM simulated rainfall showed significant improvement in R^2 and root mean square error (RMSE). The result showed that R^2 values are higher showing the good performance of bias correction.

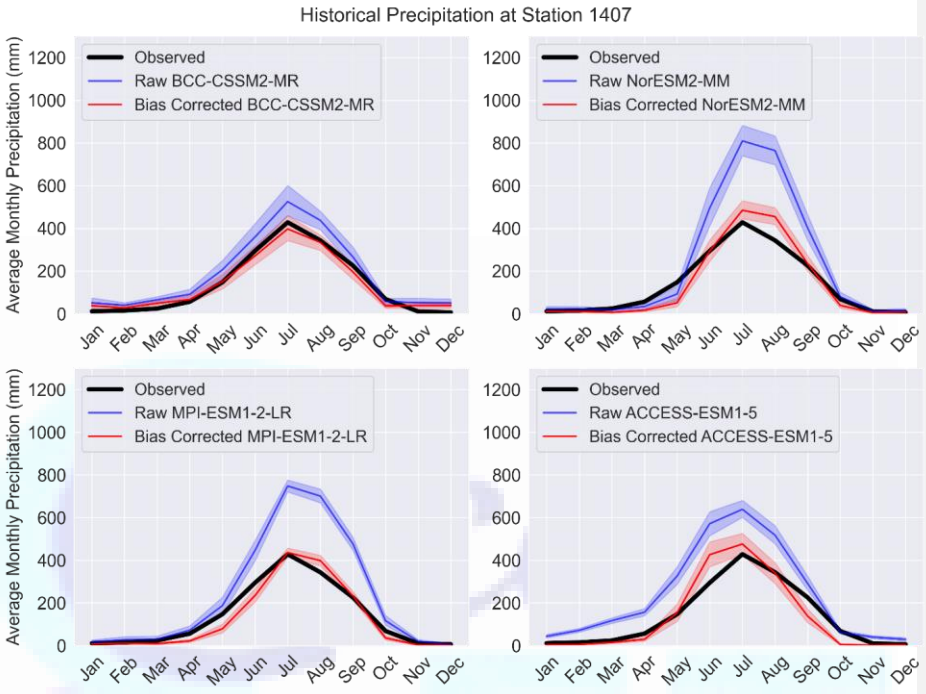

Figure 0.2: Comparison of observed, raw and bias corrected precipitation. (Ilam Station)

The monthly precipitation GCMs before and after bias correction with observed data at station Kanyam is shown in Figure 0.3. The GCMs show not significant variability and bias throughout the year compared to the observed mean monthly rainfall except BCC-CSM2-MR model. However, the variability seems to be comparatively lower during the pre-monsoon and post-monsoon periods and higher during the monsoon. The bias in GCM precipitation is notably reduced to match the observed values. The observed, raw and bias-corrected GCM precipitation are close to each other with a smaller spread between them at a 95 % confident interval.

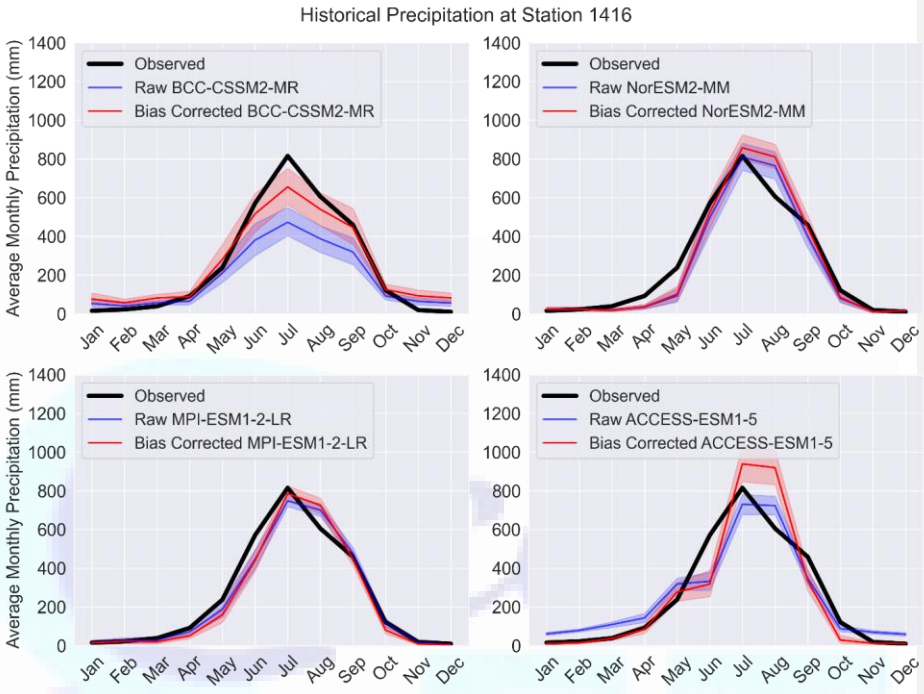

Figure 0.3: Comparison of observed, raw and bias corrected precipitation. (Kanyam Station)

CHAPTER 6: CONCLUSION AND RECOMMENDATION

This study's findings support the necessity for bias correction precipitation forecasts to remove biases between observed and raw model data. ACCESS-ESM1-5, MPI-ESM1-2-LR, BCC-CSM2-MR and NorESM2-MM are the best models for forecasting precipitation events for Kankai river basin and it's surrounding. Similarly, thirteen bias correction methods were applied on selected representative GCMs and result revealed that Bernoulli's Weibull method is best bias correction method for bias correction of precipitation in this region. Precipitation GCMs show significant variability and bias throughout the year compared to the observed mean monthly rainfall. However, the variability seems to be comparatively lower during the pre-monsoon and post-monsoon periods and higher during the monsoon period. It can also be noted that the GCMs generally overestimate precipitation, even more so at higher elevations (stations 1407, 1419) compared to lower elevations (stations 1421, 1416).

REFERENCES

Buytaert, W., Vuille, M., Dewulf, A., … R. U.-H. and E., & 2010, undefined. (2010). Uncertainties in climate change projections and regional downscaling in the tropical Andes: implications for water resources management. *Hess.Copernicus.Org*, *14*, 1247–1258. https://doi.org/10.5194/hess-14-1247-2010

Dahal, V., Shakya, N. M., & Bhattarai, R. (2016). Estimating the Impact of Climate Change on Water Availability in Bagmati Basin, Nepal. *Environmental Processes*, *3*(1), 1–17. https://doi.org/10.1007/s40710-016-0127-5

Dimri, A., Niyogi, D., Barros, A., … J. R.-R. of, & 2015, undefined. (2015). Western disturbances:

a review. *Wiley Online Library*, *53*(2), 225–246. https://doi.org/10.1002/2014RG000460

Goswami, B. N. (2012). South Asian monsoon. *Intraseasonal Variability in the Atmosphere-Ocean Climate System*, 21–72. https://doi.org/10.1007/978-3-642-13914-7_2

Helfer, F., Lemckert, C., & Zhang, H. (2012). Impacts of climate change on temperature and evaporation from a large reservoir in Australia. *Journal of Hydrology*, *475*, 365–378. https://doi.org/10.1016/J.JHYDROL.2012.10.008

Hopmans, J. W., & Maurer, E. (n.d.). *Impact of Climate Change on Irrigation Water Availability, Crop Water Requirements and Soil Salinity in the San Joaquin Valley*. Retrieved August 8, 2021, from http://hopmans.lawr.ucdavis.edu/

IPCC. (2013). IPCC CLIMATE CHANGE 2013 Climate Change 2013. In *Researchgate.Net*. https://www.researchgate.net/profile/Abha_Chhabra2/publication/271702872_Carbon_and_Other_Biogeochemical_Cycles/links/54cf9ce80cf24601c094a45e/Carbon-and-Other-Biogeochemical-Cycles.pdf

Khadka, A., Devkota, L. P., & Kayastha, R. B. (2016). Impact of Climate Change on the Snow Hydrology of Koshi River Basin. *Journal of Hydrology and Meteorology*, *9*(1), 28–44. https://doi.org/10.3126/jhm.v9i1.15580

Lin, C., Terrestrial, C. T.-, Oceanic, A. &, & 2017, undefined. (2017). Procedure for selecting

GCM datasets for climate risk assessment. *Pdfs.Semanticscholar.Org*, *28*(1), 43–55. https://doi.org/10.3319/TAO.2016.06.14.01(CCA)

MacAdam, I., Pitman, A. J., Whetton, P. H., & Abramowitz, G. (2010). Ranking climate models by performance using actual values and anomalies: Implications for climate change impact assessments. *Geophysical Research Letters*, *37*(16). https://doi.org/10.1029/2010GL043877

Maskey, S., Uhlenbrook, S., & Ojha, S. (2011). An analysis of snow cover changes in the Himalayan region using MODIS snow products and in-situ temperature data. *Climatic Change*, *108*(1), 391–400. https://doi.org/10.1007/S10584-011-0181-Y

Moriasi, D. N., Arnold, J. G., Liew, M. W. Van, Bingner, R. L., Harmel, R. D., & Veith, T. L. (2007). Model Evaluation Guidelines for Systematic Quantification of Accuracy in Watershed Simulations. *Transactions of the ASABE*, *50*(3), 885–900. https://doi.org/10.13031/2013.23153

Nunez, M., & McGregor, J. L. (2007). Modelling future water environments of Tasmania, Australia. *Climate Research*, *34*(1), 25–37. https://doi.org/10.3354/CR034025

Preethi, B., Kripalani, R., dynamics, K. K.-C., & 2010, undefined. (2009). Indian summer monsoon rainfall variability in global coupled ocean-atmospheric models. *Springer*, *35*(7), 1521–1539. https://doi.org/10.1007/s00382-009-0657-x

Rajbhandari, R., Shrestha, A. B., Nepal, S., & Wahid, S. (2016). Projection of Future Climate over the Koshi River Basin Based on CMIP5 GCMs. *Atmospheric and Climate Sciences*, *06*(02), 190–204. https://doi.org/10.4236/ACS.2016.62017

Squeezing of Hydropower Tunnel from Nepal Lesser Himalaya

Nitesh Shrestha*

Abstract

Underground tunnels in hard rock generally, have no or less stability issues. However, tunneling in weak and tectonically disturbed, young and fragile rocks usually faces complex and unpredicted geological problems. Stability is the major concern particularly, when tunnel aligns through poor quality, sheared, deformed, highly stratified & thinly foliated rock masses. Insitu stress increases degree of instability in tunnel. This paper quantifies stress state and deformation of tunnel at Chameliya hydroelectric project, a tunnel from Nepal lesser Himalaya, using different methods like empirical, semi analytical, analytical and a two-dimensional finite element (FE) investigation using Rocscience (RS) v. 9.0 software. Finite element modeling results highlight that the existing geological condition, rock mass parameters and tunnel configuration highly influence to stability of underground structures.

Keywords: *underground, squeezing, tunnel, stress*

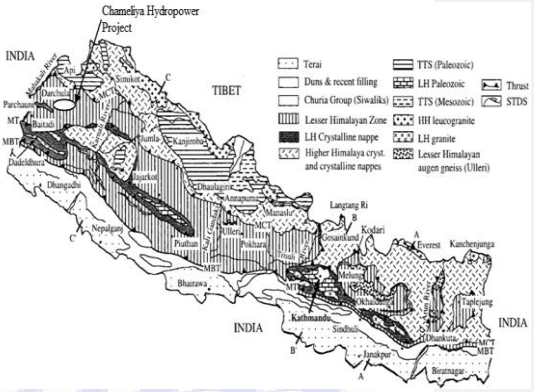

Fig.1. Location of Chameliya Hydroelectric Project [9]

***** Correspondence Author
Nitesh Shrestha*, MSc. Hydropower Development, Norwegian University of Science & Technology
Email: niteshshrestha81@gmail.com

I. INTRODUCTION

Nepal lies in north-central position in South Asia and is sandwiched between two giant countries in the world, India in the south and China in the north. It occupies one third of 2500 km long Himalayan arch. Being a mountainous country, it has tremendous potential in hydropower development due to steep terrain and fast flowing rivers. Nepal, being a developing country requires a long term & sustainable development of hydropower projects, and cost-effective option for waterway is construction of underground tunnels in these diverse geographical orientations. Nepal Himalayas has young and fragile geological formation which results challenges in underground construction. Poor rock condition, weathering, fracturing & disintegration, heavy overburden and rock stresses are major challenges encountered during underground excavations in Nepal Lesser Himalaya. Chameliya Hydroelectric Project (CHEP) is one of such projects lying in lesser Himalaya region of Nepal. Tunnel squeezing is a significant problem in weak rocks masses of Nepal Himalaya since they are unable to withstand extreme stress [1].Due to uneven topography of Nepal, most often tunnels have to be aligned under extreme overburden pressure which becomes a crucial cause for plastic deformation around tunnel contour. Very less study has been done on these young and fragile rock masses of Himalaya. Therefore, it is extremely difficult to predict the exact geological features and its effects in underground structures. So, rigorous researches are needed out to address these stability issues and correct problems related to geology. This paper, thus tries to examine a tunnel case from weak geology in Nepal lesser Himalaya finding out squeezing on rock mass and recommending some engineering solution to counter that problem.

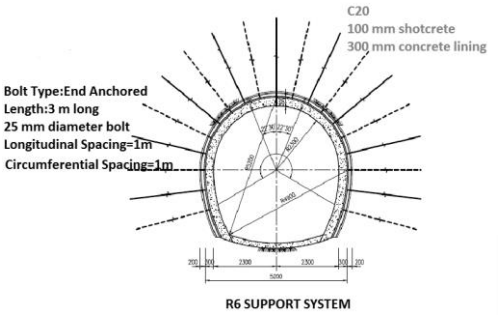

Fig. 2. R_6 Type Support System for HRT at CHEP Chainage 4+420 m [2]

Fig. 3. Severe Tunnel squeezing seen at Chameliya Hydroelectric Project

II. BRIEF DESCRIPTION OF PROJECT

Chameliya Hydroelectric Project is in Shikhar village of Darchula District, Mahakali Zone in Nepal. Project area lies in Lesser Himalayas zone, in catchment of Chameliya River (Fig. 1). Chameliya River is a main tributary of Mahakali river in Mahakali river basin. The intake structures are located at Lattenath VDC, Bitule. Project is a Peaking Run-of-River (RoR) type having limited storage in the intake pond. Design discharge of the plant is 36 m^3/s. The plant utilizes a maximum gross head of 103.7 m between elevations 884.4m amsl (Highest Regulated Water Level in the intake pond) and 780.7 amsl (the Francis turbine runner elevation). A total of 4.067 km length of headrace tunnel is there, and shape of headrace tunnel is of horse shoe configuration of 5.2 m diameter. Geology consists of fossiliferous, sedimentary to meta-sedimentary rocks like slate, phyllite, schist, quartzite, limestone and dolomite. In these zones, rocks are deeply weathered, fractured, jointed, traversed by various and large number of major and minor thrusts and faults. Various shear zones have made this zone fragile (Fig.4.). Problematic situation in the underground structure is faced when tunnel is bored through weaker rocks like phyllite and limestone (Fig.3.).

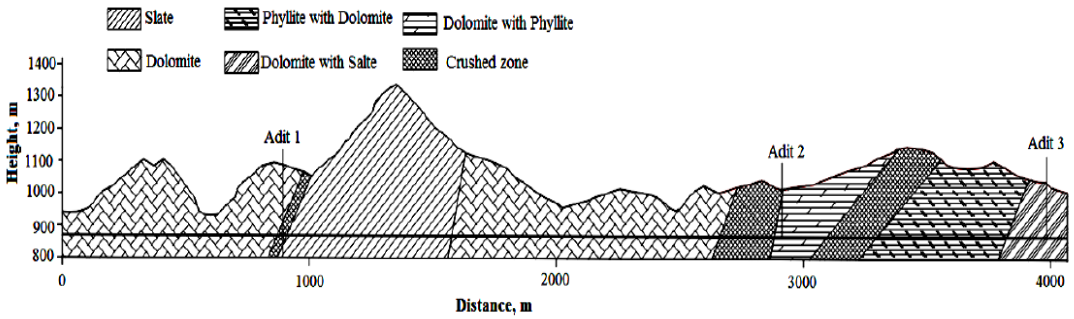

Fig. 4. Longitudinal geological section along Chameliya Head race tunnel (NEA, 1998)

III. Q-SYSTEM

CHEP has very poor rock masses. Rock masses here, are categorized in six classes, namely Q_1, Q_2, Q_3, Q_4, Q_5 and Q_6 with rock supports, namely R_1, R_2, R_3, R_4, R_5 and R_6 using Q system of rock mass classification (NEA, 1998). as shown in Table-I.CHEP has a weak rock mass with the least Q value of 0.01. For these rock masses with very less Q value, they undergo severe plastic deformation. Fig.2. shows existing R_6 support system before squeezing treatment was done.

Table-I: Rock Mass Classification for Rock mass at CHEP (NEA, 1998)

Rock Quality	Class	Support Class	Q value
Very poor	Q_6	R_6	Q<0.01
Poor	Q_5	R_5	Q<0.1
Fair	Q_4	R_4	0.1 to 1
Good	Q_3	R_3	1 to 4
Very Good	Q_2	R_2	4 to 10
Strong	Q_1	R_1	>10

IV. ANALYSIS OF PLASTIC DEFORMATION

Stability of tunnels passing through weak rock mass are significantly influenced by degree of maximum tunnel deformation and support pressure (stiffness) required to contain that deformation. Deformations are determined by various methods such empirical, semi-analytical, analytical and numerical methods. Empirical method (Singh et al (1992)) is only used for preliminary classification of squeezing. Similarly, semi-analytical method like Hoek &-Marions (2000) gives an idea about the final deformation of the tunnel wall considering the support pressure, but it neither gives an idea about the deformation of tunnel wall at the time of support installation nor does it specify the yielding of support. Analytical approach like Convergence Confinement Method gives idea about installation of optimum support at right location and support pressure required to maintain deformation within specified limit. This paper uses empirical, semi-analytical, analytical & numerical method to analyze stresses & deformation around tunnel contours.

A. Singh et. al (1992) Method

This method gives a preliminary idea on squeezing or non-squeezing rock masses based on rock mass classification system. Singh used 39 different tunnel case histories using data on Q-value and overburden to assess squeezing ground condition [3]. A clear line demarcates squeezing cases from non-squeezing cases. Analysis result is shown in Fig. 5. which shows that most of tunnel sections had excessive overburden due to which severe squeezing problem has been observed.

B. Hoek and Marinos (H/M) (2000) Method

H/M method is sophisticated approach to assess squeezing behavior of rock mass than empirical method. The extent of tunnel deformation after support installation can be calculated using H/M method. This method considers plotting of tunnel strain with respect to competency factor of rock mass which is actually the ratio of rock mass strength (σ_{cm}) & insitu stress (P_o) [4].Fig.6. shows that strain varies from 0 to as high as 50% which is significantly higher & abnormal condition. Because of this reason, there is severe squeezing problem and thus good support system is necessary.

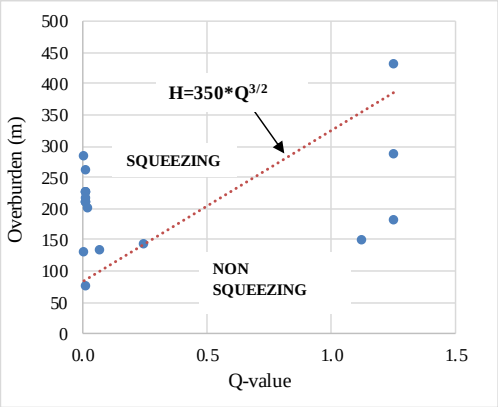

Fig. 5. Empirical method (Singh et. al (1992)) showing extreme squeezing at CHEP

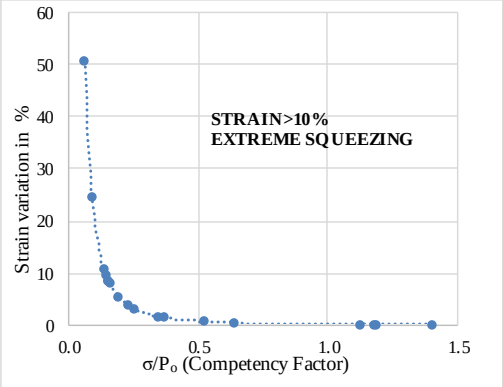

Fig. 6. Semi-analytical method (Hoek and Marinos (2000)) showing extreme squeezing at CHEP

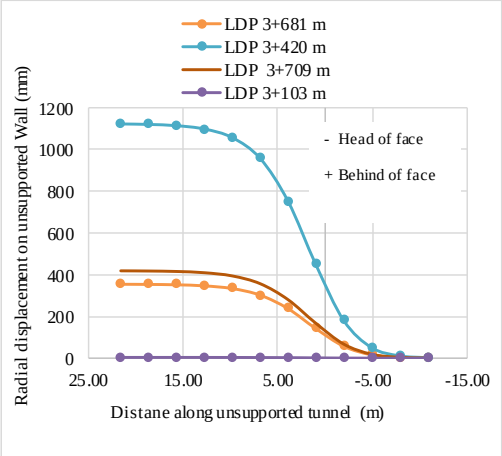

Fig. 7. Longitudinal Deformation Profiles along different chainages

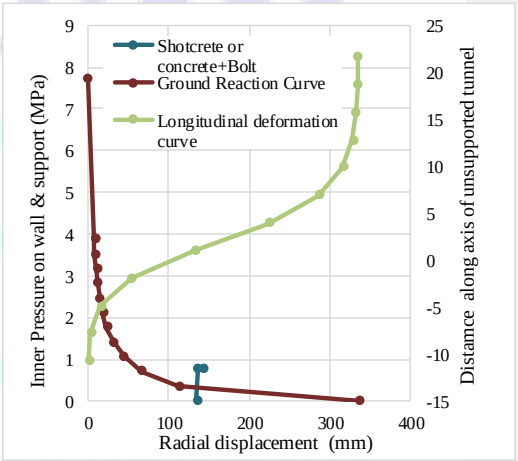

Fig. 8. Convergence Confinement Method (CCM) for Head Race tunnel Chainage 3+420 with support (Shotcrete +Bolt)

C. Convergence Confinement Method (CCM)

It is important that immediately after blasting of tunnel, final support system must not be applied. One must be careful enough to apply temporary support around tunnel so as to release stress and let tunnel to deform plastically before final support installation is carried out. CCM is one of such methods to predict or gives idea about installing optimum support at right location (how far from the face) and support pressure required to maintain deformation within specified limit. CCM incorporates elasto plastic behavior of rock mass. Various studied have been carried out for the approximation of longitudinal deformation and ground responses. A best fit curve suggested by Carranza-Torres and Fairhurst (2000) [5] has been utilized in this paper using data shown in Table-II to assess tunnel deformation.

Longitudinal displacement profile (LDP) has been constructed along different chainages considering a face length of 1m as shown in Fig. 7. Radial displacement is as high as 1.2 m , 22 m behind the face. Ground reaction curve (GRC) is plotted using section 3+420 m with 10.50 MPa overburden. Critical pressure (p_{cr}) around tunnel is around 3.8 MPa (Fig.8.). This is the point where transition of rock mass from elastic to plastic state occurs. When tunnel is not supported, maximum deformation with no internal pressure has been found out to be around 0.335 m.

Similarly, radial deformation without support increase upto 0.3 m at around 22 m behind the face. This value lowers ahead of face and becomes zero at around 10.8 m in front of the face. Face displacement of wall is found out to be lower than 0.1 m.

Table-II Data used for plotting LDP & CCM [2]

Rock Mass	Designation / Chainage (km)	3+103	3+420	3+681	3+709
σ_{ci} (MPa)	Intact compressive strength of rock	60	39	39	39
m_i	Intact rock mass parameter	10	8	8	8
N	Poisson Ratio of rock mass	0.25	0.1	0.1	0.25
Φ	Internal friction angle	30^0	30^0	30^0	30^0
GSI	Geological Strength Index	46	13	15	13
γ (MN/m^3)	Specific weight	2.72	2.40	2.40	2.72

V. TIME DEPENDENT ANALYSIS OF HEAD RACE TUNNEL OF CHEP

Creep is defined as the deformation of rock mass under a load that is less than strength of rock mass with time. Creep strain can seldom be recovered fully when loads are removed, thus it is largely plastic deformation. A time dependent creep analysis has been performed in this paper using radial displacement in the tunnel which has been analytically found out using equations (3-5), given by [6].

$$\frac{u_r}{r} = \lambda_e \frac{6_o}{2G_o} (\frac{r_p}{r})^2 * (1 + \frac{G_o}{G_f}(f(t)) \quad \ldots\ldots (3)$$

where, u_r =Radial Displacement around Tunnel

r = Radius of Tunnel

λ_e=Advance Parameter

6_o =Insitu stress

r_p =Plastic Radius of tunnel

G_o =Rock mass Shear Modulus

G_f =Rock mass Creep Modulus

$f(t)$ =Creep Function

$\lambda_e \frac{6_o}{2G_o} (\frac{r_p}{r})^2$ function of face advance effect

$1 + \frac{G_o}{G_f}(f(t)$ function of creep effect.

Value of Shear Modulus of rock is calculated from equation (4) as

$$G_o = \frac{E}{2(1+V)} \quad \ldots\ldots (4)$$

where,

E=Rock mass Young Modulus

V= Poisson Ratio

Similarly,

$$f(t) = 1(\frac{T}{t+T})^m \quad \ldots\ldots (5)$$

where,

T=Relaxation Time

t=Total Time under consideration

m=0.2 to 0.5, Constant

Since the tunnel is driven in fractured rocks, generalized Hoek-Brown failure criterion (non-linear) is used in analytical solution, considering plastic nature of the rock mass. A sample of Hoek-Brown parameters for Talcosis Phyllite at CHEP used, has been shown in Table-III.

CHEP Tunnel was assessed for creep. A total time of 2555 days corresponding to 7 years were considered to find out deformation of tunnel due to creep analytically using Panet equations (3-5). Altogether,4 different cross sections with an overburden of varying from 180 m to 285 m and rock type such as Crushed Talcosis Phyllite with

Q value 0.01 (Very Poor), Dolomite, and Phyllite were used during analysis (Fig. 10. & 11.).

Measured Convergence was as high as 1.57 m at chain age 3+420 m. Analytical solution to this chain age yielded a total convergence of 1.48 m in the roof where as a convergence of 1.28 m was noticed in side walls of tunnel (Fig. 10. & 11.). Figure 12. shows comparison of maximum tunnel wall closures at various chain ages both measured & analytical which are similar.

VI. NUMERICAL MODELING

Head race tunnel of CHEP has been simulated using Roc Science software to assess distribution of principal stresses and deformation around tunnel before and after support installation Tunnel was modeled with internal pressure reduction technique [7] by applying Generalized Hoek and Brown failure criteria. A horse shoe tunnel section of 5.2 m diameter (Fig.9.) was modeled before and after support installation. Overall geometry of model of 6 times diameter of the tunnel section was taken and restrained in both x and y direction. Stage corresponding to tunnel relaxation was computed using Vlachopoulos & Diederichs method [8] and then support installation was carried out.

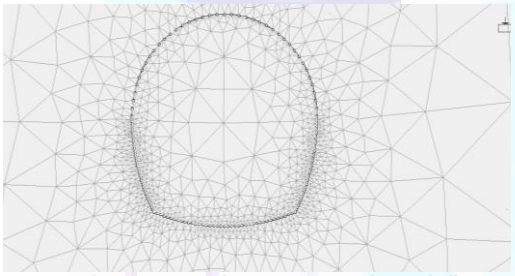

Fig. 9. Mesh Generation and Excavation on Talsocic Phyllite

Various material properties adopted for numerical simulation has been presented in Table-III. Material properties have been extracted from geological report of Chameliya Hydroelectric project by Nepal Electricity Authority (NEA, 1998). For studying the tunnel stability in plastic state, generalized Hoek and brown failure criteria [7] is selected.

Affected zone of six times dimension of tunnel in form of a box shape has been used. Triangular mesh, denser around tunnel contour, i.e. finer meshing round tunnel is used (Fig.9.) so as to increase accuracy of computation analysis.

Table-III Mechanical properties of rock mass at CH 3+420 (NEA, 1998)

Initial element loading	Field stress
Rock Type	Talcosic Phyllite
Specific Weight of Rock	27.8 kN/m^3
Elastic type Insitu Stress (σ_0)	Isotropic
Uniaxial Compressive Strength	8.77 MPa
Young's modulus	7 GPa
Poisson ratio	0.25
Failure Criterion	Generalized Hoek and Brown criteria
Material type	Plastic
Compressive strength	8.77 MPa
Peak Angle of Int. Friction	35 degree
Cohesion	0.05 MPa
Total Time	2555 days
Relaxation Time	0.2 days
Shear Modulus	2916.66 MPa
Young Modulus	7000 MPa
Creep Modulus	30 MPa

Principal stresses have been investigated around tunnel section 3+420 m as the reference section .Major principal stress (σ_1) was found to be as high as 18.60 MPa in tunnel without any support system (Fig.15) which lowers to 8.35 MPa after support installation. (Fig.16). The shear and tension failures were precisely noticed all-round the tunnel.

Due to excessive overburden, numerical modeling resulted tunnel deformation as high as 1.1 m. Thus, this project has severe squeezing problem due to heavy overburden and poor, fragile, highly jointed rock. Stress is dominant and this resulted excessive displacement around periphery of this section (Fig. 17 and Fig. 18). Maximum total displacement varies from 0 to as high as 36 cm. Numerical simulation has revealed that the maximum strain around tunnel was about 23% which is less than that suggested by Hoek and Marinos (2000) method. Strain of about13% is seen at the crown of the tunnel and of about 8% tunnel closure has been noticed at the side wall of the tunnel. Nevertheless, maximum strain of 23% is also very high and this tunnel section requires special squeezing treatment. Strength factor is also lesser than 1 (Fig.19).

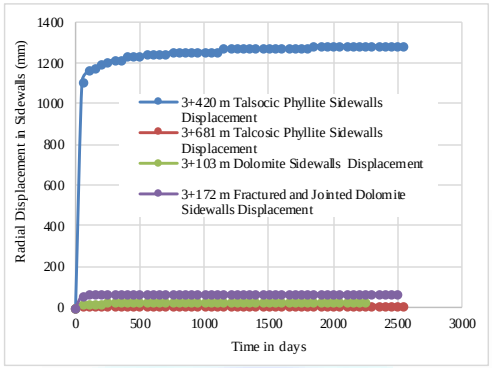

Fig.10. Time dependent side walls deformation at CHEP

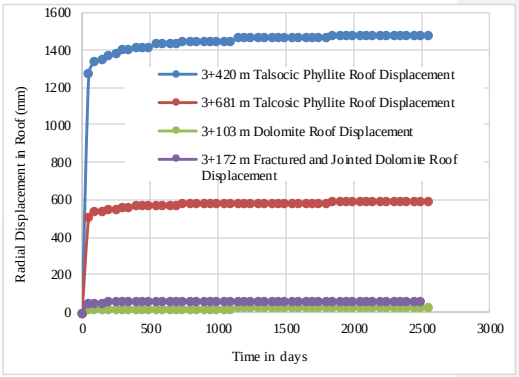

Fig. 11. Time dependent roof deformation at CHEP

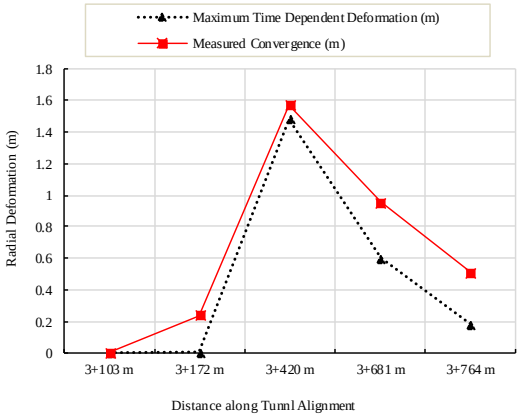

Fig.12. Tunnel Wall Closure at various Chain ages

VII. CONTROLLING SQUEEZING

A thorough study has been done for problems regarding tunnel squeezing along this hydroelectric project and have come to conclusion that the striking problem is the tunnel alignment. The alignment has very extreme overburden which has extensively helped to produce maximum squeezing problem. Now, that it is not the preliminary phase of project, so tunnel alignment cannot be changed. Therefore, the only way is to modify existing support system by increasing its stiffness. It has been shown that the modification of the support can retain squeezing problem, as shown in Table-IV below:

Table-IV Support system recommended at Chainage

Initial Support System	Modified Support Systen
Concrete Lining:0.40 m	Concrete Lining:0.90 m
Steel Set: W100*19.5	Steel Set: W200*15
Shotcrete:0.10 m M20	Shotcrete:0.30 m M50

3+420

Fig. 13. and 14. show the difference between use of existing support system and modified support system at chain age 3+420 of CHEP. Fig. 13. shows that the existing support fails in both shear and moment and has factor of safety lesser than 1. Therefore, they are not able to retain squeezing.Fig.14. shows modified support system which is has been able to retain squeezing within safety limit.

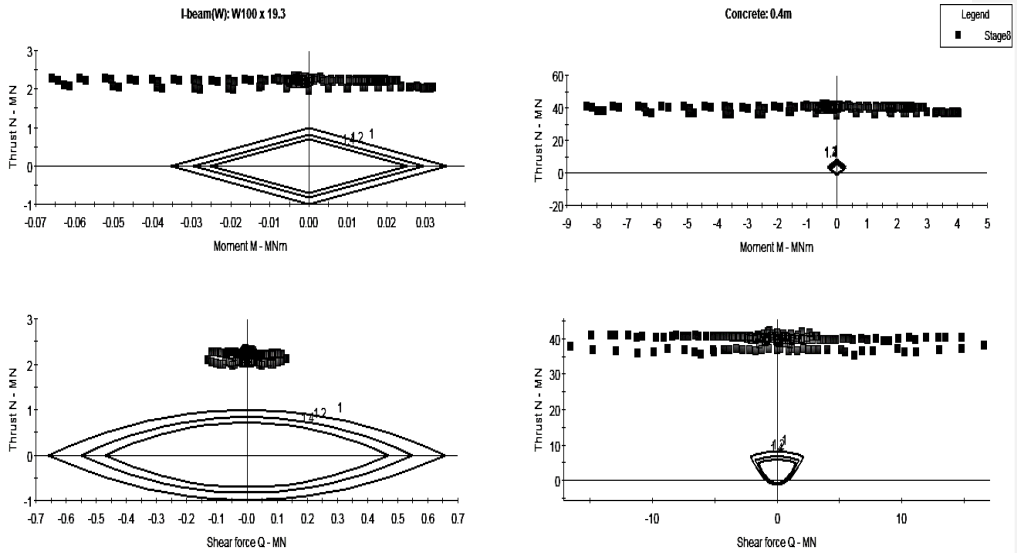

Fig. 13. Support Capacity Plot with existing Support System at Chainage 3+420 in RocScience v.9

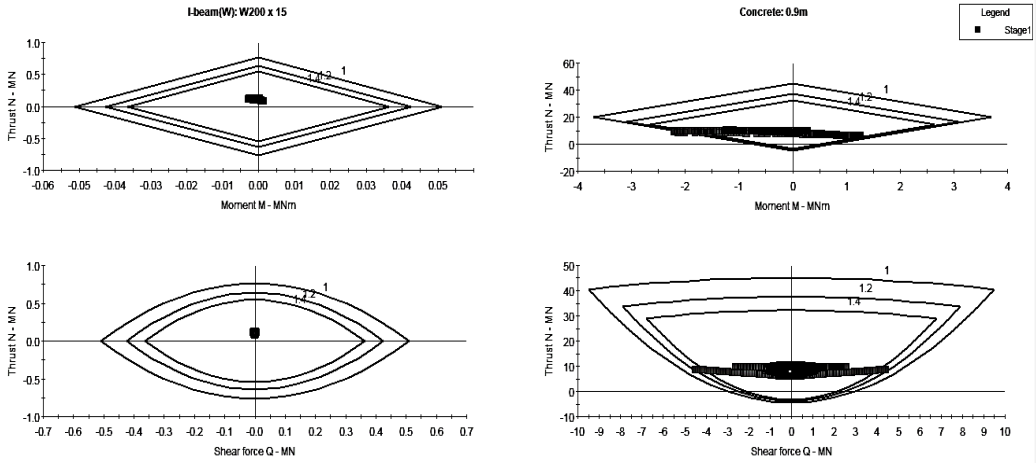

Support Element: Liner 1

Fig.14. Support Capacity Plot with modified Support System at Chainage 3+420 in RocScience v.9.0

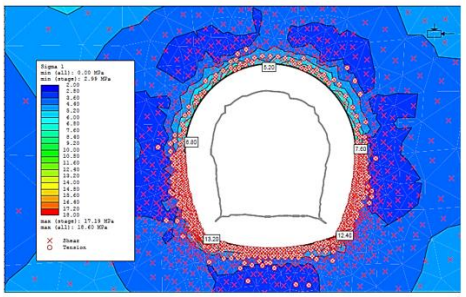

Fig. 15. Major Principal Stress variation (without support)

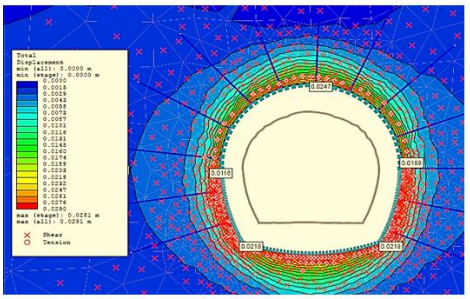

Fig. 18. Maximum displacement variation (existing support)

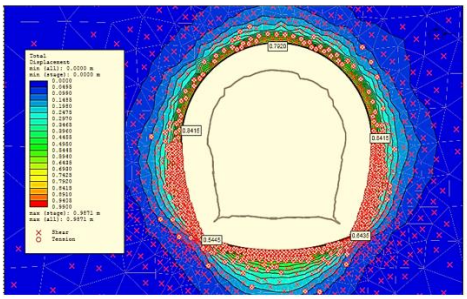

Fig. 16. Maximum displacement variation (without support)

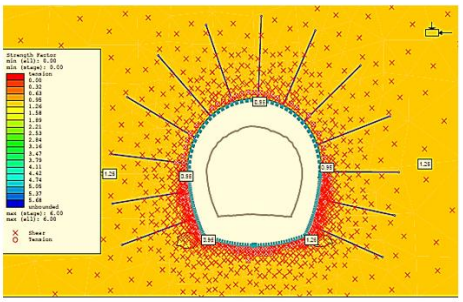

Fig. 19. Strength Factor variation (existing support)

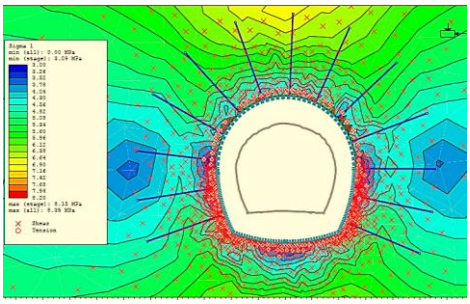

Fig. 17. Major Principal stress variation (existing support)

I. CONCLUSION

Underground civil constructions on young and weak Himalaya of Nepal is extremely vulnerable to various stability problems due to high in-situ stresses resulting excessive plastic deformation. Analysis of squeezing on one of such vulnerable tunnels at Nepal lesser Himalaya was carried out using four different methods and these were empirical (Singh et.al,1992), semi-analytical (Hoek & Marinos,2000), analytical Convergence Confinement Method (Carranza Torres & Fairhurst, 2000) with Hoek and Brown failure criteria and 2D finite element numerical analysis using Rocscience.v.9.0. Deformation at different sections was carefully calculated and subsequently compared with measured results. It has been found that above mentioned methods give precise result regarding stability issues related to squeezing in weak geology of Nepal lesser Himalaya. Analysis suggested that head race tunnel of studied project suffered from excessive tunnel deformation. Existing support system in selected tunnel section provided only around 0.75 MPa support pressure which is significantly lower

than required. Therefore, with this existing support system, there was maximum tunnel deformation of around one meter from numerical simulation which is extremely large. Thus, it is recommended that support system must be modified by increasing stiffness of support system to lower down squeezing problem.

ACKNOWLEDGEMENT

Author acknowledges Chameliya Hydroelectric Project, Nepal for geological reports and data required to produce this paper.

REFERENCES

[1] K. K. Panthi, "Analysis of engineering geological uncertanities related to tunneling in Himalayan rock mass condition," Norwegian University of Science & Technology, Norway, 2006.

[2] NEA, "Nepal Electricity Authority,Geological report on Chameliya Hydroelectric Project, Nepal," 1998.

[3] B. Singh, J. Jethwa , A. Dube and B. Singh , "Correlation between observed support pressure and rock mass quality," *Tunneling & Underground Space Techonology*, vol. 7, no. 1, pp. 59-74, 1992.

[4] P. Marinos and E. Hoek, "Predicting tunnel squeezing problems in weak heterogenous rock masses," *Tunnels and Tunneling International,32(11),45-51 and 32(11)*, pp. 34-46, 2000.

[5] C. Carranza-Torres and C. Fairhurst, "Application of the Convergence-Confinement method of tunnel design to rock masses that satisfy the Hoek-Brown failure criterian," *Tunneling and Underground Space Technology*, pp. 187-213, 2000.

[6] J. Sulem, M. Panet and A. Guenot, "An Analytical Solution for Time-dependent Displacements in a Circular Tunnel," *Int. J. Rock Mech. Min. Sci.& Geomech.Abstr. Vol. 24, No. 3*, pp. 155-164, 1987.

[7] Rocscience, "2D finite element analysis. Version: 9.008, User Manual.," Rocscience Inc., 2016.

[8] N. Vlachopoulos and M. S. Diederichs, "Improved Longitudinal Displacement Profiles for Convergence Confinement Analysis of Deep Tunnel," *Rock Mechanics and Rock Engineering* , pp. 131-146, 2009.

[9] L. F. P. Upreti BN, "Lesser Himalayan crystalline nappes of Nepal: problem of their origin," *Geological Society of America*, p. 225–238 , 1999.

AUTHOR PROFILE

Nitesh Shrestha is a hydropower engineer with his Master's of Science in Hydropower development (2018-20) from Norwegian University of Science & Technology,Norway. He has over 5 years work experience in hydropower & tunneling sector. His interests are study of underground structures in weak rock masses.

Part V: Building Technology

Development of a Model Updating Technique Using Soft Computing

Yogesh Yadav[1], Ishwor Singh Saud[2].

[1]Lecturer (M Tech Structural Engineering) at ACEM, Civil Engineering Department, Lalitpur

[2]*Structural engineer (M Tech)*

Civilonyogi1010@gmail.com[1], ishworsingh16@gmail.com[2]

Abstract

The structural models, do not necessarily predict the measured data sufficiently accurately. Because of this, there is a need for these models to be updated to better reflect the measured data. This paper introduces computational intelligence techniques to update finite element models. The model updating is formulated as a constrained optimization problem and solved using a recently developed meta-heuristic algorithm called Artificial Bee Colony (ABC) algorithm. A MATLAB code is developed using the model-updating formulations presented in this paper. Numerical simulation studies are carried out by solving for the proposed model updating technique by using pseudo-experimental data of an 8 storey framed structure and also the experimental data of ASCE three storey benchmark structure. Studies presented in this paper clearly indicate the effectiveness of the proposed computational intelligence-based model updating technique.

Keywords: *MATLAB, Artificial Bee Colony (ABC), Finite element models, ASCE three storey benchmark structure*

Introduction

Model updating of civil engineering structures has a great significance in the area of active and semi-active control of structures and structural health monitoring. Model updating is typically performed by updating the structural stiffness and mass matrices in order to obtain good matching of the responses obtained from the analytical structure from the corresponding experimental model. In view of the importance of model updating in engineering structures research is being carried out actively from past three decades. New and innovative techniques are being developed and reported regularly in the literature. This is clearly manifested from the huge haul of literature with several special issues of journals and conference proceedings [Chang (2003), Beck and Wu (2006)]. Model updating is typically being carried out using experimentally identified natural frequencies, mode shapes, frequency response functions etc. Since civil engineering structures are mammoth, the finite elements of these structures will obviously have a large number of degrees of freedom. This poses a serious problem for model updating as the number of unknown variables in the form element stiffness and or mass matrices increases. One alternative is to handle this problem is parameterization, using which we can reduce the

number of unknown variables in the model updating process. However, the parameterization is usually carried out based on the user's discretion. Here the user's experience comes into the picture. Hence, with parameterization, the process of model updating become subjective. Alternative formulations for model updating has been attempted in the literature by applying the orthogonality concepts, connectivity and/or boundary condition to correct/update the analytical model with Lagrange multiplier or generalized inverse method[Wei (1990), Farhat and Hemez (1993), Lin et al. (1995), Hua et al.(2009a,2009b)].In these type of approaches, the, stiffness and mass matrices obtained using the finite element idealisation of the structure are modified in order to correlate the natural frequencies and mode shapes obtained from the numerical model with the experimental model. Recently computational intelligence algorithms are being popularly used in the majority of civil engineering applications including structural system identification, structural health monitoring and also vibration control. Keeping this in view in the present work an attempt has been made to develop a computational intelligence-based model updating algorithm. In the present work, the modelling updating procedure is formulated as a constrained optimization problem and solved using the recently developed meta-heuristic algorithm called Artificial Bee Colony (ABC) algorithm. The proposed model updating algorithm is formulated in such a way that the natural frequencies and mode shapes are correlated and the mass and stiffness orthogonality is maintained. Numerical simulation studies have been carried out using framed structures. An eight-storey framed structure is employed by generating pseudo-experimental data in order to verify the proposed model updating procedure. Later the experimental data available in the literature related to ASCE three storey benchmark structure is used to demonstrate the effectiveness of the proposed algorithm.

Methodology

The following are the steps involved in the model updating process, which are common to every model irrespective of their type, properties, conditions etc.:

Step-1: Collect the corresponding response data after conducting the experiment from the experimental model.

Step-2: Develop a mathematical tool using the standard mathematical formulation that defines the experimental model using a computer program.

Step-3: Calculate the error between the experimental and analytical response data. If the error is very large, then re-conduct the experiment. Otherwise, select a proper optimization tool.

Step-4: Vary different parameters of the model (Material or Geometric) in the optimization process within their acceptable ranges and run the optimization process.

Step-5: Input these parameters in the mathematical tool developed and calculate the error again.

Step-6: If the error reduced, then update the numerical model with the optimal parameters obtained and this updated numerical model can be used for simulating the experimental model.

Step-7: If the error is not reduced, then there might be some problem with the experimentation or computation and it is suggested to repeat those steps again. The flow of computations is shown below:

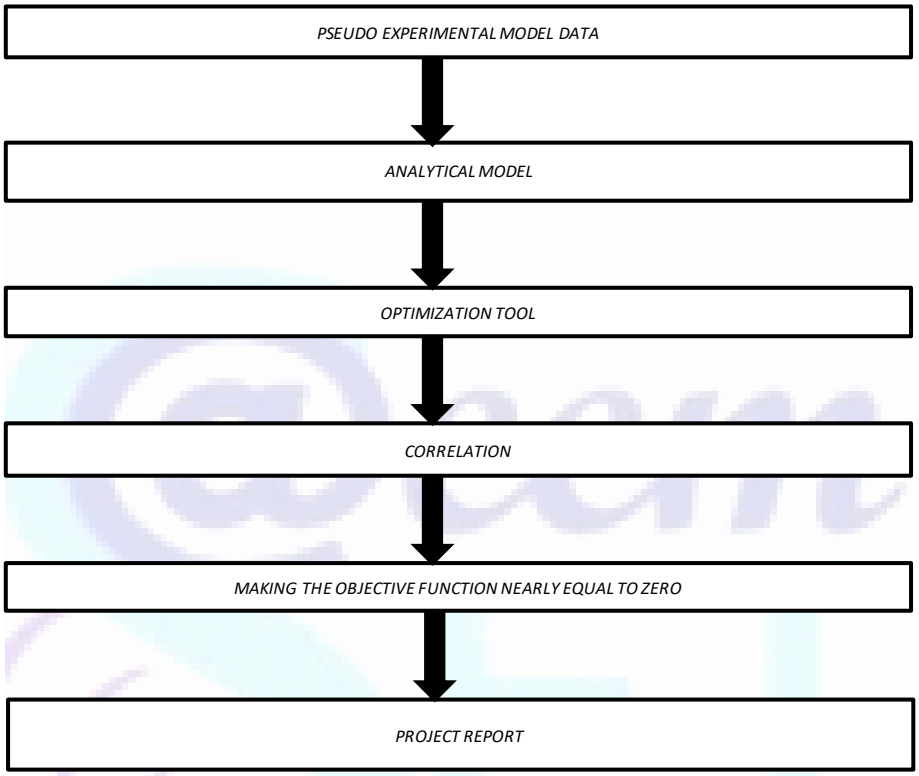

Formulation details

The dynamic equilibrium equation for any finite element idealisation can be written as

$$M\ddot{x}(t) + C\dot{x}(t)\ \ Kx(t) = F(t) \qquad (1)$$

With initial conditions $x(0) = x_0$ and $x(0) = x_0$

Where matrices M, K and C represent mass, stiffness and damping respectively. x is displacement, $\dot{x}$ is the velocity and $\ddot{x}$ is the acceleration vector

A free vibration problem can be formulated by assuming that the dynamic response is harmonic in nature. Accordingly substituting

$$\left.\begin{aligned} x &= \phi \sin\omega t \\ \dot{x} &= \phi\omega\cos\omega t \\ \ddot{x} &= -\phi\omega^2 \sin\omega t \end{aligned}\right\} \qquad (2)$$

Accordingly substituting the equations (2) in equation (1), and setting damping and also the external force to zero, the following relationship can be obtained.

$K\phi = \omega^2 M\phi$ or $K\phi = \lambda M\phi$ (3)

It should be mentioned here that the damping in equation (1) is set to zero and the force vector is also set to zero as the objective function is to obtain undamped free vibration.

Solving Equation (4) by using any popular Eigensolver, the Eigenvalues representing the natural frequencies ($\sqrt{\omega^2}$) and Eigen vectors representing the mode shapes of the structure can be obtained. It is well known that the structural modes are orthogonal to stiffness and mass.

$$\phi^T M\phi = I \quad ; \quad \phi^T K\phi = \mathrm{diag}\left(\omega_1^2, \omega_2^2, ..., \omega_n^2\right) \equiv \lambda \tag{4}$$

M represents mass matrix and K represents the stiffness matrix.

Formulation of objective function for model updating

As mentioned earlier, the proposed model updating procedure is formulated as an optimization problem and solved using recently developed meta-heuristic called ABC algorithm. The fitness or objective function is formulated as follows

$$OBJ = \sum_{i=1}^{NF} ABS(\omega_i{}^E - \omega_i{}^A) + \sum_{i=1}^{NF}[1 - MAC(\Phi_i^E, \Phi_i^A)] + \sum_{i=1}^{NP} ABS(POV_i^E - POV_i^A) + \sum_{i=1}^{NP}[1 - MAC(POM_i^E, POM_i^A)] \tag{5}$$

With the following constraints

The details related to proper orthogonal decomposition with the following constraints.

$$\left.\begin{aligned} &[\overline{\phi}_i^A]^T [M] [\overline{\phi}_i^E] \neq 0 \\ &[\overline{\phi}_i^A]^T [K] [\overline{\phi}_i^E] \neq 0 \text{ where } i = 1, 2, 3 \ldots\ldots m \end{aligned}\right\} \tag{7}$$

Sum of non-diagonal elements of matrix $[[\overline{\phi}_i^A]^T [M] [\overline{\phi}_i^E]]$ are ≈ 0.

Sum of non-diagonal elements of matrix $[[\overline{\phi}_i^A]^T [K] [\overline{\phi}_i^E]]$ are ≈ 0.

Where NF is the number of natural frequencies, superscript, E represents experimental, superscript, A represents analytical. POM and POV represent the proper orthogonal modes and proper orthogonal vectors respectively. These POMs and POVs can be obtained using proper orthogonal decomposition. Similarly, MAC is the Model assurance criteria. The proper orthogonal decomposition and also the model assurance criteria are discussed in the next section

Proper orthogonal decomposition

POD Kerschen and Golinval (2002) provides a substratum for the spectral decomposition of a spatiotemporal signal and its property of mean-square optimality provides an efficient denotes of capturing the ascendant components of a high dimensional signal through a few ascendant scales of fluctuations called Proper Orthogonal Modes.

The acceleration response function at the i^{th} (i= 1 to k time steps) step obtained at n spots looks like

$$\ddot{v}(t_i) = \begin{bmatrix} \ddot{v}_1(t_i) \\ \vdots \\ \ddot{v}_n(t_i) \end{bmatrix} \quad (6)$$

The matrix of the response correlation $R_{uu} \in R^{nxn}$ in the time domain got to be $R_{uu}=\langle \ddot{v}(t)\ddot{v}^T(t)\rangle$, where $\langle . \rangle$ represents time averaging operator. Further, its spectral decomposition is acquired as $R_{uu} = \sum_{i=1}^{n}\lambda_i \phi_i\phi_i^T$ where λ_i represents eigenvalues of R_{uu} and ϕ_i represents eigenvectors which form an orthonormal basis. The first few ascendant modes known as the proper orthogonal modes have the greatest amount of energy and required to be selected. If $E= \sum_{j=1}^{n}\lambda_j$ is the total energy content in the data, then $\sum_{j=1}^{p}\frac{\lambda_j}{E} \geq K$ is the p modes need to capture K energy of the measured accelerations. λ_i are the proper orthogonal values (POVs) and ϕ are the proper orthogonal modes (POMs).

Model assurance criterion

The model assurance criterion (MAC) is used to estimate the degree of correlation between the analytical mode shapes and experimental mode shapes. The value of MAC is in between 0 and 1. MAC can be calculated by the following formula,

$$MAC_{jk} = \frac{\left|\{\phi_{mj}\}^T\{\phi_{ak}\}\right|^2}{[\{\phi_{ak}\}^T\{\phi_{ak}\}]\,[\{\phi_{mj}\}^T\{\phi_{mj}\}]} \quad (7)$$

Here, MAC is modal assurance criterion;
$\{\phi_{mj}\}$ represents experimental mode shapes.
$\{\phi_{ak}\}$ represents analytical mode shapes.

A value of MAC closes to 1 suggests that the two mode shapes are well correlated, while a value close to 0 indicates that the mode shapes are poorly correlated.

Artificial bee colony (abc) algorithm

The Artificial Bee Colony (ABC) algorithm is a swarm predicated meta-heuristic algorithm. This method was founded by Karaboga in 2005 for optimizing numerical problems.

In ABC model, the colony consists of three components. They are1) Employed bees, 2) Onlookers and 3) Scouts. It is postulated that the number of employed bees is equal to the number of the sources of the food situated around the hive. Employed bees go to their food source and come back to hive and dance on this area. The employed bee whose food source has been forsaking becomes a scout and commences to probe for finding an incipient aliment source. Onlookers watch the dances of employed bees and operate food sources based on dances.

The following are the steps of the algorithm: -

- Food sources are produced initially for all the employed bees.
- REPEAT
    - Each employed bee peregrinates to a food source in her memory and finds the nearest source, then determines its nectar amount and dances in the hive.
    - Each onlooker watches the dance of employed bees and selects one of their sources based on the dances, and then peregrinates to that source. After selecting a neighbour around that, she determines its nectar amount.
    - Food sources which are deserted are determined and are superseded with the new food sources discovered by scouts.
    - The best food source, so far found is stored.
- Till the requirements are met.

The flow chart of the ABC algorithm is shown in Figure 1.

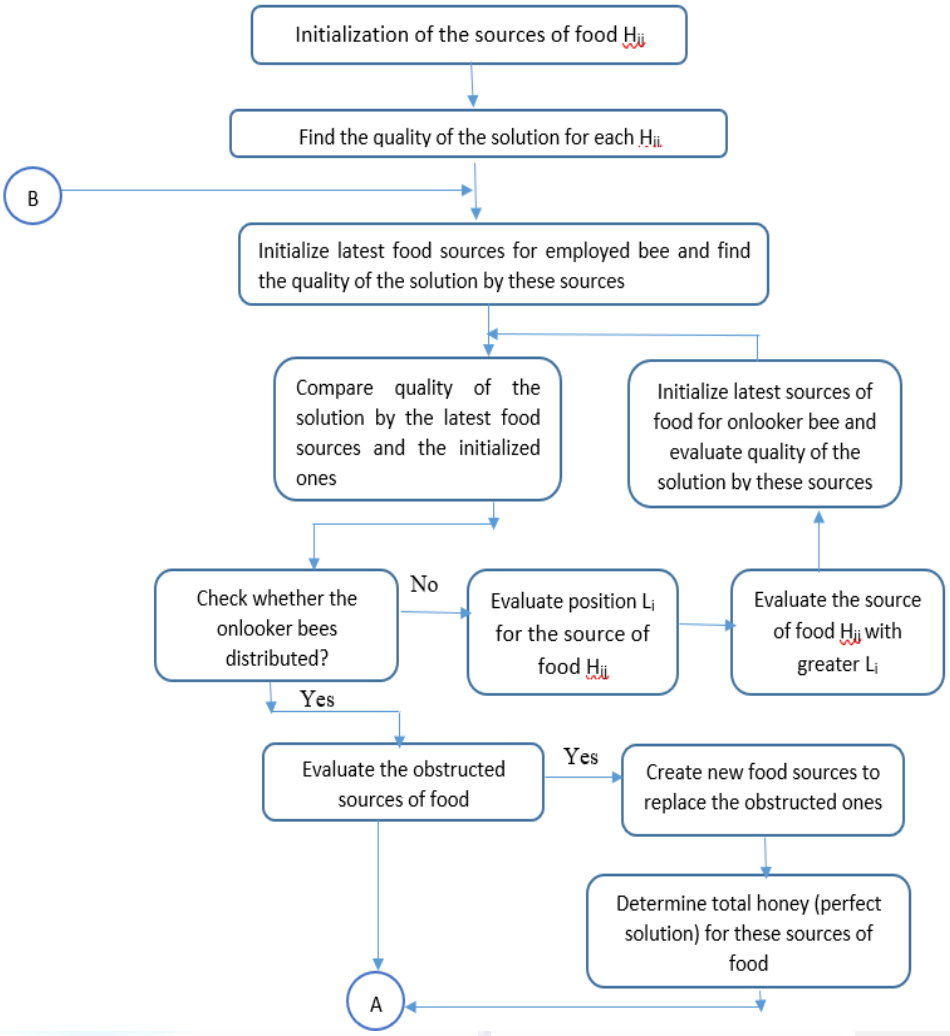
Initialization of the sources of food H_{ij}
Find the quality of the solution for each H_{ij}
B
Initialize latest food sources for employed bee and find the quality of the solution by these sources
Compare quality of the solution by the latest food sources and the initialized ones
Initialize latest sources of food for onlooker bee and evaluate quality of the solution by these sources
Check whether the onlooker bees distributed?
No
Evaluate position L_i for the source of food H_{ij}
Evaluate the source of food H_{ij} with greater L_i
Yes
Evaluate the obstructed sources of food
Yes
Create new food sources to replace the obstructed ones
Determine total honey (perfect solution) for these sources of food
A

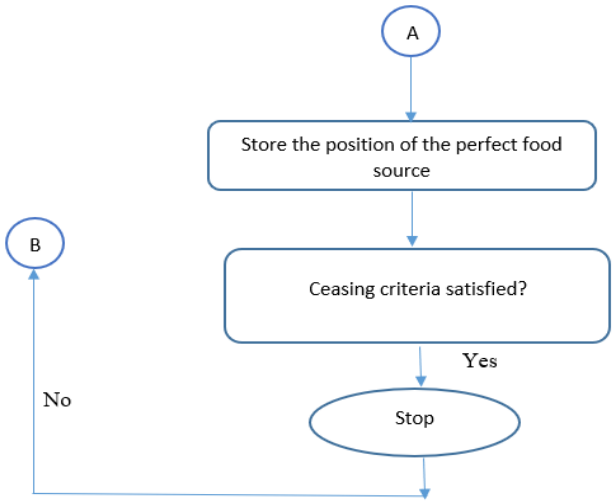

Figure 1. Flow chart of ABC algorithm

Numerical studies

A MATLAB code is developed for the proposed model updating technique discussed in the earlier sections. Numerical simulation studies have been carried out by solving an 8 storey framed structure shown in Figure 2. In order to simulate model updating procedure analytical stiffness and mass matrices of the framed structure are multiplied by a random stiffness factor ranging from 0.8 to 1.0. The resulting responses are assumed as experimental data and model updating procedure is carried out accordingly.

In this example, an 8 DOF framed structure is taken into consideration. The stiffness, damping, masses of the storeys are given below. The frame is idealized as a shear building model. In order to alter the model for the purpose of demonstrating the updating model procedure. The mode shapes and the mode frequencies obtained from this model is assumed as to be the experimental modal data. The modal frequencies (in Hz) of the actual system, the updated model, and the analytical model with a varied number of observed modes are shown in Table 1 below.

Natural frequencies for 8-DOF:

Structural properties of the 8-DOF system.

Stiffness for level 1 is 5529 KN/m and for level 2-8 is 2723 KN/m

Masses for level 1–7 is 49.48kg and for level 8 is 45.06kg

Damping for all level is 1%.

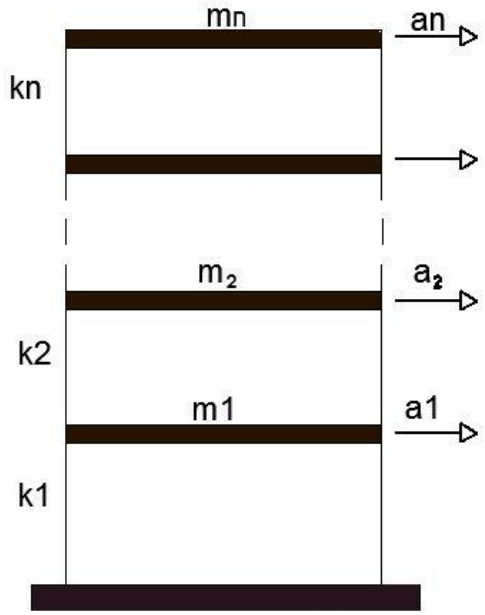

Figure 2. Eight storey framed structure

Table1. Performance of the proposed model updating technique-comparison of natural frequencies of eight storey framed structure

Pseudo-experimental frequency	**Numerical model frequency**	**Percentage change**
(Hz)	(Hz)	(%)
0.2205	0.2182	1.04
0.6189	0.6103	1.39
1.0005	1.0033	-0.28
1.4259	1.4296	-0.26
1.7755	1.7768	-0.07
1.9404	1.9412	-0.04
2.0949	2.0830	0.57
2.2607	2.2256	1.55

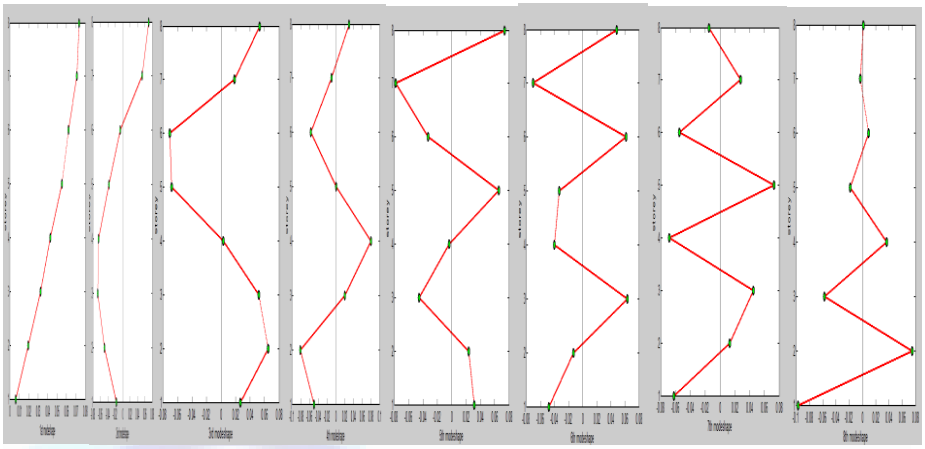

Figure 3. Numerical Example 1: Comparison of mode shapes:

The IASC-ASCE SHM benchmark structure is a four-storey, two-bay by two-bay steel frame quarter-scale model structure fabricated at the earthquake engineering research laboratory at the University of British Columbia (UBC). The plan dimensions of the scaled-down model is 2.5 m x 32.5 m and the height is 3.6 m. Further details about this model can be found in Johnson *et al* (2004). An analytical model of the structure is shown in Figure 4.

The shear building model is utilized for the SHM benchmark problem to get the simulated data. In the present model, the floor beams and floor slabs move as rigid bodies. Therefore, there is one DOF's per floor. The natural frequencies obtained using the proposed model updating procedure are compared with the experimental natural frequencies and are shown in Table 2. The experimental mode shapes are compared with the theoretical mode shapes obtained using the proposed model updating technique is shown in Figure 5. It can be observed from the results furnished in Table 2 and Figure 5, that there is a very close agreement in the values clearly demonstrating the effectiveness of the proposed model updating procedure.

Figure 4. IASC-ASCE SHM benchmark structure

Table 2. Comparison of natural frequencies obtained using the model updating technique with the experimental data

Frequencies (Hz) taken From the experimental data of IASCE-ASCE Benchmark	**Analytical Frequencies (Hz) obtained using the proposed model updating technique**	**Error %**	
9.4156	9.4147	0.096	
25.5579	25.4107	0.576	
38.6830	38.6472	0.093	
48.0317	47.9509	0.168	

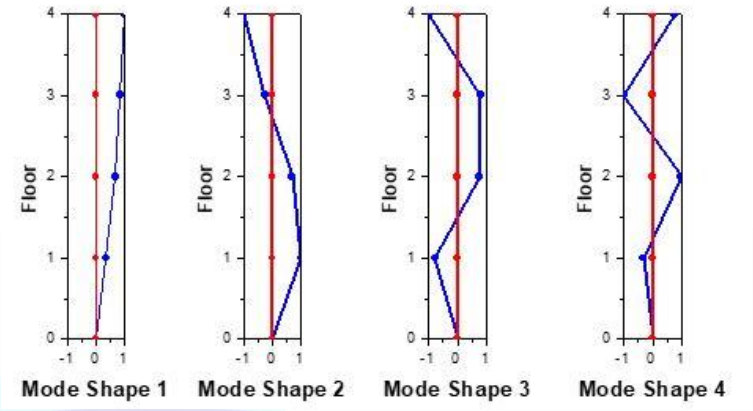

Figure 5. Comparison of experimental mode shapes with the theoretical mode shapes obtained using the proposed model updating technique

Conclusion

In this paper, a model updating technique using soft computing technique is presented. The problem of model updating is formulated as a constrained optimization problem and solved using a metaheuristic algorithm. In this paper, a recently developed Artificial Bee Colony (ABC) algorithm is employed for solving the constrained optimization problem. Numerical simulation studies have been carried out by solving two frame examples to demonstrate the effectiveness of the proposed model updating procedure. Among them, one is the IASC-ASCE benchmark experimental structure. The numerical investigations presented in this paper clearly demonstrate the effectiveness of the proposed model updating procedure and reemphasizes the utility of computational intelligence technique in the field of structural engineering.

References

1. E A Johnson *et al*, 'Phase I IASC-ASCE structural health monitoring benchmark problem using simulated data', Journal of Engineering Mechanics, Vol 130, No 1, pp 3-15, 2004. DOI: 10.1061/(ASCE)0733-9399(2004)130:1(3).
2. Farhat, C., Hemez, F.M. (1993), "Updating finite element dynamics models using element-by-element sensitivity methodology." AIAA J., 31(9), 1702–1711.
3. Yuen, K.V., Beck, J.L., Katafygiotis, L.S. (2006), "Efficient model updating and monitoring methodology using incomplete modal data without mode matching." Structural Control Health Monitoring. 13(1), 91–107.

4. Lin, R.M., Lim, M.K., Du, H. (1995), "Improved inverse eigensensitivity method for structural analytical model updating." J. Vibr. Acoust., 117(2), 192–198.
5. Zhang J, Sato T, Iai S. Support vector regression for online health monitoring of large-scale structures by a novel signal processing technique. Earthquake Engineering Struct Dyn 2007;36(7):909–25
6. S W Doebling et al, 'A summary review of vibration-based damage identification methods', The Shock and Vibration Digest, Vol 30, No 2, pp 91-105, 1998.
7. Park *et al*,. (2001): Determination of an optimal regularization factor in system identification with Tikhonov regularization for linear elastic continua. Int. J. Numer. Methods Eng, vol. 51, no. 10, pp. 1211–1230.
8. Hua, X.G *et al*, (2009b), "Adaptive regularization parameter optimization in output-error-based finite element model updating," Mech. Syst. Signal Process. 23(3), 563–579

Science Engineering and Technology (SET) Conference – 2021

Experimental Investigation on The Mechanical Properties of Cement Mortar Incorporated with Graphene and C&D Waste

Asmita Subedi[1], Ankush Jha[2*], Pashupati Deo[3], Aagya Dahal[4]

Department of Civil Engineering, Ramaiah Institute of Technology, Bangalore, Karnataka[1234]

subediasmita07@gmail.com[1], jha.ankush1@gmail.com[2], deopashupati2664@gmail.com[3], aagya.dahal1@gmail.com[4]

Abstract

Concrete is one among the essential materials utilized in engineering works. The two main properties which attribute to the reliability of concrete as a universal choice are strength and durability. Despite its remarkable properties, it has few shortcomings, namely, low tensile strength, low ductility, and unavoidable cracks. All of these inadequacies are the result of the relatively porous microstructure of concrete. The use of nanomaterials is the most influential and powerful alternative to overcome these limitations. In this paper, a comparative study of the mechanical properties of normal strength mortar over the mortar reinforced with graphene has been presented. Making use of the construction demolition waste in different proportions, namely, 25% and 50% as the partial replacement for fine aggregate, graphene was incorporated in the cement mortar of 1:3 grade in the proportion of 0.1%, 0.4%, 0.7%, and 1% by weight of cement respectively. The proportion of construction demolition waste and graphene were consequently varied and the corresponding change in mechanical properties, namely, compressive strength, tensile strength, and flexural strength of cement mortar was observed on the 7th day, 14th day, 21st day, and 28th day respectively and the same was compared with the result of normal mortar. It was observed that these mechanical properties increased with an increase in the proportion of graphene up to a certain limit after which it decreased. However, the optimum percentage of graphene varied along with the variation in the percentage of C&D waste.

Keywords: *Concrete, Nano Materials, Graphene, C&D Waste, Mechanical Properties*

1. Introduction

Cement concrete is one of the fundamental building and construction material used worldwide. It is durable and has outstanding properties to supplement the construction field under docile environments. Although highly durable, the porous internal structure of the cement concrete greatly limits the tensile strength of the concrete. Various conventional methods considered to overcome this weakness are to incorporate concrete with fibers such as steel fibers, polymer fibers, carbon fibers etc. However, these fibers have their own limitations. Steel fibers are prone to corrosion whereas polymer fibers even by providing good tensile strength lack consistency. Moreover, the addition of these fibers significantly affects the workability of concrete. All these fibers mainly focus on improving the macrostructure of the concrete which is not enough to resolve the limitations regarding the concrete.

Commented [ARS4]: [1]Reference needed various conventional methods considered (source of those consideration is essential)

The microstructure of the concrete is the major area where the focus needs to be concentrated as the strength of the concrete is mainly attributed to its microstructure. The main hydration product of cement-based materials, the CSH-gel, is a nano-structured material (Quercia et al. 2014). The adhesive property of the CSH gel formed after hydration process is the source of the mechanical strength of the

concrete. Thus, to improve the mechanical properties of the concrete, one needs to improve the microstructure of the concrete. This has led to increased research in the field of Nano science which is seen as the most powerful alternative to solve the problem.

Commented [ARS5]: [2]Statement

Nano science relates to the study of properties of particles in the Nano scale. Nano as the name suggests refers to the magnitude of 10^{-9}. Nano Science deals with every particle in molecular or atomic scale. The various properties of the material significantly come into light at this scale. This application of Nano science in the field of construction has already begun in recent times. Due to exceptional mechanical properties and signs to revolutionize the construction industry, the interest to study the Nano materials for the construction field has increased among the researchers. Antonio et al. (2016) described the advancement of researches in the field of nanomaterial graphene for the improvement of the mechanical properties and durability of concrete. Similarly, Nandhini et al. (2016), investigated the effect of addition of graphene oxide in fly ash concrete while Ming-li et al. (2016) studied the effect of addition of functionalized graphene (FGN) on the mechanical properties, fluidity and microstructure of cement mortar and Hassani et al. (2014) studied the effect of graphene oxide on the mechanical properties and durability of concrete pavement. All these studies focused on incorporating mainly functionalized graphene to improve the mechanical properties of cement mortar and concrete. Although the results seemed favourable, functionalized graphene being very reactive are not stable in physiological solution. Thus, it is very difficult to control the properties as per our requirement.

Commented [ARS6]: [3]Defination: Source

Another Nano material under research is Graphene. The mechanical properties of Graphene exhibit its potential to be used in the construction industry as reinforcements. Graphene having extremely high aspect ratio in the range of 1000:1 to 2,500,000:1 can be used to significantly improve the microstructure of the concrete thus avoiding considerable cracks (Makar et al. 2005).

With the advancement in technology, modernization and urbanization is spreading rapidly throughout the world. This has resulted in frequent changes in building design and orientations. The materials, debris and rubble resulting from these frequent modelling and construction due to design changes known as the construction demolition waste has added further burden to the construction industry and environment as whole as the disposal mechanism of these wastes are not well established. It is in this light; researches are going on to recycle these wastes to be used again in the construction industry which will not only solve the disposal problems but also supplement in the construction field.

Cement based concrete mainly consist of cement, fine aggregates, coarse aggregates, admixtures and water (S Sanju et al. 2016). Recycled construction demolition waste can be used as a full or partial replacement of coarse and fine aggregates which will ease out the pressure on the environment and will also economize the construction industry. Many researches have been done to replace fine aggregate with construction and demolition waste. Monish et al. (2012) carried out an experimental investigation to study about the effect of the replacement of the fine aggregate by demolition waste on the workability and the compressive strength of concrete while Raman et al. (2017) studied the replacement level of the natural river sand by demolished waste in concrete. Most of these studies have focused on replacing fine aggregates compared to coarse aggregates. However, these wastes do not have the same strength as the materials they have replaced. The general problems faced are increased moisture content and low strength concrete. To overcome the cons faced by using recycled construction demolition waste, appropriate additives are to be introduced. Nano materials in this case can solve this problem. Thus, in this research an experimental investigation was conducted to study the mechanical properties of cement mortar by incorporating graphene as additive to strengthen the mix after replacement of coarse aggregate by construction and demolition waste in various proportions.

2. Experimental Program

2.1. Materials

Ordinary Portland Cement (OPC) 43 Grade was used as binding material in the mortar. The sand used was Manufactured Sand (M-sand) which was sieved in a proper manner so as to achieve Zone II gradation. The Construction and Demolition Waste (CDW) was used as a partial replacement to fine aggregates in the cement mortar. The CDW was sieved though 4.75mm sieve and zoning was done to achieve the grade requirements of Zone II. The sand was replaced by 25% and 50% CDW. Industrial graphene purchased from United Nanotech Innovations Pvt. Ltd., Bangalore was used. The physical properties of the materials used has been presented in Table 1 to Table 3.

Table 1. Physical properties of cement

Physical Properties	Test Results	IS 8112-1989 Standards
Fineness	6.8%	10%
Specific gravity	3.1	3.15
Standard consistency	30%	25-35%
Initial setting time	90 minutes	Minimum 30 minutes

Table 2. Physical properties of sand

Zone	Specific gravity	Loose density (kg/m^3)	Bulk density (kg/m^3)
II	2.42	1496	1634

Table 3. Physical properties of graphene

Physical properties	Range of values
Tensile modulus	>1000 GPa
Tensile strength	>5 GPa
Bulk density	0.30 gm/cc
Average diameter	10-15µ
Average thickness	10-15nm
Purity	>98%
Number of layers	10-15
Surface area	112 m2/gm

2.2. Mix Proportion

Several trial mixes were carried out on cube moulds of size 7.07cm as per the Indian Standards with the variation in water cement ratios ranging from 0.35 to 0.7 for cement: sand ratio of 1:3. The ratio of cement: sand of 1:3 with water cement ratio of 0.5 yielded the optimum strength with good workability. Henceforth, 1:3(cement: sand) ratio by weight and 0.5 water cement ratio was adopted for further investigations. The various mix proportion used has been presented in Table 4.

Table 4. Varieties of mortar mixes

S.No.	Mix type	Cement	Sand (kg)	CDW	Graphene	Water (ml)
1	Conventional Mortar	1.8	5.4	Nil	Nil	900
2	M-C25	1.8	4.05	1.35	Nil	900
3	M-C50	1.8	2.7	2.7	Nil	900
4	M-C0 (G-0.1%)	1.8	5.4	Nil	1.8	900
5	M-C0 (G-0.4%)	1.8	5.4	Nil	7.2	900
6	M-C0 (G-0.7%)	1.8	5.4	Nil	12.6	900
7	M-C0 (G-1%)	1.8	5.4	Nil	18	900
8	M-C25 (G-0.1%)	1.8	4.05	1.35	1.8	900
9	M-C25 (G-0.4%)	1.8	4.05	1.35	7.2	900
10	M-C25 (G-0.7%)	1.8	4.05	1.35	12.6	900
11	M-C25 (G-1%)	1.8	4.05	1.35	18	900
12	M-C50 (G-0.1%)	1.8	5.4	2.7	1.8	900
13	M-C50 (G-0.4%)	1.8	5.4	2.7	7.2	900
14	M-C50 (G-0.7%)	1.8	5.4	2.7	12.6	900
15	M-C50 (G-1%)	1.8	5.4	2.7	18	900
Total Quantiy		27	71.55	20.25	118.8	13500

2.3. Fabrication of Mould

The mould used was rectangular in shape with cast iron frame resting on a wooden board with 12 compartments spaced by granite blocks so as to form prisms of size 160mm×40mm×40mm as per the standards of BS EN 1015-11. Fig 1 shows the mould specimen.

Figure 1. Mould with prism compartments

2.4. Dispersion of Graphene

In cement-based materials, the Graphene molecules tend to agglomerate due to strong Vander Wall's force of attraction resulting in poor dispersion. In order to ensure the proper dispersion of Graphene in cement mortar, ultrasonic process was adopted. The ultra sonicator was employed to disperse the Graphene. 20 KHz frequency and 50% amplitude of ultrasonic pulse was applied.

A predetermined quantity of Graphene was weighed in a weighing balance sensitive to 0.001gm and mixed with calculated volume of water in a beaker. Not more than 3gms of Graphene was mixed in one shift to assure homogeneous dispersion. Graphene and water were poured in a glass beaker and stirred well. The probe of the ultra sonicator was inserted inside the beaker and sonication process was allowed

to take place for 20 minutes time. The dispersed mixture was then carried to concrete laboratory where it was added to mortar at the time of mixing.

2.5. Test Methodology

2.5.1. *Flexural Strength Test*

The cured specimen was taken out from water and allowed to lose its dampness. After those suitable markings were made in the specimen to conduct the flexural strength test. The test was carried out as per BS-EN 1015-11. Suitable markings were done as shown in the figure 2.

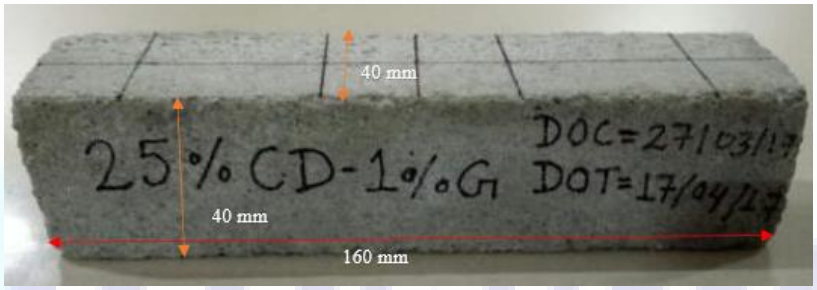

Figure 2. Flexural strength test specimen

In flexural strength testing machine, the three-point loading of the prism specimen was carried out till it failed. The dial gauge reading was converted to kg force and ultimate load carried by the specimen was noted down and flexural strength was computed by using the formula given belowin Eq. (1).

$$\sigma f = \frac{Pl}{bd^2} \quad (1)$$

where, σ_f = flexural strength in MPa, P= load applied in Newton, l= span of the specimen in mm, b= breadth of the specimen in mm, d= depth of the specimen in mm

Three specimens were tested at every 7, 14, 21 and 28 days from the day of curing and the average value was taken as the flexural strength of the specimen of a particular mix. Out of the two broken halves of the flexural strength testing specimen, one halves was used for determination of compressive strength and the next halve was used for the determination of split tensile strength.

Commented [ARS7]: [4]Image distortion fig 3

Figure 3. Flexural strength test set up

Figure 4. Flexural strength test specimen at failure

Commented [ARS8]: [5]It would be better to provide the failure specimen failure crack pattern and explain the failure mechanism rather than test specimen

2.5.2. *Compressive Strength Test*

One half of the broken specimens were tested on 7, 14, 21 and 28 days from the day of curing. Compressive strength test was carried out confirming to BS EN 1015.Uniformly distributed load was applied on the specimen on the cross-section area of 40mm×40mm till the specimen failed under crushing load. Three halves of the broken specimen of a particular mix were tested and the average value was taken as the compressive strength of the particular mix. Compressive Strength was calculated using the formulae given below in Eq. (2).

$$\sigma c = \frac{P}{A} \qquad (2)$$

Where, σ_c = compressive strength in MPa, P= load applied in Newton, A= cross section area of specimen in mm^2

Figure 5. Compressive strength test specimen in zig and test setup

2.5.3. *Split Tensile Strength Test*

Other halve of the broken specimen of the flexural strength test was tested for split tensile strength test on 7, 14, 21 and 28 days from the day of curing. Line load was applied on the specimen on the section of 40mm till the specimen failed. Three samples from a particular mix were tested and average value was taken as the split tensile strength of the particular mix. Split Tensile Strength was calculated using the formulae given below in Eq. (3).

$$\sigma t = 2P/\pi bd \qquad (3)$$

Where, σ_t = split tensile strength in MPa, P= load applied in Newton, b= breadth of the specimen in mm, d= depth of the specimen in mm

Figure 6. Tensile strength test set up

3. Results and Discussions

The table 5 below indicate the 28-day compressive strength, flexural strength and split tensile strength for various tested samples.

Table 5. Strength of Specimens

Mix Type	Flexural Strength	Compressive Strength	Tensile Strength
NORMAL	5.58	24.83	3.00
25% CD	5.32	19.01	2.45
50% CD	5.09	17.78	2.16
NORMALWith 0.1% G	6.79	25.75	3.62
NORMAL 0.4% G	6.56	28.20	4.06
NORMAL 0.7% G	7.65	28.81	4.46
NORMAL 1% G	6.90	32.50	4.04
25% CD With 0.1% G	5.94	21.46	3.20
25% CD With 0.4% G	7.24	27.59	3.83
25% CD With 0.7% G	6.67	22.07	3.18
25% CD With 1% G	5.66	21.46	3.76
50% CD With 0.1% G	5.83	18.39	2.45
50% CD With 0.4% G	6.22	22.99	2.90
50% CD With 0.7% G	5.32	18.39	2.77
50% CD With 1% G	6.11	19.31	3.77

All measurements are in MPa

3.1. Compressive Strength

The results of compressive strength values for cement mortar with varying percentage of construction and demolition waste and varying percentage of graphene are shown in figure 7.

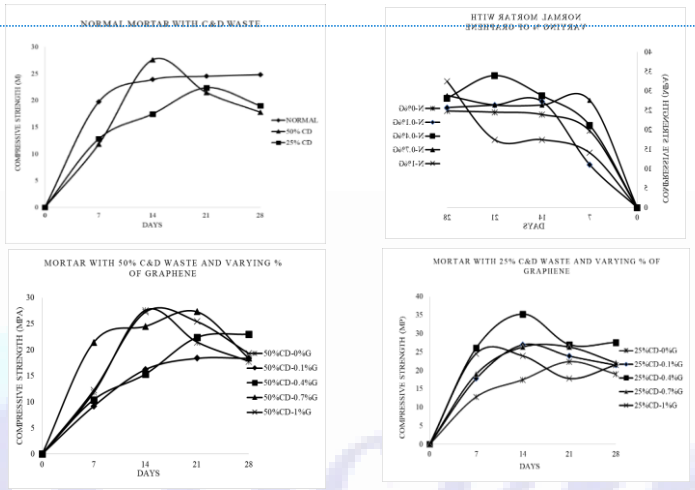

Figure 7. Compressive Strength Test Results

From the above graphs, it is seen that there is decrease in compressive strength of mortar incorporated with 25% and 50% construction and demolition waste compared to the normal cement mortar. This may be because of the formation of transition zone between C&D waste and sand, forming the weak zone in mortar. Moreover, C&D waste being more porous in nature results in increased porosity thus decreasing the compressive strength of cement mortar.

Also, there is increase in compressive strength of mortar with the incorporation of graphene in different proportions. This is because graphene is a nanoparticle which fills the nano voids decreasing the porosity thus reducing the transition zone in mortar leading to the increase in compressive strength.

It is seen that the incorporation of graphene in varying percentage in mortar with 25% C&D waste has led to increase in the compressive strength where in addition of 0.4% graphene by weight of cement has shown the optimum result. This is because with the increase in % of graphene, the graphene molecules tend to come close to each other leading to their re-agglomeration thus resulting in poor distribution of graphene molecules in the mortar.

It is seen that the incorporation of graphene in varying percentage in mortar with 50% C&D waste has led to increase in the compressive strength. The addition of 0.4% graphene by weight of cement has shown the optimum result. The curve of varying percentage of graphene has shown the greater values of compressive strength in 14th day and later decrease in 28th day, this is because the hydration product increases with the day and so does the Ca(OH)2 thus increasing the alkalinity of the mortar.

Commented [ARS9]: [6]Unit of Compressive Strength in figures must be consistent (M,MPA, MP =MPa). It would be better to provide numeric reference to the each figure (a, b, c and d) and explain each figure in the caption

3.2. Flexural Strength

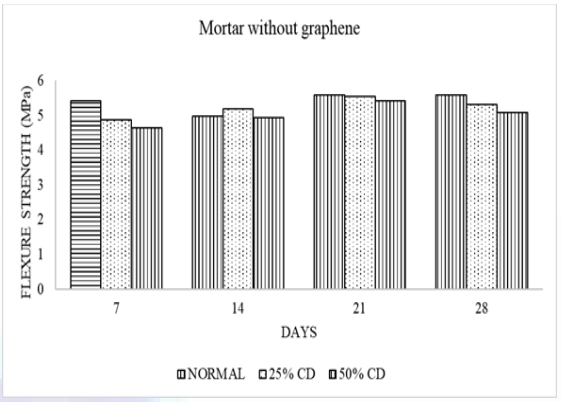

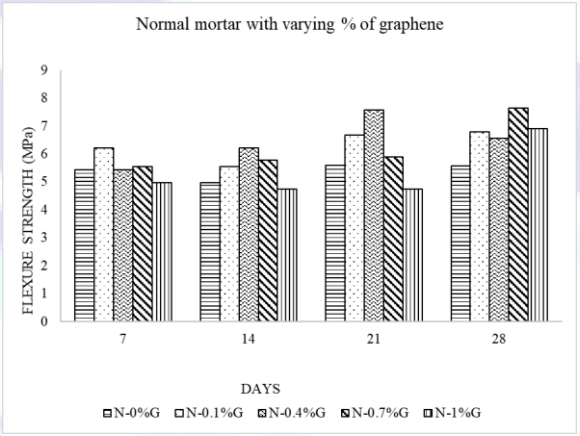

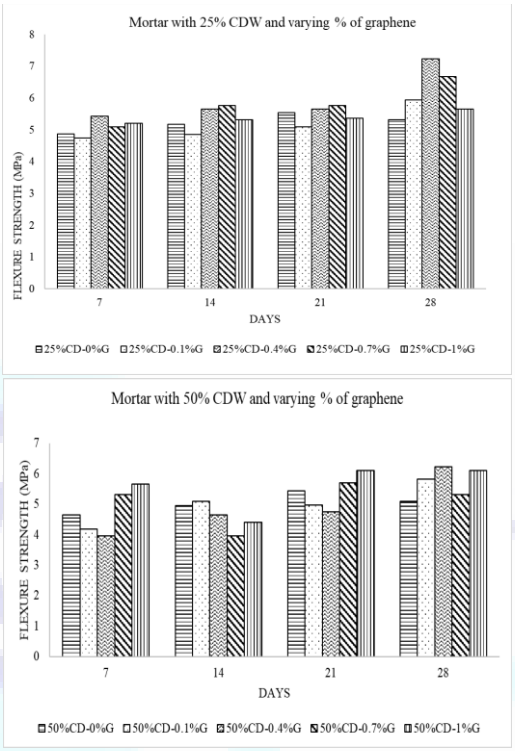

Figure 8. Flexural Strength Test Results

Figure 8 shows the flexural strength test results. It is seen that there is decrease in flexural strength of mortar incorporated with 25% and 50% construction and demolition waste compared to the normal cement mortar. This is due to the formation of transition zone between C&D waste and sand particles and also due to the increase in porosity of mortar. This weak zone initiates the cracks in the bottom fibers where tensile stress is developed when the flexural load is applied. These cracks propagate to the compression zone and the specimen fails under lesser flexural load.

There is increase in flexural strength of mortar with the incorporation of graphene in different proportions. This may be due to the fact that graphene fills the nano voids and reduces the transition zone between C&D waste and sand particles. So, when the flexural load is applied, there are not enough weak points to initiate the cracks thus improving the flexural strength. The incorporation of graphene in varying percentage in mortar with 25% and 50% C&D waste has led to increase in flexural strength of mortar with the addition of 0.4% graphene by weight of cement showing the optimum result.

3.3. Split Tensile Strength

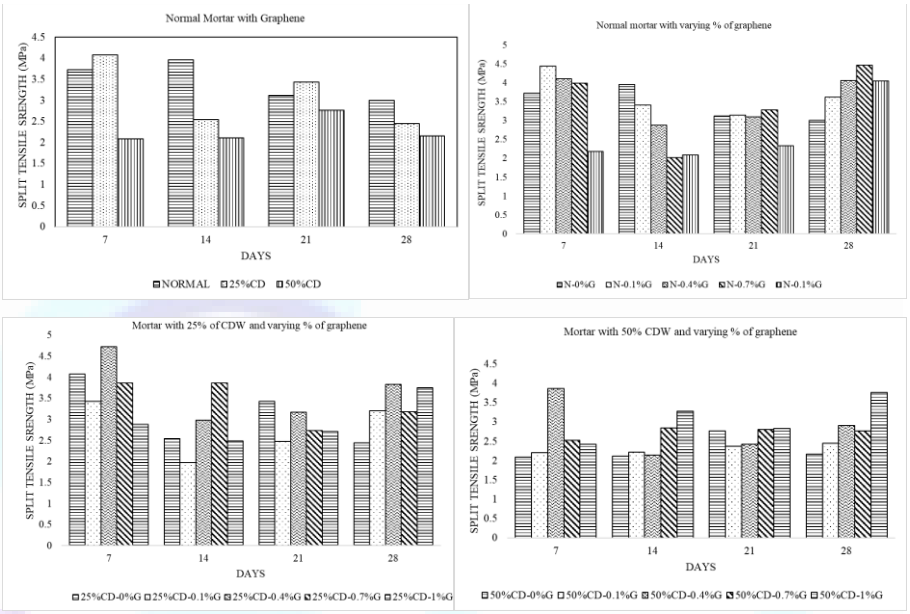

Figure 9. Split Tensile Strength Test Results

Figure 8 shows the split tensile strength test results. The incorporation of graphene in varying percentage in mortar has led to increase in split tensile strength of mortar. The addition of 0.4% graphene by weight of cement has shown the optimum result for mortar with 0%, 25% and 50% construction and demolition waste.

4. Conclusions

i. The results obtained from the analysis gives us the fair level of idea that with the increment of proportion of Graphene, there is considerable increase in the flexural, compressive and tensile strengths up to a certain limit.
ii. The increasing trend ceases after a specific proportion which varies with the variation of C&D waste replaced.
iii. The flexural, compressive and split tensile strength decreases with the use of C&D waste.
iv. The optimum results in case of flexural and compressive strength tests were in case of .4% replace however, there was significant increase in the strength with addition of .4% and 1% graphene by weight of cement.
v. To sum up, with the addition of graphene, there was positive compensation of loss only for the 25% replacement of sand by construction and demolition waste. This trend was not continuous for 50% replacement of sand.
vi. Thus, it can be concluded that 25% replacement of sand with 0.4% Graphene is the optimum value as per the results obtained.

References

[1] Antonio, V.R., & German, C.S. (2016). Optimizing content graphene oxide in high strength concrete. International Journal of scientific research and management.

[2] Cao, M., Zhang, H., and Zhang, C. (2016). Effect of graphene on mechanical properties of cement mortars. Journal of Central South University, 23(4), 919–925.

[3] Hassani, A., Fakhim, B., Rashidi, A., & Ghoddousi, P. (2014). The Influence of Graphene Oxide on Mechanical Properties and Durability Increase of Concrete Pavement. International Journal of Transportation Engineering, 10.2219.

[4] Makar, J., Margeson, J., & Luh, J. (2005). Carbon nanotube/cement composites-early results and potential application. Proceedings of the 3rd International Conference on Construction Materials: Performance, Innovations and Structural Implications (pp.110). Vancouver, Canada.

[5] Monish, M., Vikas, S., Agrawal, V.C, & Rakesh, K. (2012). Utilization of demolished waste as fine aggregate in Concrete. Journal of Academic Industrial Research. 1(7).

[6] Nandhini, S., & Padmanaban. (2016). Experimental Investigation on Graphene oxide Composites with Fly Ash Concrete. International Journal of Modern Trends in Engineering and Science.

[7] Quercia, G., Spiesz, P., & Brouwers, H. J. (2014). Effects of nano-silica (ns) additions on durability of scc mixtures. Durability of Reinforced Concrete from Composition to Protection, 125–143.

[8] Raman, J.V.M. (2017). Study on replacement level of concrete waste as fine aggregate in concrete. International Journal for Research in Applied Science and Engineering Technology, V(II), 241–246.

[9] Sanju, S., Sharadha, S., & Revathy, J. (2016). Performance on the Study of Nano Materials for the Development of Sustainable Concrete. International Journal of Earth Sciences and Engineering, 9(3),294-300.

Preparing comprehensive earthquake catalogue of Nepal to compare the G-R parameter from Maximum Likelihood Method (MLM) and Least Square Method (LSM)

Radhesh Shrestha, Ramesh Khanal, Pawan Chhetri
Department of Civil Engineering, Advanced College of Engineering and Management

Abstract

Earthquake catalogues from 1900 AD to 2021 AD were downloaded from the International Seismological Centre (ISC), United States Geological Survey (USGS) and Global Centroid Moment Tensor (GCMT). Collected catalogues were homogenized to moment magnitude and merged into a single catalogue to perform declustering of the catalogue. Declustured catalogue was used to perform completeness analysis to calculate magnitude frequency parameter. In this study, an attempt bas been made to compare the G-R parameters calculations from the MLM and the LSM for declustured catalogue for Nepal as a single source and only MHT as a source. The Z-Map tool was used for the MLM whereas graphical analysis on catalogue after completeness analysis is used for the LSM. It was observed that G-R parameters were 3.59 and 0.72 from LSM and 5.51 and 0.61 from MLM when complete catalogue was considered as a single source zone. Similarly, calculated parameters were 3.06 and 0.71 from LSM and 6.72 and 0.98 when calculation was made for only MHT as a source. MHT is the subduction interface, with suggested b value is around 1. From the results it can be observed that for a well characterized source zones MLM represents seismicity of the source better than LSM.

Keywords: *G-R parameters, Maximum likelihood method, Least square method, Source characterization*

Introduction

Himalaya is situated in the subduction interface between Indo gigantic plate and Eurasian plate, which is continuingly slipping from past 55 million years. (Dhakal, 2012). Nepal is located in the central part of this subduction boundary zone. Due to which large number of major significant earthquake (1255, 1408, 1505, 1833, 1934, and 2015 AD) were experienced in the past. These major earthquakes have moment magnitude larger than 7.6 and caused huge loss of life and properties (Thapa et. al 2017). In the past number of attempts has been made for the seismic hazard analysis of the Nepal. For all seismic study and hazard analysis of a region, at first preparation of proper earthquake catalogue which can represent the seismicity of that region is must (Woessner and Wiemer,2005). Earthquake catalogue is the collection of detail spatial, temporal and size information about earthquakes of a selected region in a time frame. Catalogue may contain earthquake magnitude of different magnitude scale which has to be homogenised into single magnitude scale. If catalogue is prepared from different sources they have to be merged into single earthquake catalogue using suitable methods. Finally merged catalogues were used for the further analysis. In the past numbers of attempt has been made to prepare the earthquake catalogue of Nepal for various research works. But theses catalogue has been outdated and old in the context of 2021 AD.

G-R parameters (a, b) values are the major factor that can be calculate from earthquake catalogue for the further seismic hazard analysis. Magnitude frequency parameters (a & b value) are the major factor that affect the seismic hazard analysis. For Nepal, seismic records are less compared to seismic cycles. Due to the lack of sufficient data for hazard analysis, the uncertainty may arise in seismic hazard estimation. Among others, G-R parameters (a & b value) have more effect on hazard estimation, which

lead to necessity of proper calculation of the parameters. The Maximum Likelihood Method (MLM) and the Least Square Method (LSM) are the common methods to compute G-R parameters. In this study an attempt has been made to prepared the declustured earthquake catalogue of Nepal and used that catalogue to make the comparison between calculated a & b value for both LSM and MLM methods without source characterization and with characterization of MHT as a source.

Data Compilation

For the development of a comprehensive earthquake catalogue primary earthquake catalogues are fundamental. We used the instrumentally recorded earthquake catalogues reported by various seismological agencies. The comprehensive catalogue for Nepal was prepared by merging the data of earthquake magnitudes obtained from International Seismological Centre (ISC), United States Geological Survey (USGS) and Global Centroid Moment Tensor (GCMT). Historical earthquakes are not included in this catalog since the magnitude of historical earthquakes are derived using empirical relations based on intensity of earthquake, hence, are subjected to high uncertainty (Rajure completeness). The magnitudes from 1901 AD to May 2021 AD were taken but due to repetition of events in different catalogues it was important to remove all the repeated duplicate events. The events were considered duplicate if they had similar magnitudes along with 10 seconds or less time difference and space origin difference of 0.5° or less. The repeated events were removed manually and checked using a computer program. Discrepant data were discarded on the basis of the catalogues and priorities given in the order of GCMT, USGS and ISC respectively. The collected data were recorded in various magnitudes such as Richter scale, Moment Magnitude, Surface Magnitude and Body Wave Magnitude, and were converted into Moment Magnitude for declustering and completeness work.

Homogenization

Even though the use of a uniform single magnitude scale is desirable it is not always possible due to the changes in instrumentation, the data reduction method, the magnitude formula, the station distribution, etc. (Kanamori 1983). As a result, various magnitude scales such as ML, Ms, mb, etc. have been developed and are currently in use. Moment magnitude, M_w, is found to characterize the earthquake source size more accurately than other magnitude scales and also does not saturate even at large earthquakes hence, it is widely preferred as the uniform magnitude scale for seismic hazard assessment worldwide. So the catalogue was unified and homogenized in terms of $M_{w,GCMT}$. Various empirical relationships between Mw and classical magnitude scales (ML, Ms, and mb) have been presented by many authors, either derived from global data sets (e.g., Ekström and Dziewonski 1988; Scordilis 2006; Bormann and Saul 2008) or by using records of earthquakes in different regions and environments (e.g., Papazachos et al. 2002; Stromeyer et al. 2004; Yenier et al. 2008; Grünthal et al. 2009). So, the selection of the correct and favorable empirical relations for our study region and requirement was deemed necessary.

Most of the current studies rely on Scordilis (2006) empirical relation for homogenization of Earthquake Magnitudes, however, these relations were developed by considering global seismicity, and relatively less weightage was given to the seismicity of the Himalayas during this study (Citation-Angbajan et al). So the empirical relation given by Scordillis (2006) is not appropriate for our seismic hazard analysis. So we have used the empirical relations suitable for the South Asian region given by Nath et al. (2016) to homogenize our earthquake catalogue.

The empirical relations for the conversion of various magnitude scales to Mw as given by Nath et al (2016) are listed as follows:

Table *1*: Magnitude conversion from other source to $M_{w,GCMT}$

S.N	Catalog	Equation	Magnitude range
1	ISC	$1.168 * m_{b,ISC} - 0.663$	3.8 - 7
2		$0.499 * M_{L,ISC} + 2.88$	3.5 - 7.3
3		$0.978 * M_{ISC} - 0.1634$	4.7 - 7.2
4	USGS	$1.082 * m_{b,USGS} - 0.413$	4.6 - 6.4
5		$1.15 * M_{s,USGS} - 0.628$	4.5 - 5.6
6		$1.21 * M_{s,USGS} - 1.45$	5.7 - 7
7		$M_{s,USGS}$	7.1 - 7.5
8		$1.017 * M_{w,USGS} - 0.118$	5.1 - 7
9		$M_{w,USGS}$	7.1 -7.8

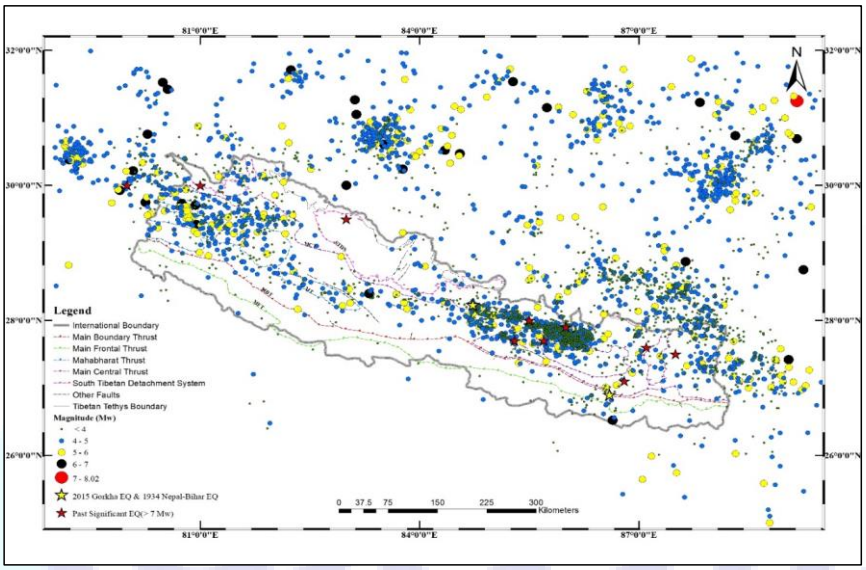

Figure *1*. Spatial distribution of merged catalogue

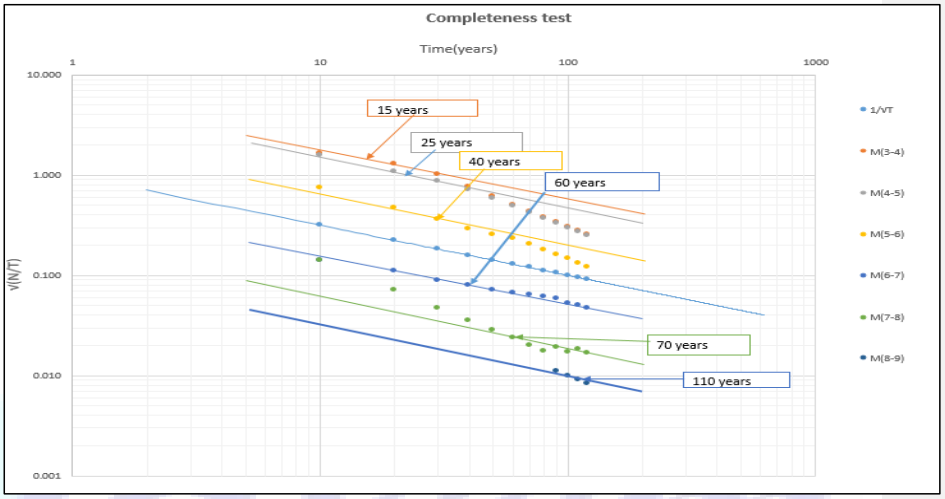

Figure 2. Completeness test of declustered earthquake catalogue

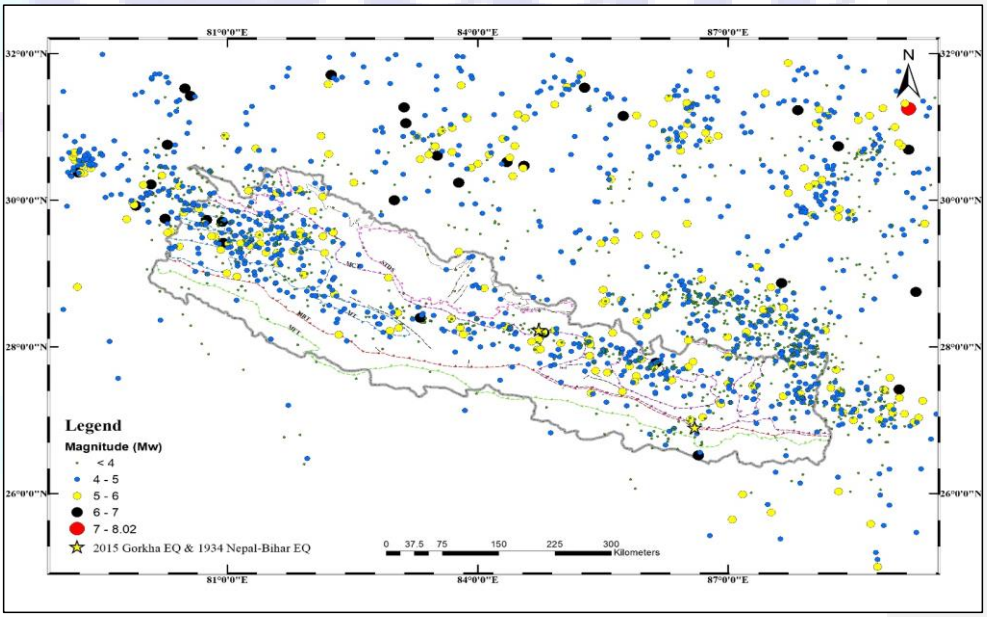

Figure *3*. Spatial distribution of declustered earthquakes data by Gardener and Knopoff

Declustering

The main earthquake event is generally followed by a large number of aftershocks and sometimes even preceded by foreshocks. These events are known as dependent events as they are temporarily or spatially dependent on the main shock. For the preparation of the earthquake catalogue, a set of independent events are required which follows Poisson Distribution. However, the data in the catalogue is filled with both the dependent (Foreshocks and Aftershocks) and independent events from which dependent events shall be identified and shall be removed. Different algorithms are established for identifying the dependent and independent events but still, the identification process is not absolute as a single algorithm might not be suitable for all the seismic locations. This is because, while developing an algorithm, various assumptions based on seismic location, recorded data, etc., are made which may be suitable for a particular seismic region but not for all the seismic locations around the world. There are many algorithms that can be used to remove the dependent events; they are: Gardner and Knopoff (1974), Reasenberg (1985), Zhuang et al. (2002), Hainzl et al. (2006). In our study we have applied the algorithm given by Gardner and Knopoff (1974), it utilizes windows method for identifying aftershocks within seismicity catalogs which is based on space-time distances as a function of the mainshock magnitude[1] .

Completeness Analysis

The time interval of different magnitudes of data for that particular magnitude completeness period can be assessed by Steep (1972) method. For the better completeness period, the collection of earthquake magnitude data should be large as far as possible to overcome less variance of data while using statistical analysis [2]. It is assumed that earthquake patterns follow the Poisson distribution. In this method, different magnitudes and different scale times are separated then each data mean rate of occurrence (μ) is evaluated. The rate of occurrence of earthquake data is the function of the cumulative number of earthquakes in the given time interval. Whether the mean rate of occurrence of particular magnitude is constant or deviated is computed by a line($1/\sqrt{T}$), where T is the time interval. The time interval of completeness of data is the time interval length where data lies on a constant line($1/\sqrt{T}$) or the point on the constant line($1/\sqrt{T}$) where the slope of data is changed[3]. This can be computed by visual examination from graphs. For small earthquake magnitudes, the time interval of the completeness period is small and for large earthquake magnitudes, the time interval of the completeness is also large.

Magnitude Frequency relationship (G-R relationship)

After the completeness period calculation, the activity of the earthquake pattern can be computed by Gutenberg Richter relation. It is the empirical relation between magnitude(M) and number of earthquakes exceeding at a particular period of time (Nm). Mathematically,

$$LogNm = a - bM;$$

where 'Nm' is the number of earthquakes per year with magnitude equal to or greater than M. To analyze by a simple method, we take the logarithmic of Nm for computation by straight-line coefficient methods. Mathematically, 'b' is the slope of the line and 'a' is the intercept corresponding to the value of LogNm when M is equal to zero. The 'a' value describes the total activity of earthquakes in a particular region and the b value describes the relative number of large and small earthquakes [4]. Both LSM and MLM methods were used to calculate G-R parameters.

Source Characterization

ource characterization was done only to locate the position of Main Himalayan Thrust (MHT). Fault map of Nepal, proposed by Nepal geological society was digitized using ArcGIS. Using the digitized map, position of Main Frontal Thrust (MFT) was identified accurately. Coupling data for more than 50% coupling downloaded and adopted from the study of Stevens & Avouac (2015) to locate the actual subduction zone of Main Himalayan thrust. Zone above the Main Frontal Thrust (MFT) up to line defined by more than 50% coupling as calculated by Stevens & Avouac (2015) was taken as MHT source.

Results and Discussion

Complete and comprehensive earthquake catalogue of Nepal and its surroundings regions from 1900 AD to 2021 AD was prepared in this study. This catalogue can be used for the proper earthquake source characterization of Nepal and to perform seismic hazard analysis in future.

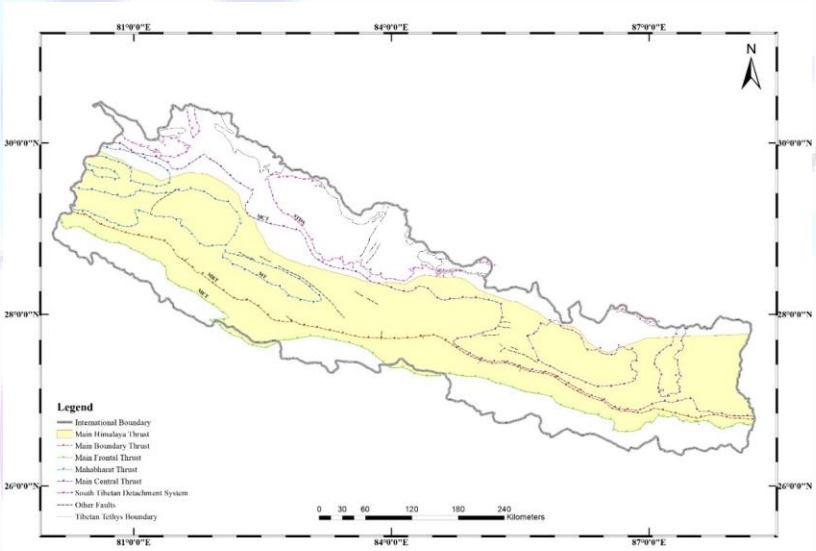

Figure 4. Subduction Interface of Main Himalaya Thrust for coupling more than 50%

Table 2. Results of G-R parameter calculation

G-R parameter	Nepal as a single source		Only MHT as a Source	
	LSM	MLM	LSM	MLM
a	3.59	5.51	3.06	6.72
b	0.72	0.61	0.71	0.98

Result for both source considerations calculated from LSM and MLM are shown in Table 2 and were compared with previously validated seismic hazard analysis of Nepal and Global seismicity parameter suggested for Nepal. Since the global b value for the seismicity of Nepal is suggested to be near 1, which matches the result obtained from the maximum likelihood method when considering MHT as the earthquake source. Also Stevens et al 2018 calculated a value as 6.02 and b vale as 1 for MHT, Which

also insight the accuracy of MLM. Finally, conclusion can be drawn that, only the proper source characterization based on the seismicity can represents the activity of the earthquake in that region, while performing any seismic hazard analysis. And Maximum likelihood method can predict the seismicity of Nepal better than least square method.

References

[1] T. Van Stiphout, J. Zhuang, and D. Marsan, "Seismicity declustering," *Community Online Resour. Stat. Seism. Anal.*, no. February, pp. 1–25, 2012, doi: 10.5078/corssa-52382934.

[2] J. C. Stepp, "Analysis of completeness of the earthquake sample in the Puget Sound area and its effect on statistical estimates of earthquake hazard.," *Proc. 1st Int. Conf. Microzonazion*, vol. 2, no. 1, pp. 897–910, 1972.

[3] A. Nasir, W. Lenhardt, E. Hintersberger, and K. Decker, "Assessing the completeness of historical and instrumental earthquake data in Austria and the surrounding areas," *Austrian J. Earth Sci.*, vol. 106, no. 1, pp. 90–102, 2013.

[4] S. Rajaure and L. P. Paudel, "A comprehensive earthquake catalogue for Nepal and its adjoining region," *J. Nepal Geol. Soc.*, vol. 56, no. 1, pp. 65–72, 2018, doi: 10.3126/jngs.v56i1.22747.

Properties and Applications of Agricultural Straw in Construction

B. Nepal [1], A.R. Shrestha[2]

[1,2] University of Liverpool

bhooma.nepal@gmail.com

Abstract

Rice and wheat are the major agricultural products and a staple food for more than half of the world's population. Straw is a major by-product of rice and wheat whose annual production amounts to a total of about 1500 million tonnes. Straw is mostly used as roofing and packing material, livestock feed, fertilizer and fuel in small quantities. These uses are however unprofitable and most farmers look for easy ways of disposal such as burning. Legislation has been put in place in most countries after objections regarding air pollution, but burning is still a common practice. In the last few decades, the use of straw has advanced from laboratory studies to industrial applications. Driven by cost considerations and environmental concerns, this residual by-product now has the potential for more sustainable uses. This paper focuses on current applications and potential uses of rice and wheat straw in construction and also presents physical, mechanical and chemical properties of rice and wheat straw.

Keywords: *Rice straw; Rice husk; Wheat straw; sustainable construction.*

1. Introduction

Straw is a term commonly used for all residues after wheat and rice grains have been collected by grain harvesting, and includes major parts of the stem, leaves, and spikelet. Husk or hull is the outermost layer of the grain that is separated from the rice or wheat grains during the milling process. Rice grain, often referred to as paddy rice or rough rice is primarily used for human food, with the remainder used for animal feed and green and sustainable materials. Globally, approximately 750 million tons of rice paddy and a similar amount of wheat is produced each year (FAOSTAT, 2019).

Official statistics on straw utilization are hard to find. Modernization in rural areas leads to growing access to modern cooking and heating fuels, which means that in most regions, rice straw will no longer be used as a source of energy for cooking and heating. Therefore, by making a proper utilization of agricultural straw fibers in construction is no doubt a significant step towards low carbon and sustainable construction.

2. Experimental investigation of agricultural straw

A considerable effort is going on in the context of international research to explore the properties of cheap agricultural crops and crop residues as a possible material for sustainable construction. The basic advantage of natural fibers being environment friendly, low cost and availability. The disadvantage being a high variation of their properties, which may lead to unpredictable concrete properties (Chin and Nepal, 2019).

Rice and wheat straw were investigated and several material properties are presented in Table 1.

Table 1: Material properties of rice and wheat straw (Chin and Nepal, 2019)

Types of properties		Rice Straw	Wheat Straw
Chemical properties	Nitrogen (%)	0.44	0.17
	Carbon (%)	42.00	45.05
	Hydrogen (%)	5.95	6.04
	Oxygen (%)	51.61	48.74
	Cellulose (%)	47.48	35.00
	Hemicellulose (%)	14.14	21.30
	Lignin (%)	6.38	17.50
Physical properties	Water absorption capacity (24 h) (%)	332.33	269.55
	Density (g/cm^3)	1.10	0.60
	Tensile test (N/mm^2)	198.54	278.00

The vario MICRO cube was used for the CHNX analysis for this experiment. Straw was dried for 24 hours at 105 °C in an oven prior to the analysis. Each sample was analysed with a standard method with helium as a carrier gas after weighing 10-15 mg into tin boats with a micro balance. The results in Table 1 show that oxygen is the largest content for both the straws followed by carbon. Hydrogen is also present with an amount of 5.95 %, but the presence of Nitrogen is in only a trace amount. Trubetskaya et al. (2016) analysed wheat straw and rice husk and reported 46.6 and 37.8 % of carbon, 42.5 and 35.5 % of oxygen respectively. The results are in good agreement with the test results in Table 1.

Fibertech TM 2010 was used for the determination of the chemical composition of rice and wheat straw according to the Van Soest method. Fibertech TM 2010 is a semi-automated incubation and filtration system for the quantitative determination of dietary fiber. Solid samples were dried for 4 hours at 105 °C in an oven prior to defat in cold extraction unit. The samples were kept in hot extraction unit where hemicellulose and cellulose were extracted. After cooling to room temperature, the sample was ignited at 525 °C to determine the quantity of lignin. From the analysis, it is seen that cellulose is the major chemical contained in the rice and wheat straw followed by hemicellulose. Trubetskaya et al. (2016) also investigated the chemical composition of the rice husk and wheat straw. Compared to these results of 35.00 % cellulose in wheat straw, the literature reported 35.90 % in wheat straw.

Water absorption is a material's ability to absorb and transmit water through it by capillary suction. The fibers are oven dried at 60 °C for 24 hours and brought to a saturated condition, weighed again and brought to an oven dry condition. The samples were submerged in the water for several durations (1, 2, 5,10, 30, 60 min and 24 h) to determine the water absorption coefficient. The water absorption was determined by weighing the samples before and after wetting. Water absorption was lower in the wheat fibers at 269.55 %, the rice straw water absorption was higher by 23.30 %. Bouasker et al. (2014) also studied the water absorption for different straws and found that the water absorption was about three times the weight of the straws. Agricultural straw has a very high-water absorption capacity. For large volume fractions of straw in composite, the designer should appropriately include for water absorbed by straw in the calculation.

The density of rice and wheat straw was found by using the true density analyser using the principle of Helium pycnometer. Helium can enter the smallest pores and is used to measure the unknown volume of a material to a known weight. Rice straw is denser than wheat straw at 1.10 g/cm^3. Bouasker et al. (2014) also published the test results for the density of wheat straw which was determined by a pycnometry test. The research indicated that wheat straws have a density of about 0.87 g/cm^3. The test results from this research confirm closely with

that of Bouasker et al. (2014). Density test results indicate that wheat straw are less compact and have less cellulosic material compared to the same volume of rice straw. Density is necessary to determine the quantity of straw required in the mix design of composite.

The tensile strength of the rice and wheat straw was determined by using a simple grip mechanism. The cross sectonal area was determined by using a digital Vernier caliper, tension force generated on the straw using the grip mechanism (Nepal et al. 2017 a, b). Tensile strength for rice and wheat straw was determined to be 198.54 MPa and 278.00 MPa, respectively. Although rice and wheat straw have very similar composition and internal structure, tensile strength of wheat straw was 28.16 % higher than rice straw.

3. Current applications of agricultural straw in construction

3.1 Housing and insulation

Straw bales have been used in housing in America as early as the 1900's. Although known for being energy efficient and inexpensive, this technique was sporadic in rural America, due to the lack of proper documentation and guidelines. Bales should be dry, without seed heads and about twice as long as they arewide. This helps for compaction and uniformity in construction. The bale walls could be either load bearing or non-load bearing. The foremost advantage is the insulation the bale provides as theyhaveahigh R value (greater than 10) which is at least double that of wooden battens (Myhrman and MacDonald, 1997). A typical bale of straw has a U-value of 0.13W/m^{2}K which has significantly better thermal performance than that required (Jones, 2009). Figure 1 shows the different phases of straw bale house construction.

Figure 1: Different stages of straw bale house construction (Morrison)

Research carried out for the Network for Earthquake Engineering Simulation at the University of Nevada, in association with the Pakistan Straw Bale and Appropriate Buildings (PAKSBAB, 2009) studied the response of straw bale houses to earthquakes. The capacity of clay plastered, load bearing straw bales houses were simulated in cyclic loading and it was found that the building performed was significantly improveddue to its flexibility and lightweight.

Straw bale building is now at a crucial point in its development. Straw as a building material excels in the areas of cost and energy efficiency. So advancements in design guides and construction methods can make this material even more appealing. Straw bale houses are sustainable, low cost, energy efficient, highly insulating for both heat and sound and also possess a low risk of fire.

Garas et al. (2010) studied the applications and strength of rice straw posts and walls to support the roof of a

building. Cement mortar was used to bind rice straw and bricks. The results were promising as the walls and posts behaved well as a support system. The literature emphasizes the use of rice straw bricks as it is aesthetically pleasing, strong and sustainable building material.

3.2 Composite materials for fiber reinforced concrete

Composite materials combine more than one material or substance, most commonly a matrix material and reinforcing fibers. The fiber and the matrix will act together if a good bond exists between the resin and the fiber. Composites can be extremely strong and are also very flexible for manufacturing processes. Composites have long been used in airplanes and defense, but are gradually making inroads in the automobile industry. Glass fibers have been the most common reinforcing materials for composites, but these pose health and environmental problems for disposal and require high energy inputs for manufacturing. Rice straw fibers and stems, which are resistant to decomposition as a result of their high silica content prove suitable (REI, 1997). Plant fibers can be surprisingly strong, lightweight and inexpensive. A comparison of tensile strength of various natural fibers commonly used for composites is listed in Table 2.

Table 2: Comparison of Tensile Strength of various materials commonly used for composites (Nepal et al., 2015)

Material	Tensile Strength (in MPa)
Sisal	347-378
Coconut	95-118
Bamboo	73-505
Jute	250-350
Rice Straw	48

Grozdanov et al. (2006) investigated the potential use of rice straw fibers as polypropylene reinforcement. They studied using reinforcement of rice straw in maleated polypropylene. By using extrusion and compression moulding process, rice straw composites containing 20-30% by weight rice straw were prepared. Both of these studies have shown that rice straw could be used as bio-degradable eco-friendly reinforcement in polypropylene composites, to minimize environmental pollution rather than to perform a strong reinforcing effect. The composites showed an acceptable strength upto 30% by weight of rice straw. The mechanical properties and impact resistance of rice straw could be improved by modification of the rice strawas polymer composites thus opening a new dimension of use of rice straw fibers in industrial applications.

Conclusion

Rice and wheat straw are available in many countries in abundant quantities as agriculture residue. The opportunities are huge in terms of the ever-growing quantity of availability of straw. If only a small part of this market, it would definitely create a very large demand for straw. A more exciting dimension is possible in terms of use of straw in sustainable housing and eco-friendly concrete. Straw bales used in housing should be regulated by means of design guidelines. However, the economics behind the high cost associated with collection, handling, transport and treatment before extraction of energy is a drawback. The supply chain of straw is disorganised and needs to be defragmented.

The properties of rice and wheat straw show that the straw have sufficient tensile strength to be used as straw composite matrices for use in construction. The fibers have high water absorption, this needs to be carefully accounted for before using as a reinforcement filler in composite. Straw is also an organic, biodegrable material so further research is required in durabilty aspect.

References

Bouasker, M., Belayachi, N., Hoxha, D., & Al-Mukhtar, M. (2014). Physical characterization of natural straw fibers as aggregates for construction materials applications. Materials, 7(4), 3034-3048.

Chin, C. S., & Nepal, B. (2019). Material Properties of Agriculture Straw Fiber-Reinforced Concrete. In Ecological Wisdom Inspired Restoration Engineering (pp. 109-120). Springer, Singapore.

FAOSTAT (2019) Production. See http://faostat3.fao.org/download/Q/QC/E (Accessed 05/08/ 2021).

Garas, G., El Kady, H., & El Alfy, A. (2010). Developing a new combined structural roofing system of domes and vaults supported by cementitious straw bricks. ARPN Journal of Engineering and Applied Sciences, under publication.

Grozdanov, A., Buzarovska, A., Bogoeva-Gaceva, G., Avella, M., Errico, M. E., & Gentille, G. (2006). Rice straw as an alternative reinforcement in polypropylene composites. Agronomy for sustainable development, 26(4), 251-255.

Jones, B. (2009). Building with straw bales: a practical guide for the UK and Ireland. Green Books & Resurgence Books.

Morrison A. Photo Gallery - Straw Bale Workshops. See http://www.strawbale.com/photo-gallery-straw-bale-workshops/ (Accessed 08/08/2021).

Myhrman M. & MacDonald S. O. (1997). Build it with Bales: A step-by-step guide to Straw-Bale construction. Bale Publishers, Tucson, Arizona.

Nepal, B., Chin, C. S., & Jones, S. W. (2017a). Cementitious material with bio-based recycled agricultural waste. Academic Journal of Civil Engineering, 35(2), 589-596.

Nepal, B., Chin, C. S., & Jones, S. W. (2017b). Comparative study of the use of man-made and natural fiber reinforced concrete for ground floor slab applications. International Journal of Structural and Civil Engineering Research, 182-185. https://doi.org/10.18178/ijscer.6.3.182-185

Nepal, B., Chin, C. S., & Jones, S. (2015). A review on agricultural fiber reinforced concrete. Sustainable Buildings and Structures, 125-130.

REI (Renewable Energy Institute) (1997) Alternative Uses of Rice Straw in California. California Air Resources

Board, California, Report 94-330.

Trubetskaya, A., Jensen, P. A., Jensen, A. D., Steibel, M., Spliethoff, H., Glarborg, P., & Larsen, F. H. (2016). Comparison of high temperature chars of wheat straw and rice husk with respect to chemistry, morphology and reactivity. Biomass and bioenergy, 86, 76-87.IEEE.